TIME-DEPENDENT DEFORMATION IN UNCONSOLIDATED RESERVOIR SANDS

A DISSERTATION SUBMITTED TO THE DEPARTMENT OF GEOPHYSICS AND THE COMMITTEE ON GRADUATE STUDIES OF STANFORD UNIVERSITY IN PARTIAL FULFILLMENT OF THE REQUIREMENTS FOR THE DEGREE OF DOCTOR OF PHILOSOPHY

Carl Tingyu Chang

June 1998

Abstract

This dissertation discusses observations, implications, and micromechanical mechanisms of time-dependent deformation in dry reservoir sands from the Wilmington Field, Long Beach, California, and the South Eugene Island Field, Gulf of Mexico, with grainsizes between 10 to 300 μm under elevated pressures. Experimental results obtained in a triaxial loading system at confining pressures of 20 - 30 MPa and axial stresses of 40 MPa provide evidence of viscoelasticity as indicated by time-dependent deformation and ultrasonic pulse transmission data. Creep strain data suggests that dry sand deformed under high pressures has a fundamental creep and relaxation time constant. These results may provide a mechanism that explains creep, dispersion, and low differential stress observed in unconsolidated reservoir rocks. The combination of creep and relaxation implies that the dry rock matrix is viscoelastic which may result in dispersion even in the absence of pore fluids. The viscoelasticity of the dry sand matrix adds an additional relaxation time constant besides those associated with pore fluid motion thus complicating previous descriptions of frequency dependent moduli. Control groups of Ottawa sand mixed with small amounts of Montmorillonite clay suggest that the phenomena is controlled by the deformation of intergranular clay and not the deformation of quartz grains. Creep tests on synthetic idealized "two grain" models could replicate the creep strain observed in the sands with equal volume fractions of Montmorillonite clay indicating clay's role in the overall matrix rheology. It appears that microporosity reduction in the clays allows the quartz sand matrix to viscously rearrange its grains hence leading to time-dependent deformation.

Acknowledgments

Funding for this research was provided by the Department of Energy, The Gas Research Institute, and the Stanford Rock and Borehole Geophysics consortium. I would like to thank Mark Zoback, my mentor, teacher, example and guide, for believing in me. I would also like to thank Amos Nur, for letting the students come first. I'd like to thank Gary Mavko for introducing me to rock physics in the classroom, and Jack Dvorkin for encouraging my study of granular materials. Special thanks to Ronnie Borja of civil engineering, for tolerating my incessant and irrelevant questioning in soil mechanics class and for serving as my defense chair. This research wouldn't have been possible without the engineers at New England Research - Randy Martin, Chris Knudsen, Greg Boitnott, Martin and Terri Smith. Dan Moos, of Stanford Geophysics, provided many of the critical questions that motivated this research. Gilbert Palafox participated in the marathon of experiments that lead to my graduation. Special thanks to the administrative staff: Linda Farwell, Margaret Muir, Laurie Reynolds, Jeanette Ochoa, and Marianne Lang for handling red tape so I could focus on rock mechanics.

Thanks to my friends and colleagues in the borehole group, Wendy, Balz, Dave and Thomas who made grad school fun. I'd like to thank the senior grad students too, Lanbo Liu, Dave Castillo, and Marian Magee for guiding me when I was green. My friends and surrogate family, Soo Chan, Chris Chan, Sumit Sen, and Pamela Sturner made life rich during my years here. Thanks to Kenneth Chung and my brothers from the San Francisco Wing Chun Kuen kept my body and spirit strong during my most soul destroying months in the lab - your names belong on this thesis.

Finally I'd like to thank my wife Kazumi for her patience.

Contents

List of Figures

Chapter 2

Chapter 3

Figure 6.12 - Summary of creep strain

Figure 6.13 - Summary of creep strain at high pressure

List of Tables

CHAPTER 1

1.1 Scope

Over the past few years, interest in the study of unconsolidated reservoir sand deformation has increased in the rock mechanics and petroleum engineering community. Investigation of the mechanical behavior is motivated by the fact that the weakest, apparently most anelastic unconsolidated formations encountered during hydrocarbon exploration are also the most desirable highly permeable reservoir rocks. Any anelastic behavior of unconsolidated sands would suggest that elastic models may not sufficiently describe the mechanical behavior of unconsolidated sands in the hydrocarbon reservoir environment. Anelastic behavior would complicate the interpretation of field data since the mechanical properties of unconsolidated sands differ from those of hard rocks (e.g. well-cemented sandstone), upon which much of the existing rock mechanics knowledge is based. For understanding of the mechanical behavior of unconsolidated sands to improve, reservoir sand samples must be tested at reservoir stress levels in a controlled environment of a triaxial loading system, in much the same way that cemented and crystalline rocks have been tested previously.

Time-dependent deformation of unconsolidated reservoir rocks is one aspect of anelasticity which has been observed but not often pursued in detail in rock mechanics studies. This physical phenomenon could apply to such field problems as wellbore stability and sand production, in-situ stress, time-varying stress and frequency-dependent elastic moduli. Unfortunately, there are few laboratory studies concerning the deformation of unconsolidated reservoir rocks under high pressures and in the absence of pore fluids to

separate the pure rock mechanics from the inertial effects of pore fluid. In this work we investigate the material properties of unconsolidated sand deformation under high pressure conditions without the complicating influence of poroelastic effects.

This chapter reviews some of the previous studies relevant to time-dependent deformation of unconsolidated reservoir rock, the scientific aims of our work, and the material presented in this thesis.

1.2 Background

Creep in soils has been widely studied for over half a century to understand better the physics of slope stability and foundation competence (e.g., Terzaghi, 1941; Bishop, 1966; Barden, 1969). Traditionally this phenomenon has been investigated at pressures below several kPa's in geotechnical studies associated with the overburden at the near surface (<10's m). These studies established that clays and clay-rich sands creep under uniaxial strain conditions in odeometer tests. The testing was generally concerned with creep effects originating from pore water expulsion. Because of limited drainage in some soils, pore pressure transients lead to time-dependent deformation. This area of investigation established the relationship between strain and time in poorly drained soil bodies under triaxial and uniaxial consolidation below 20 MPa; these observations are relevant to foundation and slope stability at the near surface.

The pressures encountered in oil and gas reservoirs associated with hydrocarbon recovery are often much higher than 20 MPa. At these stresses, soil particles can be crushed, resulting in anelasticity (Wong, 1990; Wong et al, 1992; Zhang et al, 1992; Brzesowsky, 1995). In these studies, individual grain-crushing (detected by acoustic

emission techniques) was found to be critical to the constitutive behavior of sands at high pressures. Owing to the stress dependence of grain deformation mechanisms, if we are to observe phenomena occurring at the stress conditions encountered in hydrocarbon recovery, investigation of unconsolidated sands must be extended to include pressures higher than those used in the studies relevant to soil mechanics.

The rock mechanics literature has greatly enhanced understanding of the relationship between compaction, failure, and stress state in consolidated sandstone deformation at stresses greater than those observed in soil mechanics studies. For example, Wong et al (1992) established the occurrence of shear-enhanced compaction in Berea sandstone, in which grain-crushing and compaction occurred under triaxial loads in excess of 200 MPa mean stress. Zhang et al (1992) examined the micromechanical mechanisms of grain-crushing and cementation failure that occurred during the same tests. These studies found that large-scale porosity reduction in Berea sandstone can occur under low differential loads and very high confining pressures; this phenomenon became known as shear-enhanced compaction. Both studies established that the micromechanical mechanism of shear-enhanced compaction in Berea sandstone is grain and cementation failure. They found that grain-crushing manifests itself as irreversible pore compaction, a mode of failure different from brittle shear. The relationship of shear-enhanced compaction to cementation strength implies that such behavior should occur at lower pressures in unconsolidated sands. Although the studies provide insight into load path dependent mechanical properties and pore compaction, they do not report time-dependent deformation effects.

While much can be learned about the deformation of sedimentary rock from these studies of Berea sandstone, the behavior of unconsolidated sands under high pressures (>

10 MPa) has been rarely examined this way. The study of unconsolidated sand deformation demonstrates the influence of the presence or absence of cement on the grain contact. This is an important addition to the existing rock mechanics literature of cemented sands. Unconsolidated sands have usually been avoided in studies relevant to hydrocarbon recovery because of experimental difficulties associated with intact sample preparation and system sensitivity problems. Since the deformation of granular materials is highly dependent on grain contact strength, it is important to consider cases of uncemented, unconsolidated sands other than Berea sandstone.

In studies such as those of Yamamuro et al (1996) and Karig et al (1992), unconsolidated sediments were tested in the laboratory under triaxial conditions. These compliant materials deformed with a combination of plastic and nonlinear elastic behavior under drained conditions. The tests focused on triaxial strengths and the relationship between stress and strain; neither reported any time-dependent deformation. In Karig et al it is clear from the stress-strain plots that some of the sediments from the Nankai trench did indeed exhibit creep under static loads, as is seen by the flat portions in the stress-strain curves. Since strength and plasticity information was the aim of these tests, time-dependent deformation was ignored or allowed to equilibrate so as not to contaminate the data. In both studies, creep was virtually ignored.

Both Ostermeier (1993) and Dudley et al (1994) performed studies under hydrostatic and triaxial conditions that showed creep deformation in sands. These tests involved the compression of unconsolidated reservoir rock from the Gulf of Mexico at pressures up to 100 MPa. Being highly permeable well-sorted sands, the intact sand samples were saturated and well drained. In these high-pressure tests, long-term creep was observed

under hydrostatic and triaxial loads, implying that the creep mechanism was not necessarily dependent on shear loading. In the case of Ostermeier (1993) creep continued for up to a year under laboratory conditions. Although Ostermeier (1993) suggested several grain adhesion models to describe the micromechanical mechanism of time-dependent strain, neither he nor Dudley presented a viable mechanical mechanism for creep. Nor did either explore the creep deformation in the absence of pore fluid.

Breszowsky (1995) presented creep data in vacuum dry quartz sands tested under uniaxial strain compression. Acoustic emission monitoring during compaction and creep phases of the experiment connected grain-crushing to time-dependent deformation. Scanning electron microscopy indicated that the once-rounded sand grains tested in the uniaxial strain vessel had been crushed. From these results, Breszowsky connected creep to grain-crushing under uniaxial strain conditions. This was explained by the high shear stresses applied to the samples through the uniaxial strain testing conditions. Although it was never made clear whether a combination of repacking and grain-crushing resulted in creep (since monitoring acoustic emission alone could never determine this), it was concluded that grain-crushing mechanisms resulted in creep in clean quartz sands under uniaxial strain conditions.

1.2.1 Viscoelasticity in unconsolidated sediments

The presence of creep is a mechanical property of viscous or viscoelastic materials (Cole and Cole, 1941). I show in Chapter 2 that viscoelastic phenomenology can be used to describe creep in saturated clastic materials. Ostermeier (1993) proposed that the Gulf of Mexico sands tested under hydrostatic loading crept by viscoelastic mechanisms. Creep strain histories of turbidite samples were fitted to Kelvin viscoelastic models to extrapolate

long-term strains.

Since creep in sand implies an energy loss mechanism, it follows that viscoelastic dispersion can characterize the moduli of porous rocks (Bourbie, 1987). Viscoelastic materials deformed at high frequencies should appear stiffer than those deformed under lower-frequency perturbations. This phenomenology stipulates a predictable frequency response for the material, provided that it can be described mathematically using springs and dashpots. Because the models need a viscous component in the constitutive behavior, they are often used to describe the deformation of saturated rocks where pore fluid provides the energy loss mechanism.

The squirt flow mechanism is related to viscoelasticity in porous rocks (Mavko and Nur, 1979; Dvorkin,1993). This mechanism, which uses the displacement of pore fluid in a flat elastic crack as a loss mechanism to generate modulus dispersion, requires a compliant pore that provides the spring constant of the material. The model can be used to describe the transient strain of the pore volume and the relationship between ultrasonic moduli and saturation in a poroelastic material. The transition from high- to low-frequency behavior can occur in the sonic to ultrasonic frequency bands for sandstones, given the appropriate mineral moduli, pore volume modulus, and fluid viscosity.

Some investigations have speculated that viscoelastic mechanisms play no role in dispersion in that the moduli of poorly consolidated sediments are strain amplitude dependent, rather than frequency-dependent. Here plasticity is used to explain dispersion between static and dynamic moduli (Tutuncu, 1994). The difference between static and dynamic moduli is suspected to arise from the relative strain amplitudes associated with triaxial deformation and ultrasonic pulse transmission measurements. These results suggest

that cemented sedimentary rocks under triaxial loading have strain-amplitude dependent moduli, as indicated by their plasticity and nonlinear elasticity.

Although creep has been observed in samples of poorly consolidated sands from hydrocarbon-bearing reservoirs (Ostermeier, 1993; Dudley et al, 1994), it has not been solidly connected to viscoelastic mechanisms, making the connection between dispersion and creep speculative. Creep alone does not necessarily suggest a viscoelastic rheology that gives rise to dispersion between the static and dynamic moduli. However, creep does imply that the stress phase leads the strain phase under compaction. This phase difference suggests that moduli will appear stiff under fast perturbations and compliant under slow perturbations. Establishing the connection between creep and dispersion requires creep testing, relaxation testing, and dispersion analysis, none of which are treated in the aforementioned studies.

1.3 Objectives

Investigating the mechanical behavior of unconsolidated sediments required specialized hydraulic testing hardware that differs significantly from standard rock mechanics testing equipment. Much of this hardware was unavailable commercially and was specially designed and built for this study. Chapter 2 discusses the deformation apparatus and the sample preparation techniques developed and used here.

The primary scientific objective of this work was to obtain time-dependent deformation data in dry unconsolidated reservoir sand. Chapter 3 presents the first results of time-dependent deformation under hydrostatic loading in dry sands. The results are correlated with modulus dispersion detected in the absence of pore fluids. Measurements were

performed at pressures between 10 and 50 MPa, which are the same as those encountered in hydrocarbon reservoirs. Observations were made under dry or well-drained conditions to separate the time-dependent deformation of the rock from the inertial effects of the pore fluid.

The inertial effects of pore fluids change ultrasonic stiffnesses under saturated conditions. Chapter 4 uses poroelastic squirt theory to extrapolate the influence of pore fluid on the dispersive dry rock matrix. A full harmonic response was calculated to demonstrate the combined effects of fluid poroelasticity in a viscoelastically deforming rock matrix. The results show that scanning from subseismic to ultrasonic frequencies produces peculiar harmonic responses.

The existence of creep under hydrostatic loading conditions implies that other viscoelastic effects such as stress relaxation may occur under different boundary conditions. Chapter 5 describes how this hypothesis was tested by recording increases in stress relaxation, creep, and transient pore pressure under triaxial stress conditions. The duality of relaxation and creep supports the use of viscoelastic phenomenology to describe unconsolidated reservoir rocks.

The experimental results presented in Chapters 3 through 5 provide evidence of viscoelastic behavior in unconsolidated sands without explaining the origin of the phenomenon. In Chapter 6, an experiment to isolate the micromechanics of single-grain contact deformation was devised to examine the rheological behavior of two grains and a single grain contact. From this the micromechanical mechanism of dry viscoelasticity in unconsolidated reservoir rocks could be deduced.

1.4 References

Cole, K.S., Cole, R.H.,1941, Dispersion and Absorption in Dielectrics, Journal of Chemical Physics, 9, 341-351.

Barden, L., 1969, Time-dependent deformation of normally consolidated clays and peats, Journal of the Soil Mechanics and Foundations Division, ASCE, 95:SM1, 1-31.

Bishop, A.W., 1966, The Strength of Soils as Engineering Materials, Geotechnical, 16, 91-128.

Bourbie, T.,Cousy, O. and Zinser, B., 1987, Acoustics of porous media", Gulf Publishing Company.

Brzesowsky, R., 1995, Micromechanics of sand grain failure, Ph.D thesis, Universiteit Utrecht.

Dudley, J.W., Myers, M.T., Shew, R.D., Arasteh, M.M., 1994, Measuring compaction and compressibilitites in unconsolidated reservoir materials via time scaling creep, Proc. of Eurock '94 Balkema, Rotterdam, 45-54.

Dvorkin, J. and Nur, A., 1993, Dynamic poroelasticity: A unified model with the squirt and the Biot mechanism: Geophysics, 58, 524-533.

Karig, D.E.1992 "Uniaxial reconsolidation tests on porous sediments: mudstones from site 897," Ocean Drilling Program, Scientific Results, 149, 363-373.

Mavko, G., and A. Nur, "Wave attenuation in partially saturated rocks", Geophysics, 44, 161-178, 1979

Ostermeier, R.M., 1993, Deepwater Gulf of Mexico turbidites: compaction effects on porosity and permeability, SPE Formation Evaluation, June

Terzaghi, K., 1941, Undisturbed clay samples and undisturbed clays, J. Boston Soc. Civil Eng, 29:3, 211-331

Tutuncu, A.N., Sharma, M., 1994, Grain contact adhesion and hysteresis: A mechanical mechanism of seismic waves, Geophysical Res. Lett., 21:21, 2323-2326.

Stoll, R.E., 1977, Acoustic waves in ocean sediments, Geophysics, **42**, 715-725.

Wong, T.F., 1990, Mechanical compaction and the brittle-ductile transition in porous sandstones: Geological Society Special Publications, **54**, 111-112.

Wong, T.F., Szeto, H., Zhang, J., 1992, Effect of loading path and porosity on the failure mode of prorous rocks, Applied Mechanics Review, **45**:8, 281-293.

Yamamuro, J.A., Bopp, P.A., Lade, P.V., 1996, One-dimensional compression of sands at high pressures, Journal of Geotechnical Engineering, 122:2, 147-154.

Zhang, J., Wong, T.F., Davis, D.M.,1990, High pressure embrittlement and shear-enhanced compaction of Berea Sandstone; acoustic emission measurement and microstructural

observation: Rock mechanics; contributions and challenges; proceedings of the 31st U.S. symposium; 31, 653-660.

CHAPTER 2

THE DEFORMATION SYSTEM: TECHNICAL DISCUSSION

2.1 Overview

This section covers the construction and the loading and measurement capabilities of the deformation system, including specific details of the hydraulic hardware, feedback control circuitry, and strain measurement. A brief discussion follows of special sample preparation techniques developed to test intact samples of unconsolidated reservoir rocks.

2.2 Construction

The original loading system was a triaxial loading system manufactured by New England Research of White River Junction, Vermont. It consisted of a loading frame, a pressure vessel, pressure intensifiers, and various instruments for measuring ultrasonic pulse transmission, deformation, and stress on a 1- to 2-inch diameter core sample.

The system was originally configured to test crystalline rocks and well-cemented sandstones. This configuration differs from a system that tests unconsolidated sediments. In terms of stress and strain, the system was designed to have a high axial stress range and a limited range of axial displacement. Since this extended range compromises sensitivity, we modified the system to work at lower stresses, thereby providing the degree of sensitivity necessary for testing weak rock samples. The displacement range on the axial piston was extended to accommodate the large strains accumulated during unconsolidated sediment compaction. The stress range was also decreased to allow for higher loading sensitivity.

The schematic diagram of the pressure vessel is shown in Figure 1. The frame consists of three subcomponents: the external frame, which supports the axial piston load; the confining vessel, which holds the oil bath that exerts isotropic stress on the sample; and the pressure vessel between the axial piston and loading frame, where the endcaps and sample sit.

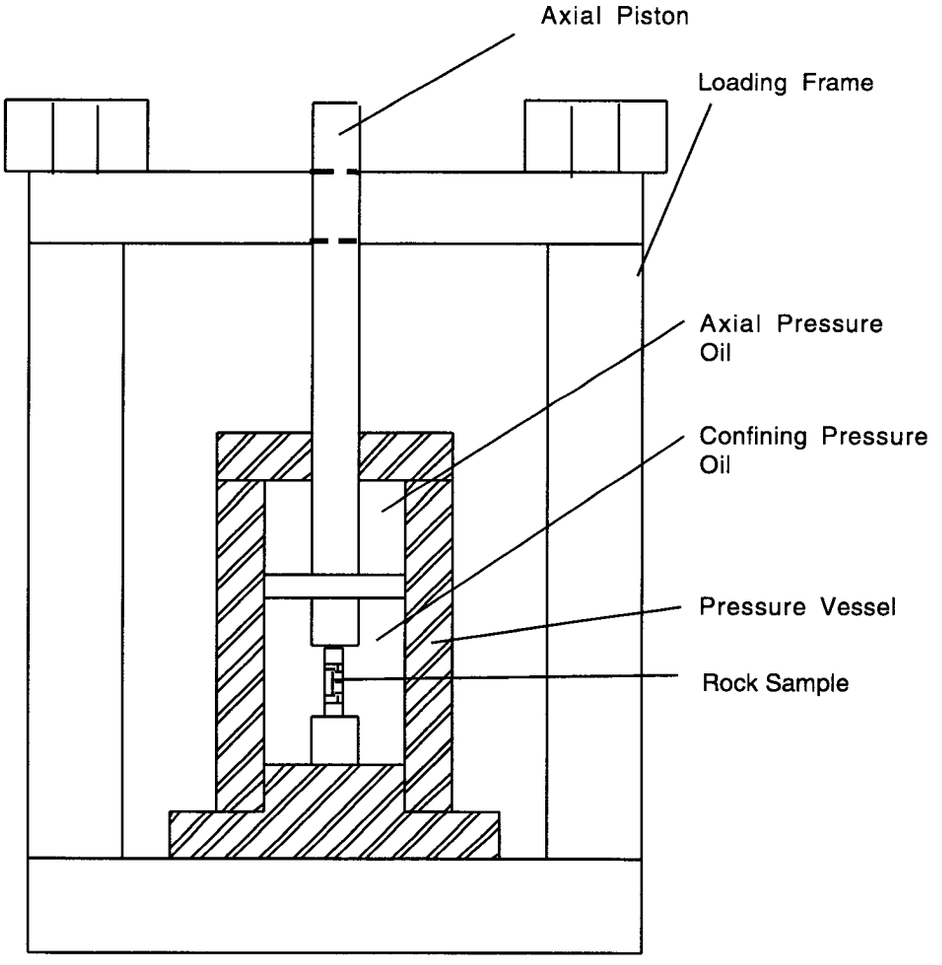

Figure 2.1: The cross-section of the pressure vessel showing the axial piston, confining pressure vessel, and rock sample.

Servo-hydraulic pressure intensifiers provide the high pressure for the system. Three pressure intensifiers feed the pore pressure, confining pressure, and differential pressure, as

shown in Figure 2. The intensifiers multiply the low-pressure power from a hydraulic pressure pump by a factor of 10 to develop a maximum of 200 MPa of confining pressure, 600 kN of differential load, and 20 MPa of pore pressure, which is limited by tubing strength rather than hydraulic power.

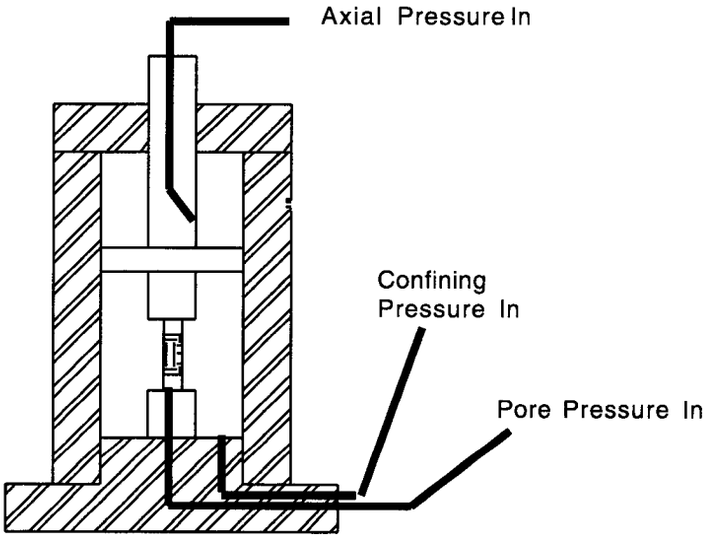

Figure 2.2: The intensifiers feed the hydraulic inputs into the pressure vessel to pressurize the confining, pore, and differential pressure.

The fluid pressure in the system is carried by Royco 756A hydraulic fluid, a clean grade of automobile transmission fluid. Depending on the type of test being done, the pore fluid can be chosen independently of the hydraulic fluid. In the tests described here, the port was always left open to atmospheric pressure unless noted. When used, pore fluids consisted of denatured alcohol. D.C. servo-motor-controlled valves regulated oil flow to the low-pressure side of the hydraulic pressure intensifiers to control the pressure precisely. The control circuitry driving the valves is discussed in a later section. A diagram of the servo-

controlled intensifier is shown in Figure 3.

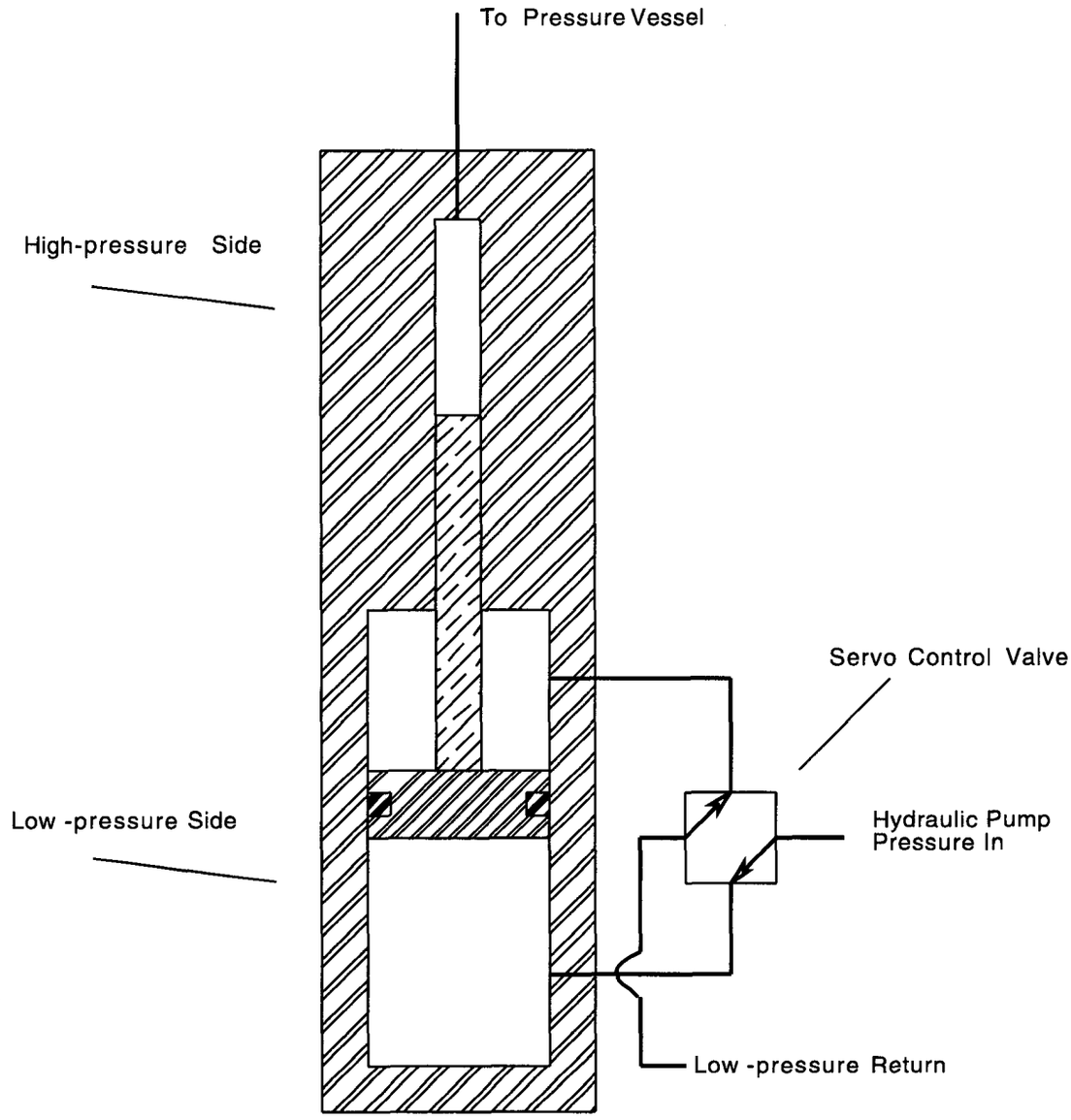

Figure 2.3: The servo-controlled pressure intensifier. This device converts small D.C. currents from the control circuitry into displacement of the intensifier. The displacement results in increases or decreases in pressure on the high-pressure side of the intensifier.

The diagram shows the high- and low-pressure sides of the intensifier. The areas of the internal pistons provide a pressure amplification ratio of 1:10 over the hydraulic source pressure generated by a 20-MPa, 7-horsepower Miller Hydraulic pump. In the valve diagram the intensifier is increasing pressure.

The pressure in both the confining pressure intensifier and the axial pressure intensifier is limited by the hydraulic pump pressure. The pump provides approximately 20 MPa of pressure, which is multiplied to a maximum of 200 MPa. If the confining press intensified to its maximum value of 200 MPa, there would be no pressure to provide any axial load, since the 20-MPa hydraulic pump multiplied by the 10 times intensifier would utilize all of the hydraulic power. It is important to remember that maximum confining pressure is achieved with no axial pressure. The pore pressure intensification system is limited by the diameter of the plumbing used to direct the pore pressure to the rock sample. Exceeding the maximum value of 20 MPa will result in the failure of the pressure relief devices (in the form of ruptured disks). The volume of the pore fluid plumbing system is 12.50 cc from the sample to the intensifier. This value is important when correction is made for the compressibility of the pore fluid between the intensifier and rock. The diameter of the high pressure side of the pore pressure intensifier is exactly 0.375 inches, which can be multiplied by the axial intensifier displacement (instrumented with a DCDT) to determine pore volume change.

2.3 Acquisition system and measurement capability

Ultrasonic velocity is measured using 1 MHz PZT crystals driven by a Panametrics 5055PR ultrasonic signal generator. Two S-wave polarizations and one P-wave polarization are collected by a digital oscilloscope. The waveforms are captured on a Hewlett-Packard 54610B 500 MHz digital oscilloscope and saved via a GPIB interface to the PC. The arrangement of the sample and crystals is shown in Figure 4. Because the rock material is very friable, ultrasonic couplants between the rock sample and crystals are not

used. During wave acquisition, the P-, S_1-, and S_2-wave transducers are switched on and off in sequence so as to not interfere with one another while ultrasonic data is recorded from each crystal.

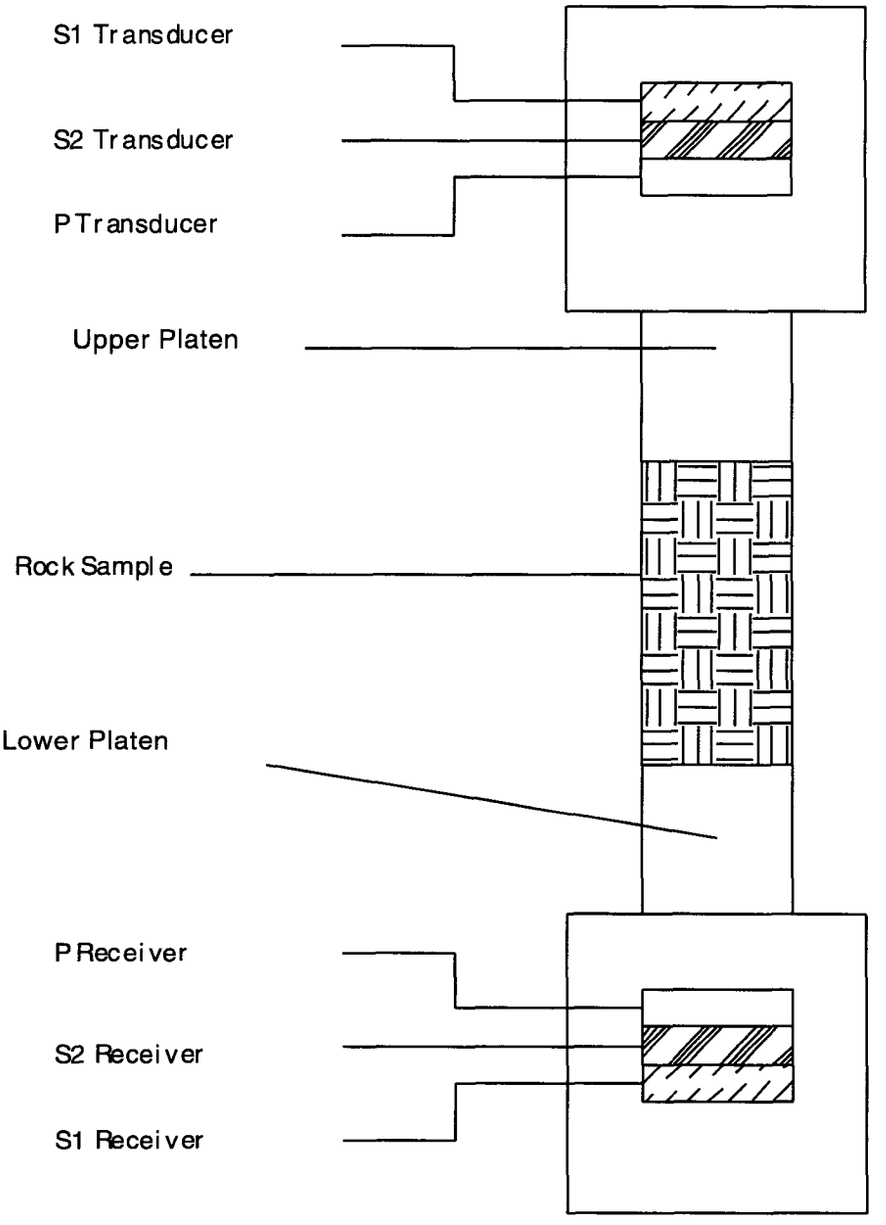

Figure 2.4: The endcaps fitted with quartz crystal ultrasonic transducers for two polarizations of S- and P-waves.

The wiring for the ultrasonic pulse transmission measurement apparatus is shown in

Figure 5. The velocity of the transducer stack is subtracted from the ultrasonic travel times using a head-to-head calibration with no rock in place. The delay between the trigger pulse from the oscilloscope and the transmitted wave determines the ultrasonic travel time. For unconsolidated sediments, the precision of this measurement is not determined by the instrumentation but rather by the operator's ability to locate the first break of the wave form. The resolved accuracy is approximately a microsecond.

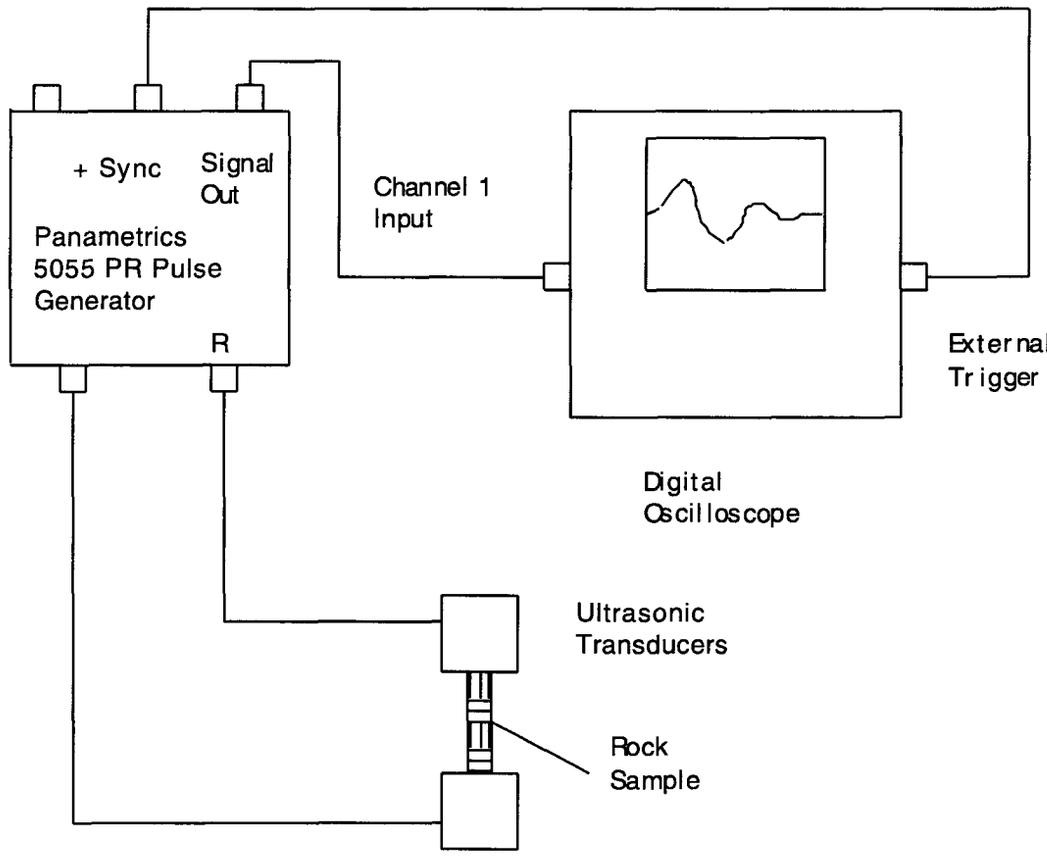

Figure 2.5: The wiring configuration of the signal generator, oscilloscope, and sample.

Two 12-bit analog-to-digital acquisition boards mounted in a 486 PC machine record data collected within the pressure vessel, including axial strain, radial strain, confining

pressure, axial load, pore pressure, pore volume displacement, and temperature. For the acquisition configurations used in all the experiments here, the accuracy of the internal transducers is controlled by the resolution of the 12-bit data acquisition system. By definition, 12-bit systems provide 4096 data points for the range of the selected measurement.

Internal displacement measurements are directly fitted to the sample to measure circumferential and axial displacements of the sample during loading. Axial strain is measured using two conductive plastic linear potentiometers, which are shown diagrammatically in Figure 6. The instrument precision specified by the manufacturer is 0.00001 inches. To insure uniaxial translation of the sample faces, the potentiometers are attached to an internal frame mounted inside the pressure vessel. Such an arrangement prevents sample buckling, which often occurs at the beginning of experiments where confining pressures are low.

We designed and built custom axial strain circuitry that specifies high range, high resolution, and large variable offset for the output voltages of the displacement gauges. Adequate measurement of displacements in unconsolidated sediments under high stresses depends on this combination of characteristics. The axial strain excitation voltages are conditioned through three stages of feedback regulation to reduce electrical noise in the excitation signal. The precision of these devices is also limited by the 12-bit cards to a strain of 0.0001. This value is high because there is a trade-off between range and resolution of the strain measurements. Conductive plastic transducers allow higher precision but limit the displacement ranges. A wide range is necessary to accommodate the large amounts of strain (sometimes as much as 10%) in the unconsolidated sands during high-pressure

compression. The transducer shafts are securely locked to the upper and lower transducer by two clamping plates; they are mounted along a frame to insure uniaxial translation of the sample faces, since sample buckling is a problem when compliant rocks are combined with compliant sample jackets.

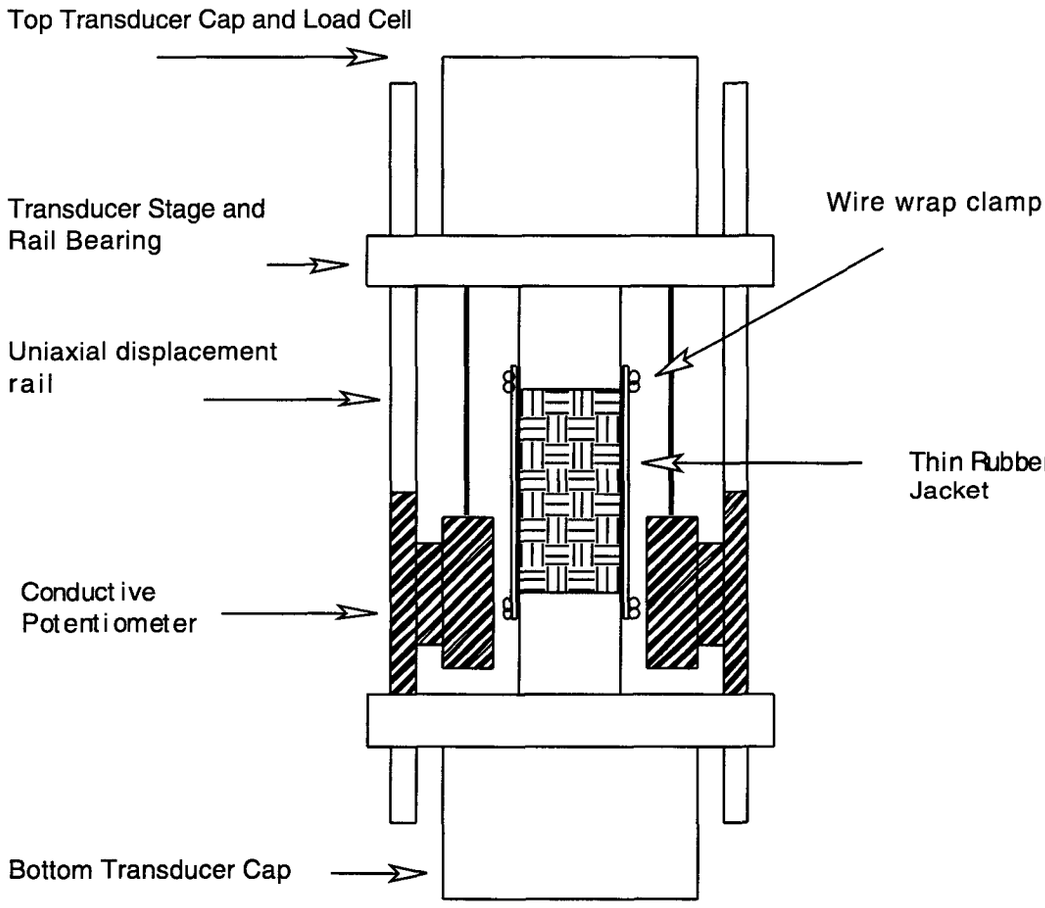

Figure 2.6: The configuration of the axial strain measurement. The vertical slide bars insure uniaxial displacement of the sample faces.

Wiring configuration is critical for linear potentiometers used under high pressure conditions. Since the confining pressure slightly deforms the plastic case of the transducer during pressurization of the vessel, the conductive plastic potentiometer will show some degree of pressure dependence. It was found by experimentation that this dependence

cancels out by wiring the outputs in the configuration shown in Figure 7. The correction is geometrical and physically normalizes the volumetric strain of the transducer.

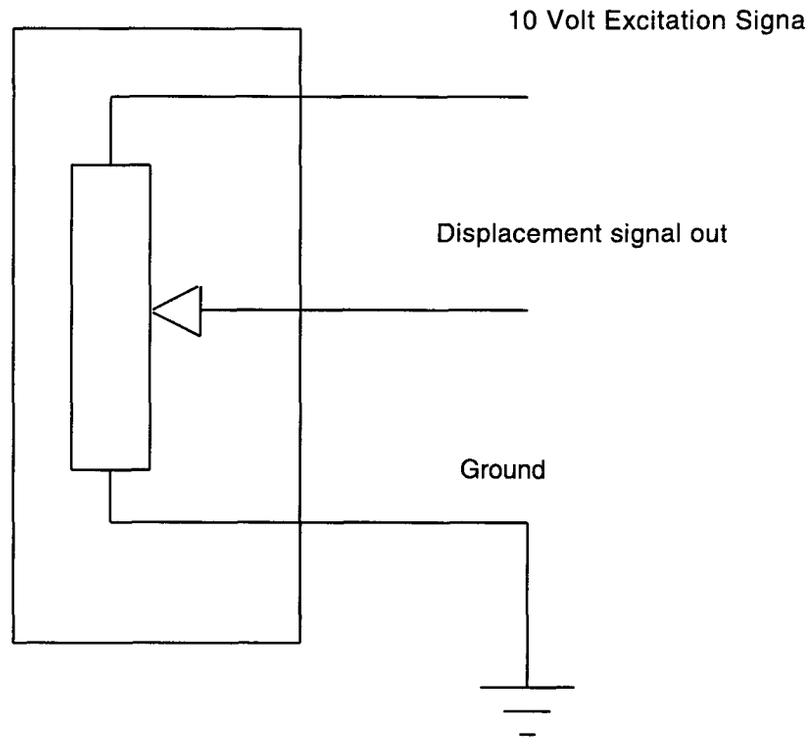

Figure 2.7: The wiring configuration of the linear potentiometers. This configuration corrects for the isotropic deformation of the case associated with changes in confining pressure.

The radial strain is measured using the chain-type circumferential strain gauge shown in Figure 8. This gauge uses a 1/4" range linear variable displacement transducer (LVDT) to measure the approximate change in the circumference of the sample. It has 2π times the sensitivity of radial transducers to changes in diametric strain. A.1475 pitch stainless steel roller chain is wrapped securely around the sample with no mechanical play. Tension is maintained on the LVDT by a small spring with an adjustable preload of 10 to 30 grams; this is too low to deform the sample. The gauge has a range of 5mm and a resolution of

0.00001 mm, which corresponds to $1x10^{-4}$ strain.

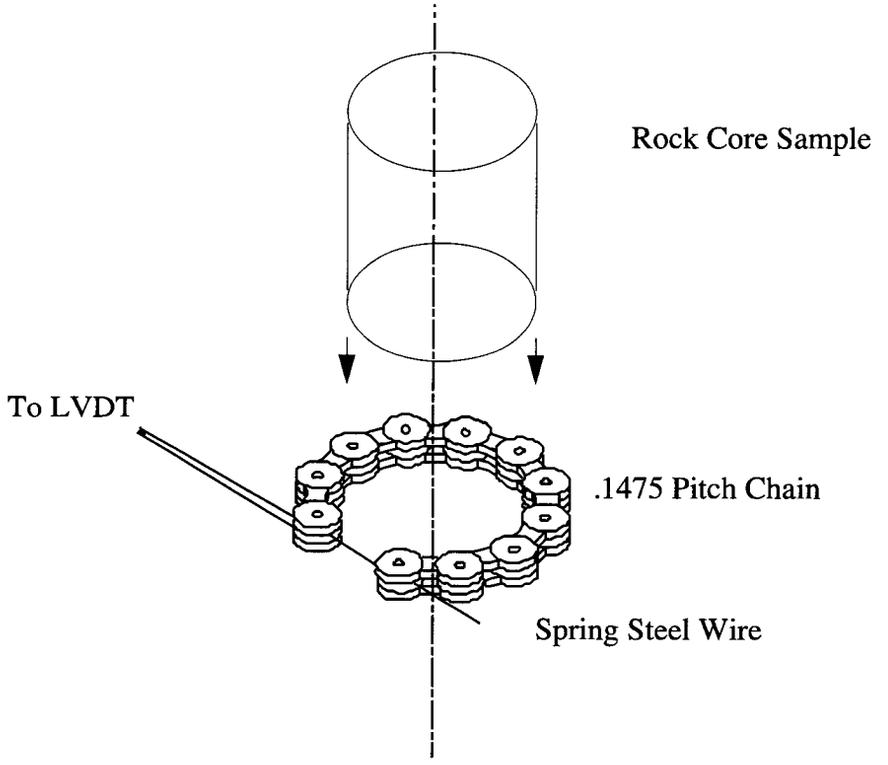

Figure 2.8: The chain displacement gauge. The chain measures the radial expansion of the cylindrical core.

2.4 The control system

Confining pressure, differential load, and pore pressure are controlled using differential feedback amplifiers. An example of this classic feedback control device is shown in Figure 9. One input of the amplifier is referenced with a user command voltage set by either the computer or the panel vernier. The other input is the transducer input. The amplifier continuously calculates the difference between the two input signals and sends out a signal proportional to this difference. As the user command voltage approaches the sensor voltage through feedback, the output of the amplifier goes to zero.

Pressure, force, and strain feedback mechanisms were configured for this work.

Pressure feedback uses the pressure gauge output to control the pressure in the confining pressure intensifier. As the user increases the pressure command signal, a control signal proportional to the difference between this signal and the actual vessel pressure moves the servo-controlled intensifier to increase the pressure. The control signal will decrease to zero as the pressure in the vessel approaches closer and closer to the user's command signal. This is a reliable method for maintaining constant confining pressure around the sample. The pressure can be increased linearly by applying a linear ramp to the user command input on the feedback amplifier.

Force feedback uses the internal differential load cell to control the differential load on the sample. The load cell voltage is fed into the amplifier and a control signal proportional to the difference between the load cell voltage and the user command voltage moves the servo-controlled axial intensifier to increase the axial pressure. Force feedback requires that the sample and load cell stay in contact. Thus, the piston must be positioned on the rock sample using pressure feedback and then switched to force feedback for increased sensitivity. This is a very reliable way to control the axial load on the sample.

Strain control uses the circumferential or axial strain gauge to control the position of either the sample jacket wall or the upper face of the sample with respect to the loading frame. In this type of control, the user sets the desired strain change on the controller input; the control signal then commands the intensifiers to advance (or retreat) appropriately until the sample reaches the predetermined dimensions. When these dimensions are met, the feedback circuitry stops the advance of the axial piston by turning off the axial intensifier.

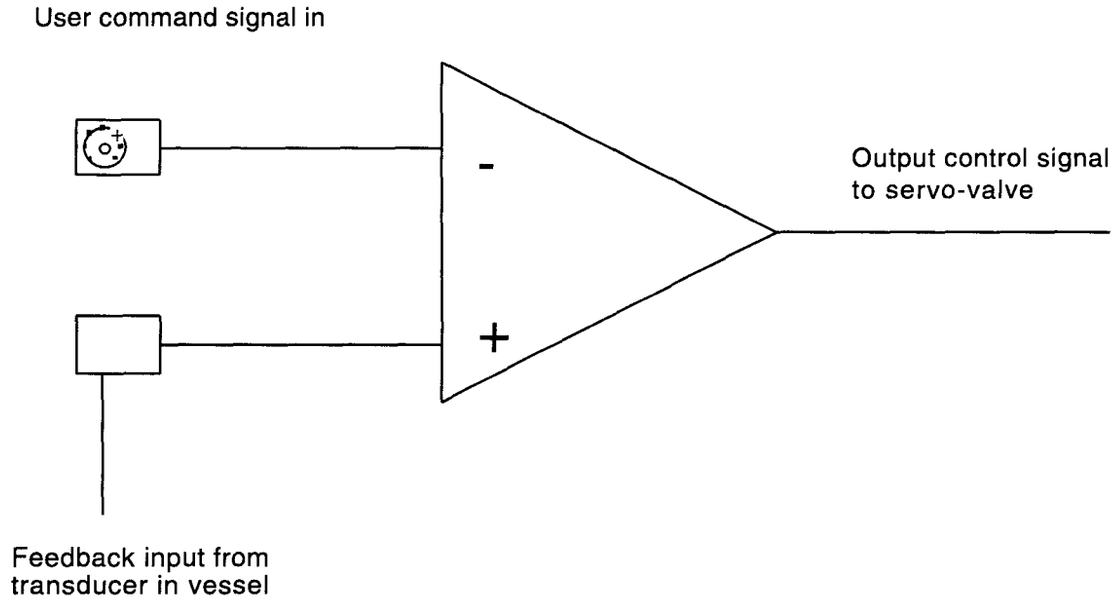

Figure 2.9: The pressure feedback amplifier. Output is proportional to the difference of the inputs. The control signal should thus approach the feedback sensor signal at equilibrium.

As in all feedback systems, there is the possibility of feedback oscillation, which occurs when the output signal overshoots the user command set point. This problem, which can result from phase lag in the feedback loop, is commonly encountered in testing viscoelastic materials where the stress leads the strain phase. One example is cases where strain control is used. Because strain control uses a direct measurement to control the stress (which leads the strain phase), and because the stress perturbation does not produce any initial strain response, the feedback correction may overshoot the desired target strain. This scenario leads to oscillation. To prevent it, one should always use low strain rates when deforming viscoelastic rocks. Another method is to perform feedback using values that do not lag or lead each other (i.e., controlling stress with stress or strain with strain). Analog filtering of

the control signal, also known as compensation, can correct unstable control loops. However, feedback oscillation is an unavoidable manifestation of viscoelasticity in samples characterized by time-dependent deformation.

2.5 Loading procedures

2.5.1 Hydrostatic loading

Hydrostatic compression of a sample within the cell is achieved by increasing the confining pressure to the desired value; the axial piston does not contact the sample during hydrostatic loading. The rate at which pressure is increased, or ramped, can be varied. Holding time and unloading rates can also be varied, thus allowing creep to be observed under hydrostatic conditions.

2.5.2 Triaxial loading

Triaxial loading involves advancing the axial piston under finite confining pressures. However, the term "triaxial" is a misnomer, because the two horizontal stresses set by the confining pressure are equal. The piston is brought into contact with the sample before the confining pressure is increased. Triaxial loading is complicated by the fact that unconsolidated rock has no strength under uniaxial compression. Once the piston contacts the sample, the confining pressure must be increased immediately to prevent sample failure.

The two pressures must be increased simultaneously: increasing the pressure too soon causes the piston to lift off of the sample (thereby breaking the force feedback loop), and not increasing the confining pressure at all causes the sample to be crushed under the piston,

since the load cell does not feed sufficient voltage back to the control circuitry. This is a consequence of testing very weak soil-like samples at high pressures. The load cell needs a wide range to perform high-pressure experiments and thus loses the sensitivity needed for the delicate initial positioning of the axial piston.

This problem was resolved by acquiring skill at moving the piston under pressure control before bringing it into contact with the sample. We then switched to force control after the internal load cell had contacted the piston. Microswitches between the piston and upper transducer allow the user to determine the proximity of the piston during lowering. A new solution involving two switchable load cells in series, one for loading and one for set-up, would provide a more reliable method of initially loading the sample.

2.5.3 Uniaxial strain

Uniaxial strain is one-dimensional compression under zero radial strain. Zero circumferential strain is maintained by measuring the circumference of the sample and feeding this value back to the confining pressure control circuit. A contraction or dilatation in the sample results in an decrease or increase in confining pressure, respectively. However, the axial piston is still free to move and thus results in a uniaxial strain experiment. One advantage of uniaxial loading is that pore volume loss is approximately equal to the axial strain, since the entire volumetric strain is in the axial direction.

Initial loading is much simpler for uniaxial stress than for triaxial stress. As the sample is touched by the piston, it dilates radially, causing the confining pressure to increase automatically in order to maintain zero radial strain. The piston can come to rest on the upper surface of the sample while exerting a finite load on the internal load cell. This safeguards the sample from instantaneous shear failure under the axial load.

2.5.4 Step strain

Constant strain can also be maintained in the axial direction. The test is performed by loading the sample under triaxial conditions, first under pressure feedback before sample contact, and then under force feedback following sample contact. The control circuitry is then switched to strain feedback and the axial load on the sample can be stepped, allowing the piston to approach a predetermined positioned. On reaching this position, the strain control circuitry holds the piston stationary by modulating the pressure in the axial pressure intensifier.

2.6 Sample preparation

2.6.1 Plunge-cutting intact unconsolidated sand samples

Because of their softness, unconsolidated sample plugs taken from intact drill cores can be plunge-cut using a drill press and a one-inch core barrel. The core barrel is fabricated from 1.125-inch stainless steel tubing that has a 0.0625-inch wall thickness and is sharpened on the inner edge of the cutting end. It is mounted onto the drill press and pressed into the drill core while the drill press is off. Using a drill press allows the sample to be taken along a straight cylindrical axis. When retracted, the core barrel extracts a one-inch diameter plug of the desired length, as is shown schematically in Figure 10. The sample remains intact inside the stainless steel tube.

2.6.2 Jacketing intact unconsolidated sand samples

The sample is then carefully pushed out of the core barrel into one-inch heat-shrink tubing, as is shown in Figures 11 and 12. After extrusion, the tubing is shrunk around the plug, whose faces are smoothed using a pair of one-inch diameter aluminum end-plugs.

When the ends are smooth and parallel, the sample is carefully placed between the transducer endcaps.

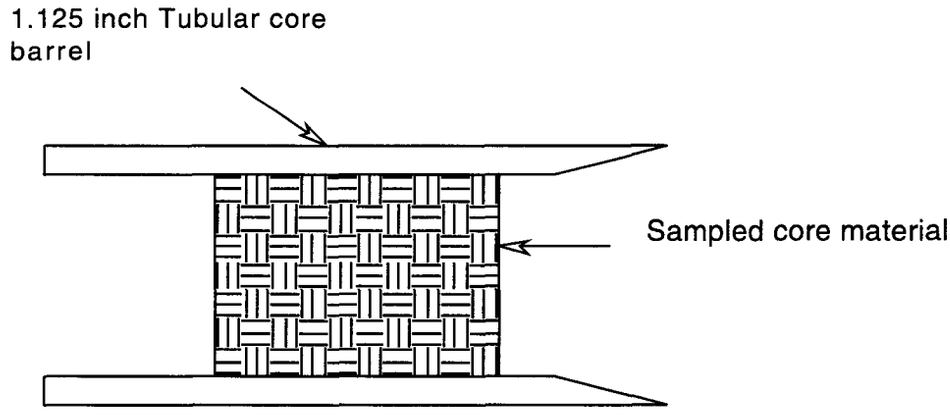

Figure 2.10: The sharpened core barrel holding the rock core. After plunge-cutting, the core material breaks off and stays inside the bore of the barrel.

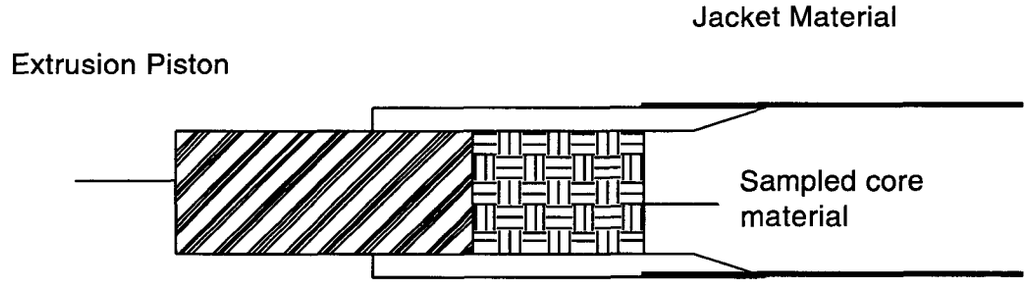

Figure 2.11: The core barrel and sample before extrusion. The extrusion piston is in position behind the rock sample. The jacketing material is slipped over the barrel.

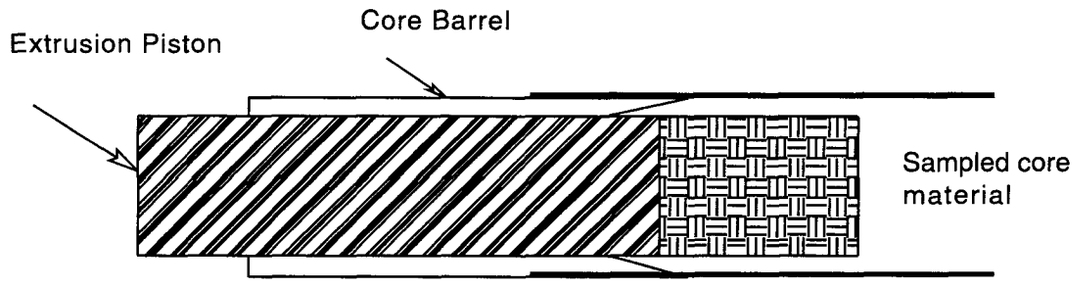

Figure 2.12: The rock sample after extrusion into the jacket. The piston is moved forward and the intact rock sample slides into the jacket.

2.6.3 Making synthetic samples with Ottawa sand and Montmorillonite clay

Clay drying for Ottawa sand/clay mixtures

Dry laboratory-grade Montmorillonite clay is mixed into Ottawa sand by volume percentages until the mixture appears homogenous. This mixture is then loaded into a sample jacket and plugged at the ends with aluminum billets. The sample is saturated with distilled water and allowed to dry for a day at room temperature while air is circulated through the pore space. Gravimetric analysis is performed to determine the moisture content. The sample is ready for testing when 0.1% water by mass remains (i.e., the resolution of gravimetric analysis).

Clay drying for block testing

Dry Montmorillonite clay used in block tests is mixed with a known amount of water and allowed to dry at room temperature. The amount of water in the mixture is determined by mass. The dry clay is weighed before water is added and the mixture is weighed again

afterward. The mass of the water in the mixture is the difference between the final and initial mass of the mix. Water content is determined by the mass ratio of water to clay. The samples are loaded into the testing vessel when the water content (in the clay only) falls below 5% by mass, which is the limit of the resolution of the gravimetric analysis.

CHAPTER 3

ANELASTICITY AND DISPERSION IN DRY UNCONSOLIDATED SANDS

Abstract

Laboratory measurements reveal frame modulus dispersion and creep behavior in room-dry samples of unconsolidated quartzo-feldspathic Upper Miocene turbidites from the Wilmington Field in California, and Lentic sand samples from the South Eugene Island Field in the Gulf of Mexico. A single standard linear solid model predicts both the dispersion and the creep response. Similar behavior is observed in Ottawa sand samples mixed with wetted Montmorillonite. In this case the magnitude of dispersion and creep increases with increasing clay content. It appears that the anelastic behavior of the Wilmington sands is due to the presence of micas and a small amount of clay. The transition frequency of 3.1×10^{-4} Hz (i.e., between high and low frequency behavior) suggests that seismic, sonic, and ultrasonic measurements of rock moduli are quite similar in the absence of fluids but the static frame modulus should be used to model tectonic processes and long-term production-related changes in oil-field environments.

3.1 Introduction

Although viscoelasticity has been documented extensively in soil and rock mechanics, it has traditionally been associated with the presence of fluids in the pore space (e.g., Biot, 1956). Laboratory measurements on saturated samples clearly demonstrate that differential motion between the fluid and frame causes dispersion (Winkler, 1983; Bourbie, 1987; Mavko and Jizba, 1991), creep (Terzhagi, et al, 1936), and attenuation (Murphy et al,

1986).

Studies of turbidites indicate that creep is prevalent in fluid-saturated weak sands, even when their permeability is high enough to allow fluids to escape during the elastic portion of the loading history (Dudley et al 1994; Ostermeier et al 1993). This suggests that in these materials the rock frame is intrinsically anelastic.

To investigate this, we studied the time-dependent response to loading in room-dry samples of unconsolidated reservoir rocks from the Wilmington Field. Additional samples of Ottawa sand mixed with varying amounts of Montmorillonite were tested to investigate the cause of the observed response. The load history was designed to allow simultaneous determination of the response to loading and unloading. Static moduli were obtained using small-amplitude strain loops. Pauses during loading were accompanied by continued deformation (creep), which was modeled viscoelastically. Ultrasonic pulse transmission experiments allowed determination of the high-frequency small-strain moduli. The results were modeled using a standard linear solid to estimate the transition frequency between high- and low-frequency values of the frame modulus.

3.2 Experimental procedure

Core samples of unconsolidated Upper Miocene turbidites were obtained from the Wilmington Field (in Long Beach, California) in wells UP941B and 169W from a depth of approximately 3000 feet. The cores from 169W were jacketed in PVC at the well site and refrigerated until testing to preserve the natural state of the matrix and fluids. Materials from UP941B were obtained from core samples archived in a non-climate-controlled warehouse. Thin section analysis indicated that the samples consisted of approximately

20% quartz, 20% feldspar, 20% crushed metamorphic rocks, 20% mica, and 10% clay. The poorly sorted grains were highly angular and had a mean grain size of 300 μm.

The samples were extracted from the whole cores by plunge-cutting at room temperature using thin-walled steel tubing; they were then extruded into soft polyolefin jacketing. The jacketed specimens were 1" in diameter and 2" long. For the UP941B samples to be tested "dry," residual heavy oil was removed by flushing, first with mineral spirits and then with air to dry the pore space, which resulted in a 5% reduction in length. The samples were wired to a transducer stack and placed in a pressure vessel for testing under room-dry conditions. The samples from 169W, which were tested "saturated," were prepared without removing the natural pore fluids.

Cyclic loading was performed in the following manner (Figure 1). The sample was initially pressurized to 10 MPa at a loading rate of 10^{-7}/s (the first loading leg). It was then allowed to sit for 5 hours to allow transient creep to subside (the creeping leg), after which the pressure was lowered to 5 MPa at 10^{-8}/s (the unloading leg). The process was repeated, with each cycle reaching a maximum confining pressure 10 MPa higher than the previous cycle, to a maximum of 30 MPa. Simultaneous travel time measurements were made by propagating P- and S-waves along the axis of the cylinder using 1 MHz quartz crystals, as represented by the open circles in Figure 1. An automated data acquisition system recorded hydrostatic stress and axial deformation, as well as the full waveforms transmitted through the sample. Samples of dry, unsorted Ottawa sand were tested in a similar fashion in order to investigate the influence of increasing clay content on the total amount of creep strain.

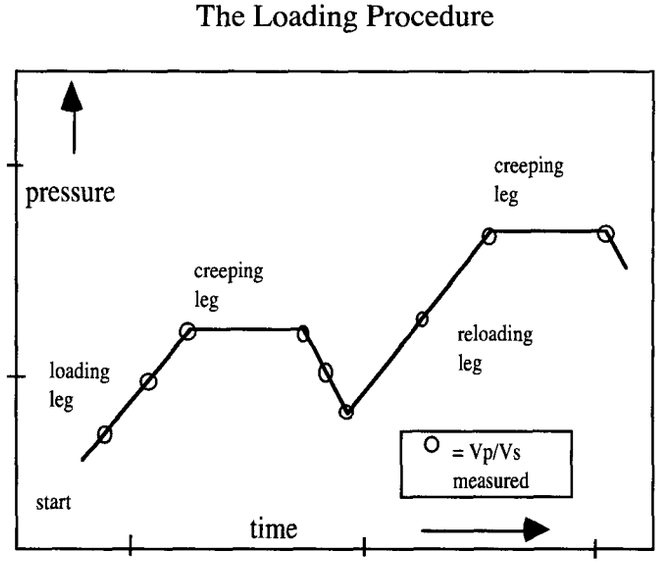

Figure 3.1: The loading process showing pressure vs. time

Small cyclic loading loops were performed to minimize strain amplitude effects caused by nonlinearity. The behavior of the samples deformed here was clearly nonlinear under both hydrostatic loading and triaxial loading. If the sample has a very nonlinear stress vs. strain response, a large amplitude strain may give a lower stiffness measurement, since we are trying to describe the behavior with a single constant. The ultrasonic measurement is a small deformation that gives a more linear measurement, since no inelastic deformation occurs. Tutuncu et al (1995) relate dispersive behavior of cemented sandstone to differences in strain amplitude. Although this seems to be the case, small unloading cycles should measure the rebound modulus without plastically deforming the matrix. This explained the large difference between static and dynamic modulus in their samples and no creeping behavior was documented.

Initial porosities were measured by gravimetric analysis of the washed grains after testing, given the mass and initial plug dimensions. The mass and volume were measured

before testing. After testing, the grain density was measured volumetrically for a subsample of the sample plug and used to calculate the total grain volume. The porosity was determined from the final grain volume and initial bulk volume.

3.3 Results

3.3.1 Wilmington sands

Stress vs. strain plots of two typical samples are shown in Figure 2. W34 was cleaned and dried to remove residual tars and had an initial porosity of 29%. W44 was tested with fluids intact and had an initial porosity of 35%. W34 is slightly stiffer, an observation consistent with the lack of soft tars within its load-bearing frame. Both samples show pronounced hysteresis and a much smaller compaction modulus than "loop" modulus. The flat portions of the curve show creep under constant load. The small loading and unloading loops fall on each other, thereby demonstrating elastic behavior. During reloading, the loading modulus decreases as the pressure is increased beyond the initial point of the unloading loop, indicating that plastic compaction of the matrix has occurred.

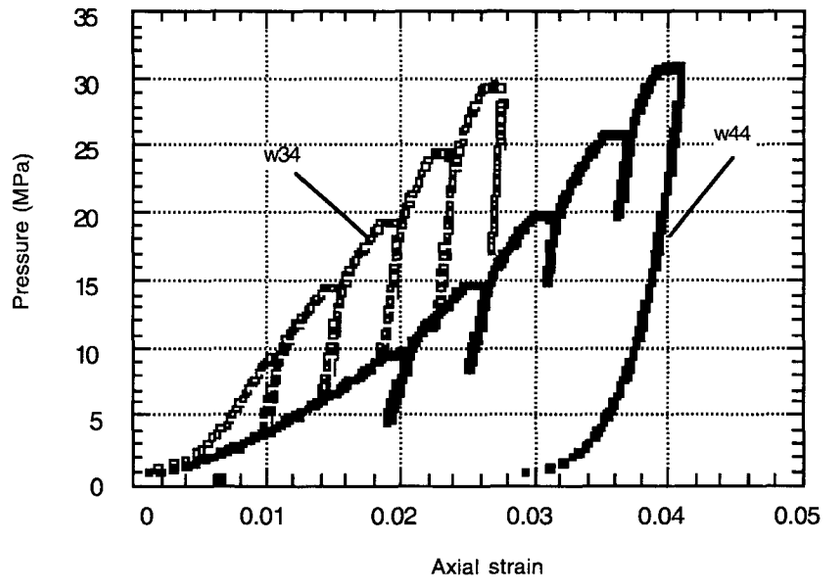

Figure 3.2: Stress vs. strain for hydrostatic cycling tests on dry (w34) and saturated (w44) samples.

Figure 4 shows ultrasonic velocities vs. porosity. Both compressional and shear velocities in the dry sample are similar to those in the saturated sample. All velocities increase with consolidation. Although saturated and dry measurements were not made in the same plug sample, the two data sets follow similar trends. Scatter in the velocities originates from using porosity alone as the state variable controlling velocity during the compaction cycles.

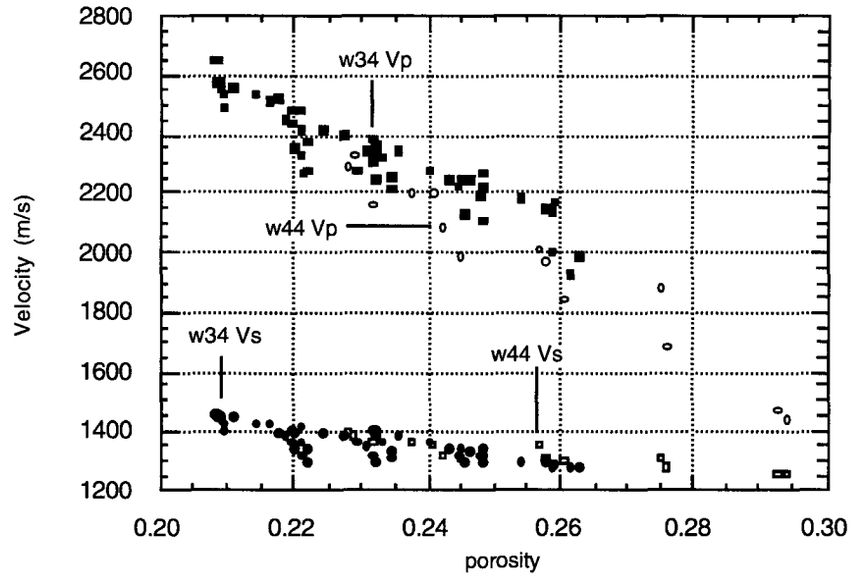

Figure 3.3: Ultrasonic velocity measurements vs. porosity for dry (w34) and saturated (w44) samples.

The bulk moduli were derived from the stress loops as well as the ultrasonic data. Linear fits to the slopes of the unloading legs of the stress-strain curve gave static moduli for a strain measured at the middle of the loop. The deformation was assumed to be isotropic and the volumetric strain was calculated as three times the axial strain. The ratio of pressure to volumetric strain gave the bulk modulus. The dynamic bulk modulus was determined from the ultrasonic P- and S-wave velocities using a density corrected for volumetric compaction at the point of measurement.

The bulk modulus derived from pulse transmission is larger than that derived from the axial strain loops in both samples (Figure 4). The dynamic modulus of each sample is approximately two times higher than the static modulus.

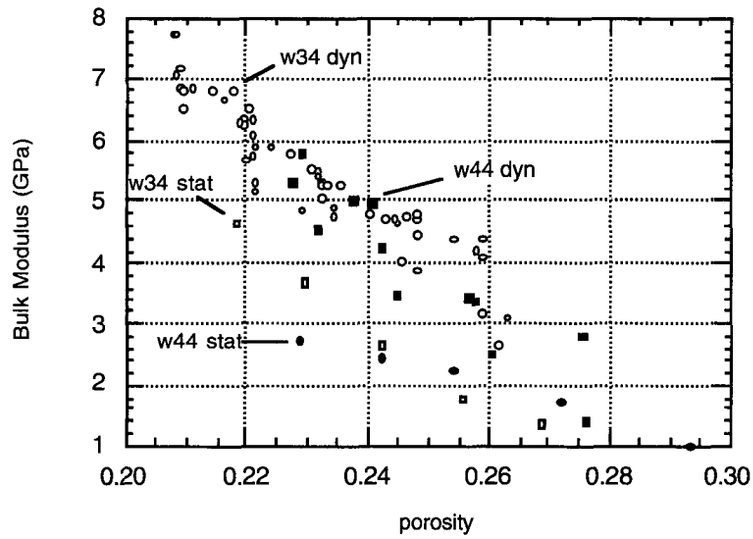

Figure 3.4: Bulk modulus as a function of porosity in dry (w34) and saturated (w44) samples.

The dynamic moduli of the two samples lie along more or less the same trend. The high porosity static moduli are also roughly equal. However, the static bulk modulus of the cleaned dried sample increases more rapidly than that of the saturated sample as porosity decreases.

3.3.2 Ottawa sands

As shown in Figure 5 dry Ottawa sand shows little hysteresis, no creep, and no difference between loading and "loop" moduli, all three effects can be observed in Ottawa sand containing 10% wetted Montmorillonite. The clean sample shows some hysteresis but little or no creep. The sample of 10% Montmorillonite added to Ottawa sand shows more creep and hysteresis. The clean sample is stiffer and shows less irreversible compaction. The ultimate strain of the dirty sample is twice as high as that of the clean sample.

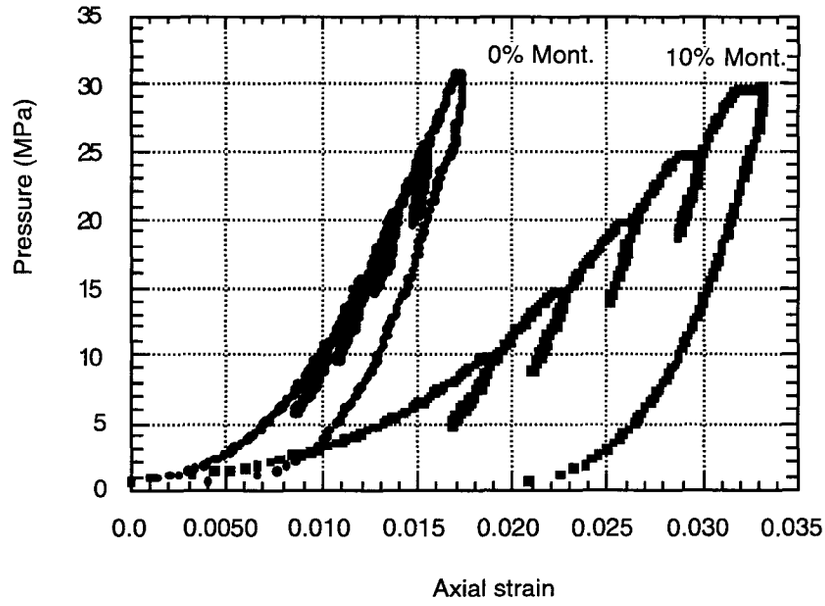

Figure 3.5: Stress vs. strain for hydrostatic cycling tests on Ottawa sand with 0% and 10% Montmorillonite clay.

Ottawa sand with 5% Montmorillonite clay

Ottawa sand samples required a small amount of Montmorillonite clay to show time-dependent deformation. In Figure 6, a mixture of Ottawa sand and 5% Montmorillonite clay shows hysteresis and creep. Using a loading scheme similar to that used to determine the static moduli of the Wilmington sand, we determined the static moduli of this synthetic sand and clay mixture. Although the clean Ottawa sand (Figure 5) did not creep or show as much plasticity as the natural samples of Wilmington sand, the addition of small amounts of Montmorillonite clay gave the Ottawa sand a stress-strain response much like that observed in the natural sand samples. Significant differences between loading and unloading moduli and creep mark the behavior of the sand-clay mixtures.

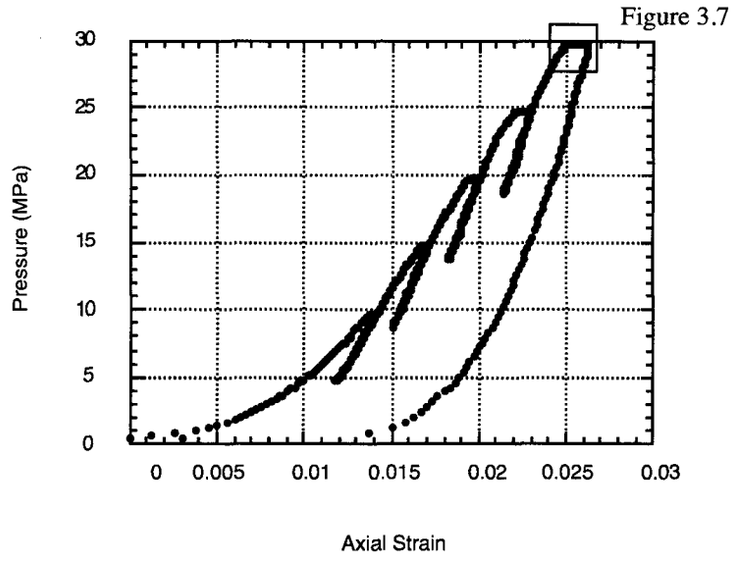

Figure 3.6: The stress vs. strain response for Ottawa sand with 5% Montmorillonite clay under hydrostatic loading. The sample was dry.

The flat spot at 30 MPa at the end of the loading leg in Figure 6 represents creep strain at constant load. In time versus strain, this creep behavior is similar to that of the natural Wilmington sand samples. The response is enlarged and plotted with respect to time in Figure 7. This sample showed creep with the same decreasing exponential form seen in the Wilmington sand samples. The strain magnitude and strain rate during this creep phase were also of the same order of magnitude as those observed in the Wilmington sands. Samples of clean Ottawa sand showed almost no creep, suggesting that the presence of Montmorillonite clay provided the mechanism for creep to occur.

Figure 8 shows the difference between static and dynamic bulk moduli in the clay-sand mixture. The material appears to be more compressible under low frequency stress cycling than under the high frequency strains associated with ultrasonic wave transmission. The ultrasonically derived moduli appear to be more pressure dependent than the static bulk moduli.

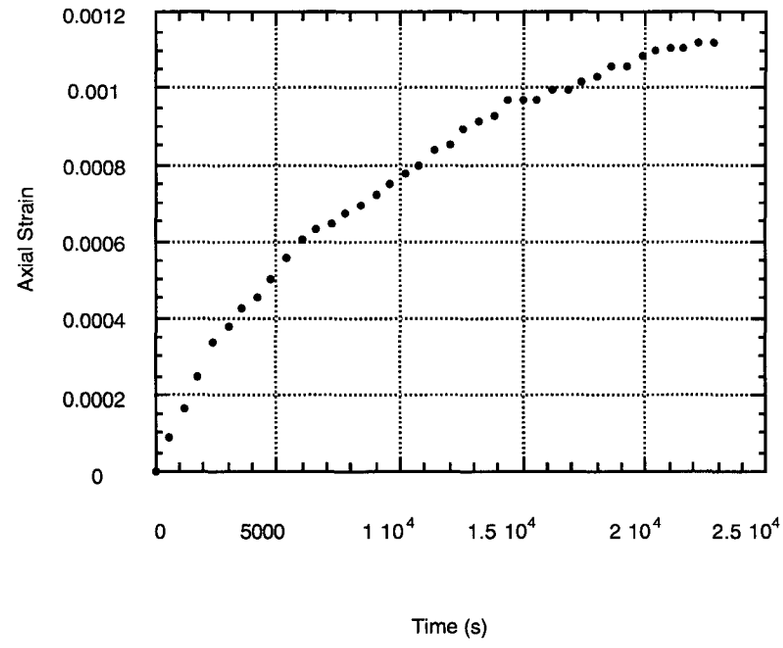

Figure 3.7: Creep strain at 30 MPa hydrostatic pressure in Ottawa sand with 5% Montmorillonite clay.

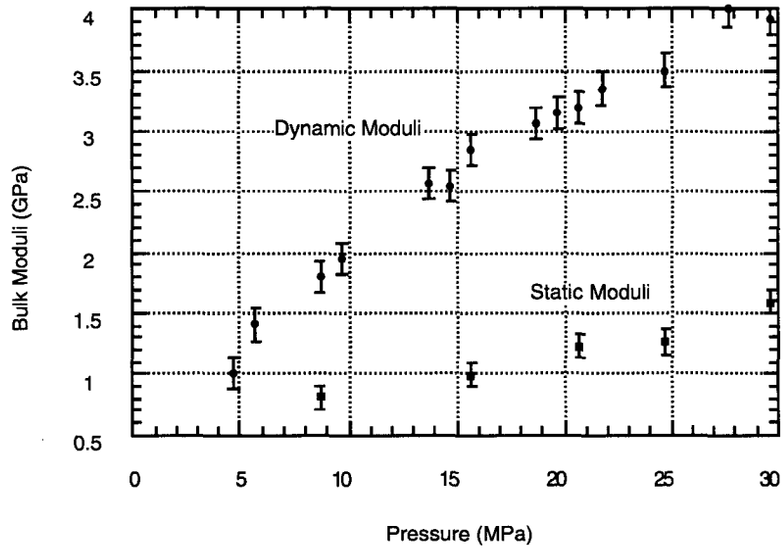

Figure 3.8: The difference between static and dynamic moduli measured during hydrostatic loading.

Ottawa sand with 10% Montmorillonite clay

To test the dependence of time-dependent deformation and dispersion on clay content, we increased the amount of Montmorillonite clay in the Ottawa sand to 10% and performed a similar analysis. The stress-strain behavior appears to have the same form as that of the 5% clay sample: it too is characterized by hysteresis and creep (Figure 9). The total creep strain is greater in the sample with more clay (Figure 10). The ultrasonic moduli also appear to increase with increasing clay content, as is seen in Figure 11. The ratio of static to dynamic moduli is approximately the same.

Figure 3.10

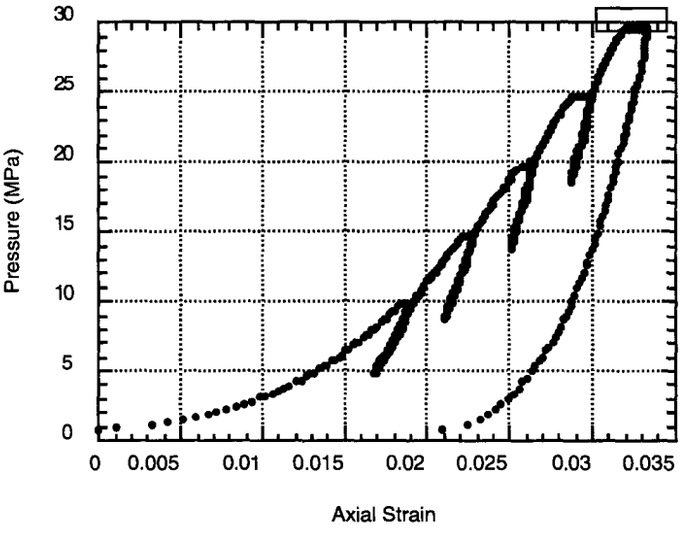

Figure 3.9: The stress vs. strain response for Ottawa sand with 10% Montmorillonite clay under hydrostatic loading. The sample was dry.

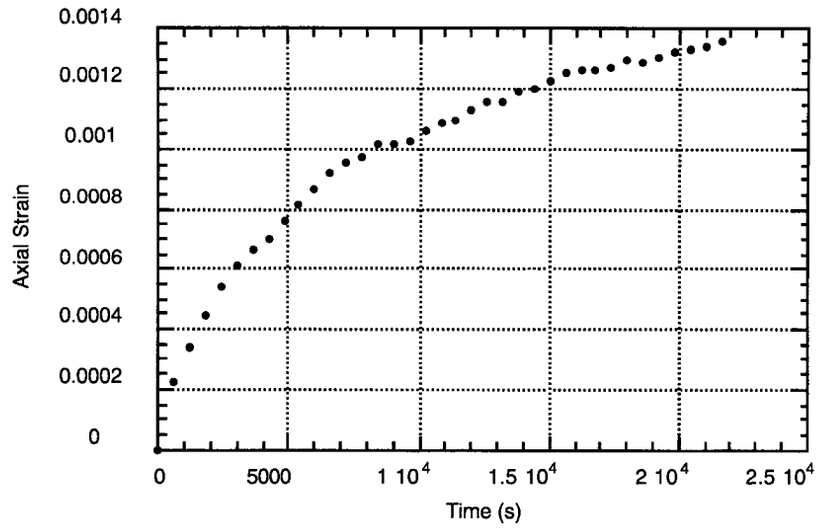

Figure 3.10: Creep in the Ottawa sand with 10% Montmorillonite clay sample under hydrostatic loading. The pressure was 30 MPa.

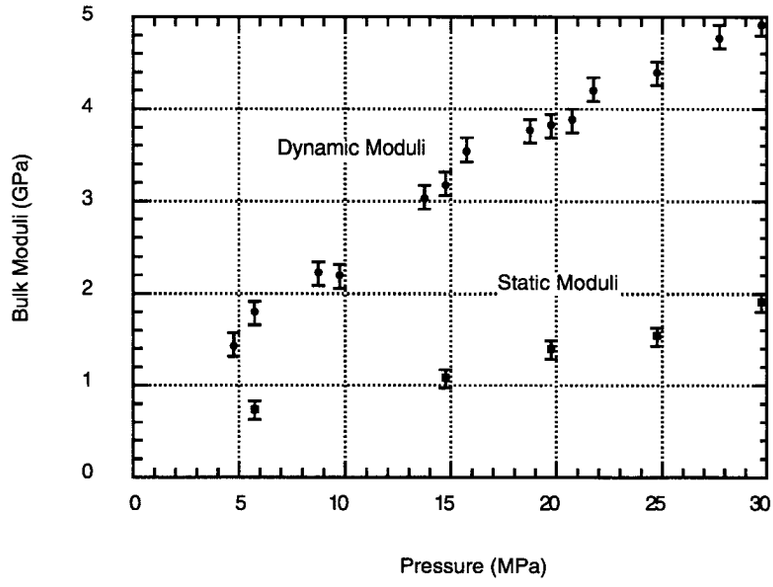

Figure 3.11: The static and dynamic moduli of Ottawa sand with 10% Montmorillonite clay measured under hydrostatic conditions.

The Ottawa sand and Montmorillonite clay mixture experiments were performed to

investigate the mechanism of anelasticity. The mean grain size of the Ottawa sand was 300 μm, which is similar to that of the turbidite samples. The clay was pure Montmorillonite prewetted with water and dried for a day at room conditions before mixing. Figure 12 summarizes the results and the turbidite creep data. Dry clay did not produce any anelastic effects; moreover, the amount of creep increased with clay content. Small amounts of clay in the natural samples could give rise to a similar mechanical behavior, as is suggested by the creep that occurred in the 10% Montmorillonite clay and Ottawa sand mixture. The data from the Ottawa samples seems to favor this mechanism as an explanation for both the creeping behavior and the dispersion.

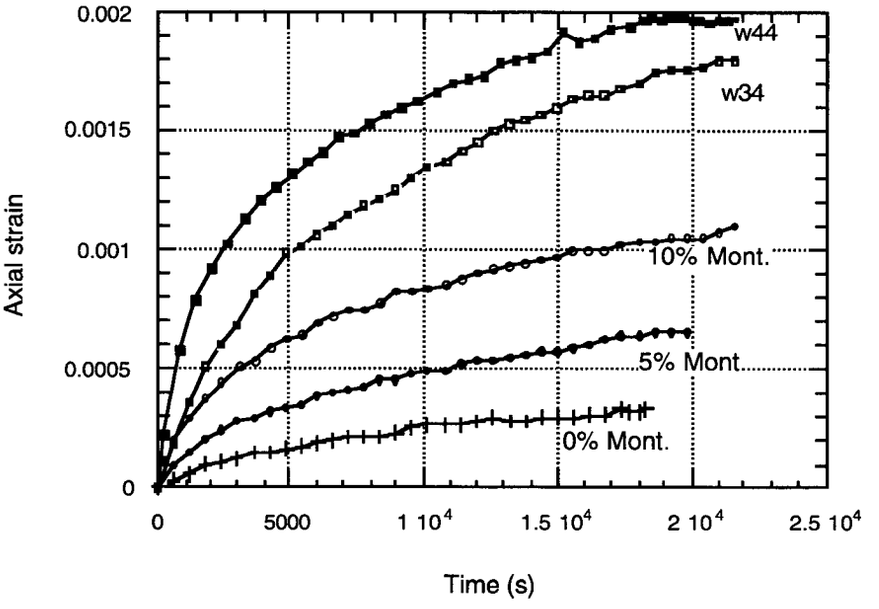

Figure 3.12: A summary of creep curves at 30 MPa for natural Wilmington (w34, w44) samples and unsaturated Ottawa sand + Montmorillonite samples.

3.3.3 Lentic sands

Hydrostatic loading of the Lentic sand from the Gulf of Mexico demonstrates that this fine-grained turbidite from the South Eugene Island field also shows significant amounts of plasticity and creep (Figure 13). The acquisition system failed at 30 MPa and did not record the entire unloading leg. The data shows a large difference between the loading and unloading slope, thus indicating plastic deformation similar to that observed in the natural samples from the Wilmington Field. This is not unreasonable, since both samples are marine turbidites consisting of quartz and feldspar grains with intergranular clay.

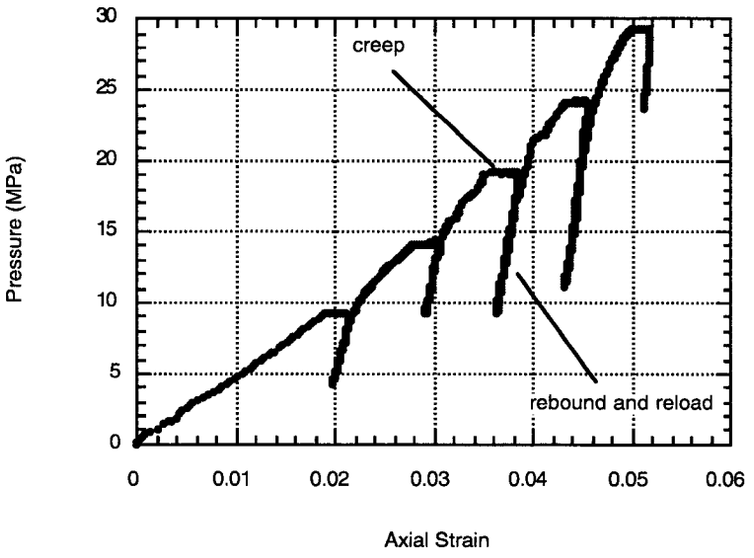

Figure 3.13: The stress-strain response of the Lentic sand under hydrostatic conditions. This was a saturated sample compressed under drained conditions.

The total amount of creep strain (Figure 14) and the creep strain rate were similar to the those of the clay-rich Ottawa sands and the Wilmington samples. The same decreasing exponential behavior with a creep time constant on the order of 5 hours characterized the mechanical properties of the natural samples. The Lentic sand sample was saturated but compacted under drained conditions. The high permeability of this fine-grained sand

provided sufficient drainage for the pore fluid to be fully relaxed.

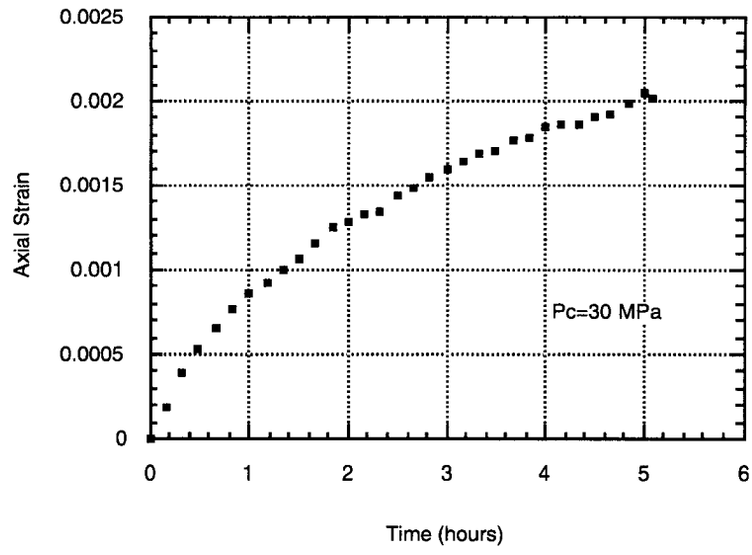

Figure 3.14: Creep at 30 MPa in the Lentic sand test.

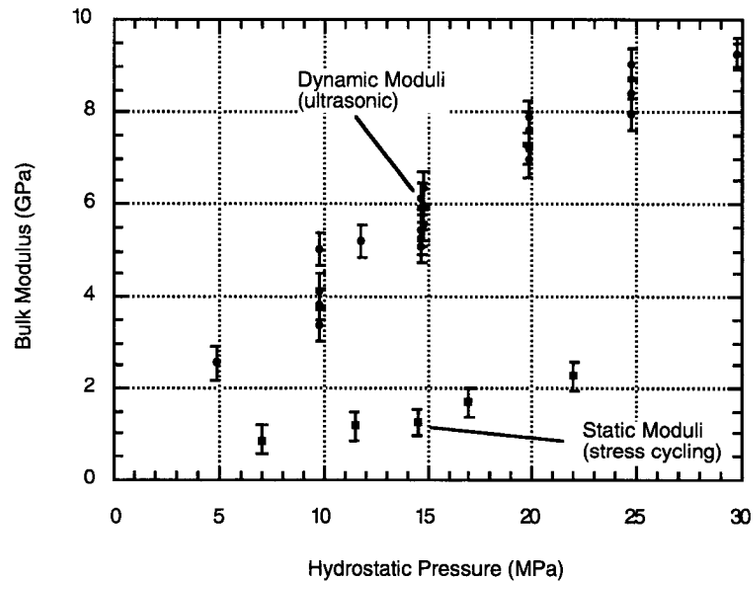

Figure 3.15: Dispersion between the static and dynamic moduli of the Lentic sand measured during hydrostatic loading.

As in the other samples, comparisons of static and dynamic moduli showed dispersion

(Figure 15). Although these values were collected at different strain magnitudes, much of the plastic and nonlinear elastic effect was removed from the modulus by using the static unloading modulus. Unfortunately, these results alone do not confirm that the mechanism of dispersion is frequency dependent moduli or strain-amplitude dependent moduli. It is clear, however, that the Lentic sand is very anelastic and demonstrates time-dependent deformation under loading.

3.4 Modeling

The model chosen to describe the sands had to describe the creep and difference between static and dynamic moduli observed in the turbidites. Two properties to be considered closely were the factor of two difference in each sample between the static and dynamic moduli, and the total amount of creep strain. These two properties are obviously not predicted from linear elastic theory. Many mechanical models have been developed to describe creep and viscoelasticity (e.g., Bourbie, 1987 and Tschoegl, 1989). These consist of idealized mechanical components to represent linear viscosity and elasticity.

We chose the standard linear solid model consisting of two springs and a dashpot. Fitting the model to the data requires determination of the two spring constants and the viscosity of the dashpot (Figure 16 inset). Thus, although the model is simple, it fully exploits the information collected in the experiments by requiring high and low frequency moduli and a relaxation time.

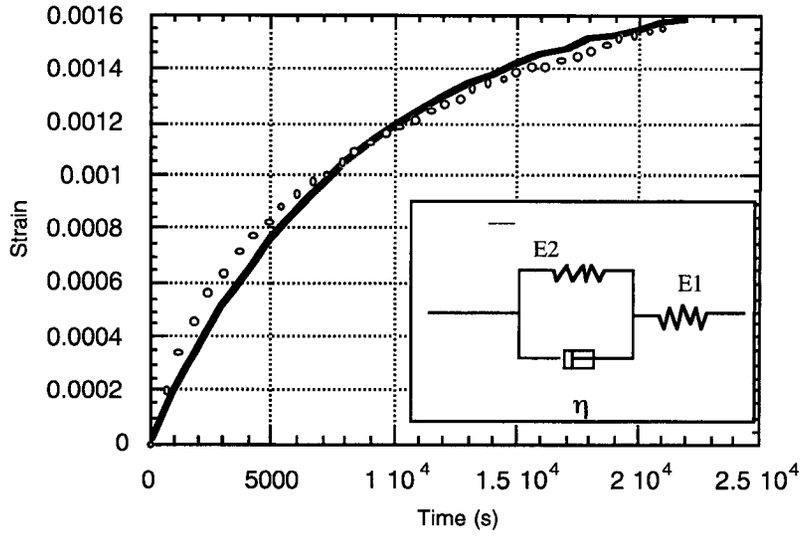

Figure 3.16: Creep data (w34-dry) at 30 MPa fit to a standard linear solid (solid line).

This model, like all viscoelastic models, will have a stiff response for high frequency strains and a compliant response for low frequency strains, depending on the relative magnitudes of the elastic and viscous contributions to the modulus. Given the deformation response to a step force, the values of viscosity and elasticity can be extracted from the creep time constants. The standard linear solid can be expressed mathematically as

$$\eta\dot{\sigma}_{11} + (\mathbf{E}_1 + \mathbf{E}_2)\sigma_{11} = \mathbf{E}_2(\eta\dot{\varepsilon}_{11} + \mathbf{E}_1\varepsilon_{11}) \qquad \text{Eqn. 3.1}$$

where η is the dashpot viscosity, E_1 is the outer spring, E_2 is the inner spring, ε_{11} is the strain and σ_{11} is the stress as defined in Figure 16 (inset).

Figure 16 shows the creep data collected on the dry sample (w34) at the 30 MPa pause in loading. The fit was achieved by estimating the model elasticities from the ultrasonic

and low frequency moduli measured in the lab. The values E_1 and E_2 can be calculated from the limiting cases when frequency approaches 0 and infinity (equations 3.2 and 3.3).

$$\mathbf{E_{low}} = \frac{\mathbf{E_1 E_2}}{\mathbf{E_1 + E_2}} \qquad \text{Eqn. 3.2}$$

$$\mathbf{E_{high}} = \mathbf{E_1} \qquad \text{Eqn. 3.3}$$

The creep response of the model was fitted to the data collected at 30 MPa by adjusting the viscosity of the dashpot. This simple model slightly under-predicts the initial deformation rate and slightly over-predicts the final deformation rate, since the real rock sample will stiffen with increasing strain.

The frequency dependent modulus for the standard linear solid (Bourbie, 1987) can be written as

$$\mathbf{E} = \frac{\mathbf{E_1(E_2 + i\omega\eta)}}{\mathbf{E_1 + E_2 + i\omega\eta}} \qquad \text{Eqn. 3.4}$$

Figure 17 shows the modulus dispersion curve calculated from the dry sample model parameters.

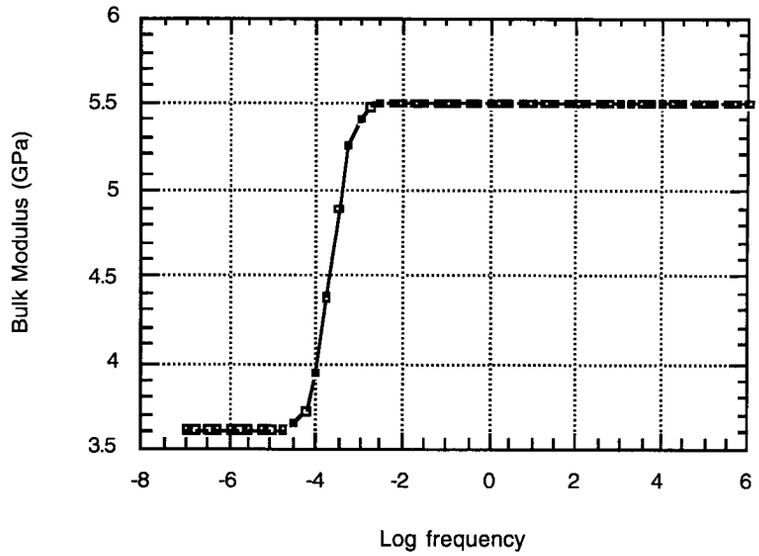

Figure 3.17: Bulk modulus vs. frequency using a standard linear solid with parameters determined from the creep fit at 30 MPa. The high and low frequency limits match the laboratory data at similar pressure.

A transition frequency between the low-frequency, relatively compliant behavior and the stiffer behavior at high frequencies is predicted to occur at approximately $2x10^{-4}$ Hz, demonstrating that anelasticity of the solid frame can result in modulus dispersion. This corresponds to a time constant of $5x10^{3}$ seconds (slightly less than 2 hours).

3.5 Discussion

Rock viscoelasticity appears to be a property of the dry matrix. The simultaneous observation of dispersion and creep in both saturated and dry samples suggests that dry frame viscoelasticity is a reasonable explanation for the dispersion observed in the Upper Terminal Zone turbidites. Using a standard linear solid viscoelastic model to describe the sample behavior is consistent with the creep behavior observed under hydrostatic loading. Observations of natural and laboratory-made unconsolidated samples suggest that the presence of intergranular clay plays an important role in the viscoelastic mechanism. The

model gives a prediction of the frequency dependence and improves understanding of how to extract mechanical properties from field data.

The logic behind modeling the material as a standard linear solid is as follows: (I) the material creeps with a decaying exponential response of the form $(1\text{-}e^{at})$, and (II) the material shows frequency dispersion. Although the gross behavior of the rock sample is consistent with the behavior of the model, there are only three measurements to define the model parameters, and it is clear that this simple mechanical model may not be the best description of unconsolidated sand. The advantage of the model is that it uses the laboratory data fully without requiring the fabrication of additional parameters not based on direct measurements.

The resulting model provides insight into the rheological properties of unconsolidated reservoir sands. The predicted transition frequency of $2x10^{-4}$ Hz is consistent with the presence of a very high viscosity component in the rock matrix that causes the material creep and dispersion. Dispersion models using the inertial effects of fluid saturation in cemented sands show much higher transition frequencies in the 1 kHz range (Biot, 1956; Mavko and Jizba, 1991; Dvorkin et al, 1994).

For the viscosity observed in them to play a significant role in the mechanical behavior of the rock, these samples must be compliant. Their very low frame modulus amplifies the effect of the viscous component. In contrast to our results, indurated samples show little modulus dispersion even in the presence of a similar amount of frame viscosity (Winkler and Murphy, 1982; Tutuncu et al, 1995).

Creep is unusual in a dry sand, since it is traditionally understood to originate from dewatering (Terzaghi, 1936; El Rafai and Hsu, 1978; Yamamuro and Lade, 1996). There

are several hypotheses that could explain dry sand creep: microcracking could be leading to cataclastic flow of the grains; strain amplitude differences between the high pressure loading of the sample and the ultrasonic measurement could give rise to different moduli because of material nonlinearity (even in a purely elastic material); or clay and mica between the grains could be affecting the overall modulus measurement for large deformation.

Microcrack propagation, grain crushing, and cataclastic flow are observed in higher pressure experiments (Zhang et al, 1990). Time-dependent microcrack propagation has been studied in fault mechanics to explain aseismic creep of faults (Costin, 1987). However, these processes usually occur at much higher pressures than those used in the lab. Furthermore, all of these processes are more likely to occur as a consequence of plastic deformation during a loading phase. Unloading moduli were measured to minimize the effects of plasticity in low-frequency measurements. Thus, a plastic process such as cataclasis does not seem consistent with observations of dispersion here.

Weak intergranular materials under high pressures could give rise to time-dependent deformation. Analysis of thin sections of the samples reveals that much of the 20% mica fraction was placed between stronger grains of quartz, feldspar, and lithic particles. The mica was deformed during the natural consolidation process along the quartz boundaries and could dramatically affect the mechanical properties of the rock. Given the amount of mechanical and microstructural evidence, this appears to be the most likely mechanism.

The prediction of a transition frequency of 3×10^{-4} Hz in this model is significant if one is trying to determine low-frequency rock properties by using seismic, sonic, or ultrasonic techniques. The predicted response dictates that these measurements are interchangeable

(in the absence of fluid saturation). However, if one needs to determine the low-frequency moduli that govern perturbations associated with oil production, a correction must be made to accommodate the dry frame viscoelastic properties of the rock unit. Thus, attention must be given to the presence of small amounts of clay and mica, since they can strongly effect the low-frequency behavior of the rock.

The modeling of the deformation of the sample with a standard linear solid could be improved upon to obtain a more accurate representation of the material at all frequencies. The rock is really viscoelastoplastic rather than viscoelastic. The model slightly under-predicts the initial strain and over-predicts the final strain. To fit the data better, strain-dependent spring constants could be used. The model is a first approximation of the mechanical behavior and can benefit from further refinements such as including strain-dependent moduli and plasticity. However, it is suitable for demonstrating the presence and effects of dry frame viscoelasticity in the samples here.

3.6 Conclusion

The presence of dry frame viscoelasticity in our samples appears to be related to the weak intergranular materials as suggested by the Ottawa sand and Montmorillonite clay mixtures. The mechanical model, along with the evidence from clay mixture tests and thin sections, suggests that increasing clay and mica content results in increasing amounts of viscoelasticity.

The creep response of the Upper Terminal Zone turbidite provides information about the mechanical behavior of the sample at high and low frequencies. The experimental results suggest that even small amounts of mica and clay between the elastic quartz grains

can cause viscoelastic dispersion in dry unconsolidated reservoir rock. By modeling the experimental results with a simple viscoelastic model to represent the roles of the intergranular clays and micas as well as the stiff minerals, we predicted the frequency-dependent modulus of the rock. The combination of experimental data, thin section data, and modeling results favors the soft intergranular mica and clay hypothesis as an explanation for the highly dispersive behavior.

Viscoelasticity will result in dispersive moduli. Although ultrasonic, sonic, and seismic measurement techniques will provide similar estimates of formation compressibility, a frequency-dependent correction will be necessary to determine moduli for low-frequency perturbations such as tectonic loading or long-term production activities in hydrocarbon reservoirs. Understanding the viscoelastic mechanisms will permit the extraction of these low-frequency moduli, thus establishing the connection between static and dynamic moduli.

3.7 References

Biot, M.A., 1956, Theory of propagation of elastic waves in a fluid saturated porous solid II. Higher-frequency range, J. Acoust. Soc. Amer., **28**, 168-178.

Bourbie, T., Coussy, O. and Zinser, B., 1987, Acoustics of porous media, Gulf Publishing Company.

Costin, L.S., 1987, Time-dependent deformation and failure", in "Fracture Mechanics of Rock, edited by B.K. Atkinson, Academic Press.

Dudley, J., Myers, M., Shew, R., Arasteh, M., 1994, Measuring compaction and compressibilities in unconsolidated reservior materials via time-scaling creep, Eurock 94, meeting proceedings, Balkema, Rotterdam, 45-54.

Dvorkin, J., Nolen-Heksema, R., and Nur, A., 1994, The squrit-flow mechanism: macroscopic description, Geophysics, **59**, 428-438.

Dvorkin, J. and Nur, A., 1993, Dynamic poroelasticity: A unified model with the squirt and the Biot mechanism, Geophysics, **58**, 524-533.

El Refai, W.T.H, and Hsu, J.R.,1978, Creep deformation of clays, Proc. ASCE J.Soiltech. Engng. Div., **104**, GT, 61-76.

Lo, K.Y., and Lee, Y.N. 1990, Time-dependent behavior of Queenstown shale, Can.Geotech, **27**, 461-471.

Locat, J. , 1994, On the development of microsturcture in collapsible soils, Proceedings of the Nato Advanced Research Workshop on Genesis and Properties of Collapsible Soils, Loughborough, U.K.,11-14 Apr, 1994.

Martin, R., 1972, Time-Dependent Crack Growth in Quartz and Its Application to the Creep of Rocks, J. Geophysical Research, **77**, 1406-1419.

Mavko, G. and Jizba, D., 1991, Estimating grain-scale fluid effects on velocity disperion in rocks, Geophysics, **56**, 1940-1949.

Mavko, G., and Nur, A., 1979, Wave attenuation in partially saturated rocks, Geophysics, 44, 161-178.

Murphy, W. F., III, Winkler, K.W., 1983. Acoustic relaxation in sedimentary rocks: dependence on grain contacts and fluid saturation, Geophysics, **51**: 3, 757-766.

Ostermeier, R.M., 1995, Deepwater Gulf of Mexico turbidites-Compaction Effects on Porosity and Permeability, SPE Formation Evaluation, June, pp.79-85.

Robertson, E.C., 1962, Experimental consolidation of calcium carbonate sediment, USGS Professional Paper; P 0350, 82-83.

Scholz, C.H., 1968, Mechanism for Creep in Brittle Rock, Journal of Geophysical Research, **73**, 3295-3302.

Tchoegl, N.W., 1989, The Phenomenological Theory of Linear Viscoelastic Behavior, Springer - Verlag, 1989, 35-156.

Tutuncu A.N., Podio A.L., Sharma M.M, Nonlinear Viscoelastic Behavior of Sedimentary Rocks: I. Effect of Frequency, submitted to Geophysics, February 1995

Terzaghi, K., 1936. The stability of slopes of natural clay, Proc. 1st Int. Conf. Soil Mech. Found.Engng., Cambridge, Mass., **1**, 161-165.

Winkler, K.W., 1983, Frequency dependent ultrasonic velocities of high porosity sandstones, Journal of Geophysical Research, **88**, 9493-9499.

Wood, D.M., 1990, Soil behavior and critical state soil mechanics, Cambridge University Press.

Yamamuro, J.A., and Lade, P.V., 1996, Drained Sand Behavior in Axisymmetric Tests at High Pressures, J. Geotech. Engr., Feb., p.109-119.

Zhang, J., Wong, T.F., Davis, D.M., 1990, High pressure embrittlement and shear- enhanced compaction of Berea Sandstone; acoustic emission measurement and microstructural observation, Rock mechanics; contributions and challenges; proceedings of the 31st U.S. symposium, **31**, p. 653-660.

CHAPTER 4

DOUBLE DISPERSION IN DRY UNCONSOLIDATED SANDS

Abstract

A dispersion relationship characterized by two transition frequencies was developed from measurements and modeling of unconsolidated turbidite sands and synthetic samples of Ottawa sand. Creep following loading indicated the presence of viscoelasticity from which rock viscosity was calculated. Using laboratory hydrostatic pressure cycling data (while monitoring ultrasonic travel times) for dry samples, we modeled the material as a standard linear solid; this yielded a relationship between frequency and bulk modulus for the dry frame. Modeling the role of fluids in the matrix using squirt flow yields higher transition frequency in the bulk modulus than that predicted by the dry ultrasonic model. The predicted values at intermediate seismic frequencies correspond well to the laboratory data, which was collected using loading rates between $1x10^{-5}$ Hz and $1x10^{-2.5}$ Hz. Results obtained by combining the saturation model for high frequency and the viscoelastic model for low frequency suggest that unconsolidated samples containing small amounts of clay have bulk moduli that increase in two separate steps as frequency increases. We call this phenomenon "double dispersion," in reference to the three moduli and two transition frequencies that are observed (rather than the two moduli and one critical frequency predicted by fluid substitution models).

4.1 Introduction

Determining in situ mechanical properties from sonic logs and seismics is especially

challenging in unconsolidated sedimentary rocks. Such rocks are prone to moduli dispersion, which can be induced by either rock viscoelasticity or poroelasticity (Chapter 3, Tutuncu, 1995; Winkler, 1982); these are two important mechanisms that govern the time-dependent deformation of unconsolidated rocks. In situations where weak unconsolidated reservoir rocks are saturated with fluids, an integrated model involving both mechanisms can be used to model time-dependent deformation more accurately than by poroelastic modeling alone. This is especially relevant at frequencies below 1 Hz. These low-frequency properties determine the response of a reservoir not only to gradual drawdown but also to changes in the near wellbore field associated with drilling and production in unconsolidated rock units.

Our study of dry viscoelasticity (Chapter 3) predicts a low transition frequency associated with matrix viscoelasticity. This model describes the viscoelastic nature of a dry sample, which does not take poroelasticity into consideration. At frequencies above 500 kHz, dispersion associated with the inertial effects of fluids in the pore space can stiffen a poroclastic rock (Biot, 1956; Brown and Korringa, 1975; Gassmann, 1951; Mavko and Nur, 1979). By combining our low-frequency viscoelastic results (Chapter 3) to represent the low-frequency behavior and a squirt model (Dvorkin et al, 1993, 1994, 1995; Mavko and Jizba, 1991) to represent the ultrasonic behavior, the wideband frequency-dependent modulus of an unconsolidated rock can be calculated. We call the combination of high- and low-frequency variations of elastic moduli parameters "double dispersion," since two distinct transition frequencies arise from two different mechanical phenomena. Thus, the resulting dispersion curve consists of three separate moduli regimes associated with three types of measurements: dry low frequency, dry high frequency, and saturated high

frequency.

4.2 Experimental procedure

4.2.1 Sample description

The samples consisted of natural and synthetic unconsolidated sediments. The turbidite sample is described extensively in Chapter 3. The synthetic samples were tested to investigate the mechanical properties of unconsolidated sediments containing different amounts of clay.

The natural samples were taken from turbidite cores from well UP941b in the Wilmington field at Long Beach, California, from a depth of 3233 feet. The sample (w34) was a fine-grained turbidite sand from the Upper Terminal zone. After plunge-cutting at room temperature with steel tubing the samples were extruded into soft polyolefin jacketing. The extrusion and jacketing procedure insures that the grain-packing remains intact. The jacketed specimen was 1 inch in diameter and 2 inches long. Before testing, residual heavy oil was removed from the samples by flushing, first with mineral spirits and then with air to dry the pore space. The samples were then wired to a transducer stack and placed in a pressure vessel for testing under room-dry conditions.

The synthetic samples consisted of Ottawa sand with varying amounts of Montmorillonite clay. After mixing, the plugs were wetted slightly with distilled water and allowed to dry under room conditions for two days. The samples were then jacketed and circulated with room-temperature air to allow additional drying. Initial uniaxial compression (50psi) precompacted the samples to increase their strength slightly. Without precompaction, the sand grains exhibited a fluid-like behavior at initial loading which

disrupted strain measurements. Table 1 summarizes the samples and their properties.

TABLE 1. Sample Properties

Sample	Sample Type	Mean Grain Sz μm	Initial Porosity	Clay Content %Volume	Pore Fluids
UTZ-w34	turbidite	300	34	10	none
o6	Ottawa sand	350	25	5	none
o7	Ottawa sand	350	26	10	none
o9	Ottawa sand	350	30	0	none
o13	Ottawa sand	350	31	10	none
o14	Ottawa sand	350	29	0	oil 756A
o15	Ottawa sand	350	32	10	oil 756A

Table 1: Initial rock properties before testing.

4.2.2 Loading procedures

Various tests were performed after the samples were placed in the pressure vessel, depending on the kind of information needed from each sample. Table 2 summarizes the content of each test. As described in Chapter 3, a comprehensive series of measurements was made at different confining pressures on these unconsolidated samples. Reported here is a subset of the measurements, in which ultrasonic pulse transmission and strain measurements were performed at a nominal confining pressure of 30 MPa. Creep strain was recorded after loading ramps were applied, keeping the confining pressure constant. For more details on the various loading procedures, see Chapter 3.

TABLE 2. The Measurements

Sample	Ultrasonic Pulse Trans	Pressure cycling & strain	Creep tests	Multiple Stress Rates	Saturation
UTZ-w34	yes	yes	yes	no	none
o6	yes	yes	yes	no	none

TABLE 2. The Measurements

Sample	Ultrasonic Pulse Trans	Pressure cycling & strain	Creep tests	Multiple Stress Rates	Saturation
o7	yes	yes	yes	no	none
o9	yes	yes	yes	no	none
o13	no	yes	yes	no	none
o14	yes	no	yes	no	yes
o15	yes	no	yes	no	yes

Table 2: Summary of the types of measurements performed in the pressure vessel

Saturated samples o14 and o15 were subjected to ultrasonic tests on synthetic samples at 30 MPa of confining pressure. A constant back pressure of 2 MPa maintained saturation. The saturant was Royco 756A oil.

Variable rate stress cycling was applied to one Ottawa sand sample (o13) mixed with 10% Montmorillonite at an initial pressure of 30 MPa to investigate strain rate dependence in the bulk modulus. These moduli at intermediate frequencies ($1x10^{-4}$ Hz < f < $1x10^{-2.5}$ Hz) were determined by using loading and unloading ramps 10 minutes to 2 hours in duration (see Table 2, test o13). The sample was loaded to 30 MPa and stress-cycled between 25 MPa and 30 MPa repeatedly at the above frequencies.

4.3 Experimental data

An increase of bulk modulus with frequency is seen in all of the experimental data. A collection of bulk modulus measurements for the tests listed in Table 2 is plotted as a function of frequency in Figure 1. This distribution begins with low-frequency loading and unloading of the samples, which gives the static bulk modulus. Simultaneous ultrasonic pulse transmission tests on these samples demonstrate the frequency-dependent moduli in

individual samples.

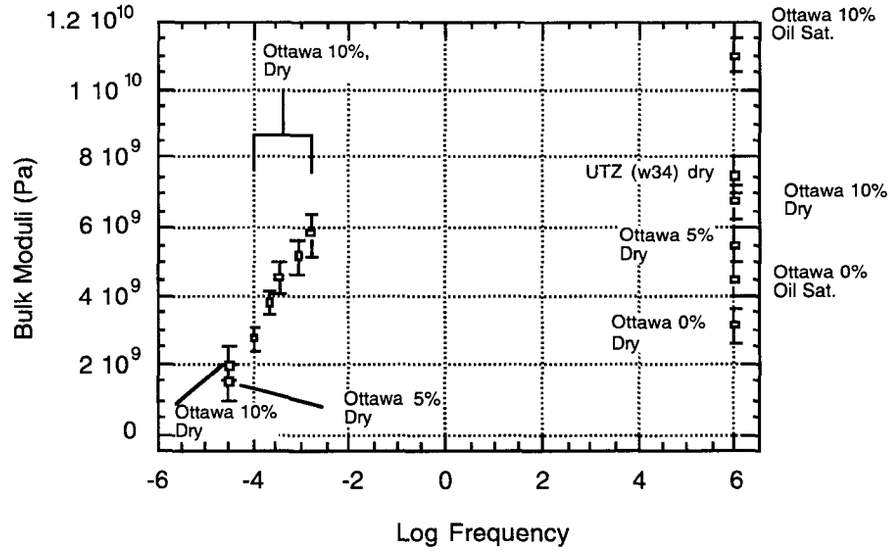

Figure 4.1: Raw moduli data collected using ultrasonic pulse transmission and pressure cycling. The percentages refer to the Montmorillonite content. Dry/Sat refers to a dry or saturated test

Ultrasonic saturated moduli in tests o14 and o15 on Ottawa sands demonstrate the stiffening effect of pore fluids at high frequency. Compared to their unsaturated counterparts, o9 (Ottawa, 0% Mont.) and o7 (Ottawa, 10% Mont.), they are significantly stiffer. These results are consistent with Marion et al (1992), where small amounts of clay were found to stiffen an unconsolidated rock, perhaps because of increasing grain adhesion.

For each type of sample with its respective clay content, there appear to be three separate moduli: dry low frequency, dry high frequency, and saturated high frequency. For example, a clean Ottawa sand will have a dry low-frequency bulk modulus of 1.5 GPa, a dry high-frequency modulus of 3.1 GPa, and an oil saturated modulus of 4.5 GPa. These three different measurements of what is seemingly one parameter (the bulk modulus) suggest that the modulus dispersion involves the mechanical properties of the dry frame as

well as those of the pore fluid.

Test o13, shown as the cluster of data points from 10^{-4} to $10^{-2.5}$ Hz (Figure 1), was determined by fitting the unloading stress-strain loops of varying loading rates with a straight line. Fitting these loops minimized effects of plasticity, since only unloading or rebound moduli were considered. This Ottawa sand/Montmorillonite clay mixture shows a significant stiffening with increasing frequency. The frequency range was limited by the ability of the hydraulic apparatus to load the sample at high loading rates.

The samples all show some time-dependent deformation, which is manifested as creep discussed in Chapter 3. This behavior is consistent with studies of Gulf of Mexico turbidites (Dudley, 1994; Ostermier, 1995). Data was recorded for approximately 5 hours. In some cases the creep still had not totally equilibrated, especially in samples containing large clay fractions. There is a relationship between clay fraction and the overall viscoelasticity of the system. Increasing clay content generally resulted in larger amounts of creep.

4.4 Analysis

Because the samples creep under constant loads applied at low frequency, we have used a viscoelastic model to describe the data. By fitting the creep of the samples to a viscoelastic model, we determined the frequency-dependent behavior of the dry rock sample. To describe the stiffening associated with fluid saturation, we used the squirt flow (Dvorkin et al, 1993, 1994, 1995; Mavko and Jizba, 1991) to calculate the expected stiffening of the dry frame modulus with the addition of pore fluid as a function of frequency. This combination results in a frequency-dependent modulus with three regimes.

The low-frequency creep and dispersive response of the samples is described using a standard linear solid model. This model is described in Chapter 3 as well as in many other texts (Tchoegel, 1989; Bourbie, 1987).

In summary, the two spring moduli are constrained by the high- and low-frequency limits of the K modulus, which are determined from the ultrasonic and pressure cycling measurements. The creep data is then fitted to the creep response of the standard linear solid containing these moduli, thus constraining the system viscosity (Figure 2).

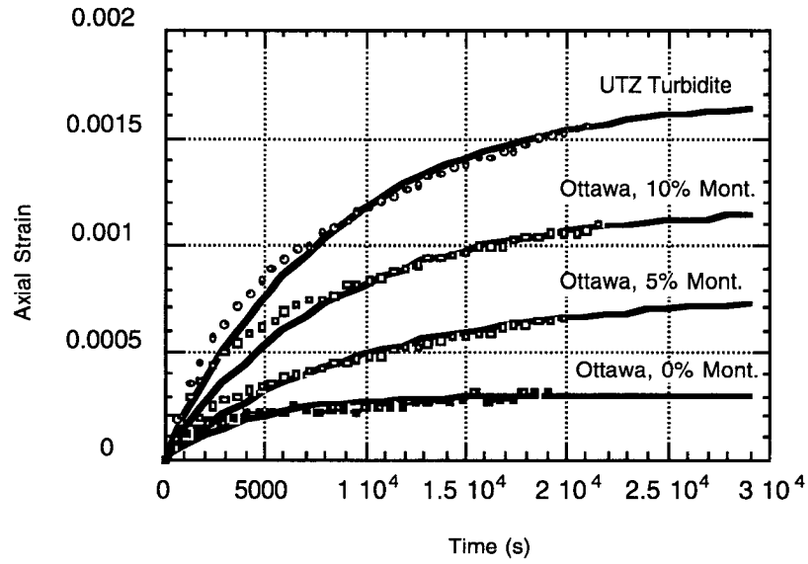

Figure 4.2: Standard linear solid creep responses fitted to the creep data. The close fits suggest that the unconsolidated samples have a narrow distribution of relaxation times that can be approximated by a single viscoelastic element.

The relaxation time of this creep response is directly related to the dispersion characteristics of the material. The model parameters are derived from the samples as shown in Table 3.

TABLE 3. The Standard Linear Solid Input Parameters

Sample	K ultrasonic (GPa)	K unloading (GPa)	E_2 (GPa)	E_1 (GPa)	η (Pa.s)
UTZ-w34	7.50	4.5	7.50	11.25	9.5e13
o6	5.50	1.5	5.50	2.06	2.0e13
o7	7.00	2.0	7.00	2.80	2.4e13
o9	3.00	1.5	3.00	3.00	1.6e13

Table 3: The component elasticity and viscosity for four experiments.

Using equation 3.4 in Chapter 3, we derived the frequency-dependent behavior for dry sands using the standard linear solid model with the parameters listed in Table 3. These are shown in Figures 5, 6, and 7 for frequencies below 100 Hz. The model predicts a transition frequency of about .0003 Hz. In Figure 5, the data collected under multiple loading rates appears to fit the viscoelastic model quite well, reflecting the appropriateness of a single-element model. The first step in the dispersion curve is caused by rock viscoelasticity, the second step by squirt flow using the Mavko-Jizba squirt relationships. A similar analysis was conducted for the natural turbidite sample (Figure 6); it shows a similar result with two transition frequencies. The mineral modulus Ko is taken as the quartz modulus of 80 GPa. The dry bulk modulus Kdry was taken to be Kunloading from Table 3. The high pressure bulk modulus Khp was extrapolated from the ultrasonic data at a pressure of 60 MPa to be approximately 8 GPa. The viscosity was taken to be 6 mPa.s which is the viscosity of Royco 756 A oil manufactured by Royal Lubricants, London, U.K., at room temperature. The calculated frequency response was not necessarily intended to predict the saturated high frequency value. It's purpose was to demonstrate the increase in stiffness associated with squirt flow under saturated conditions.

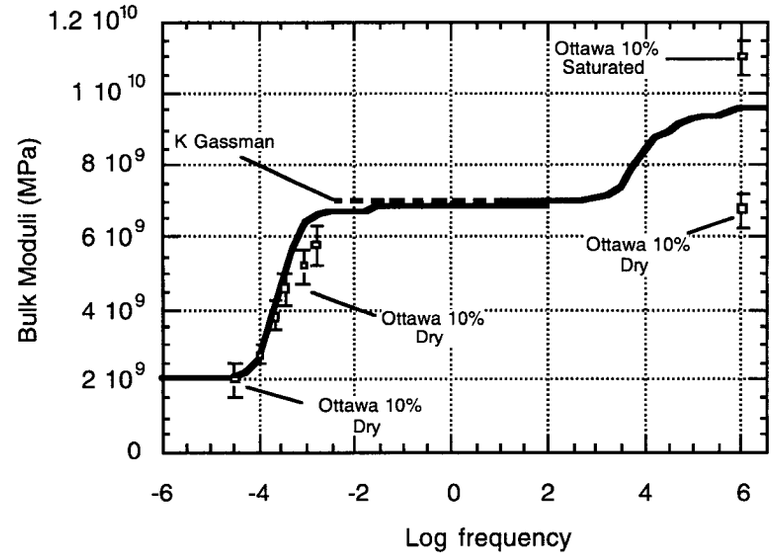

Figure 4.3: Double dispersion in Ottawa sand with 10% Montmorillonite clay. The raw data points are for both saturated and dry Ottawa sand samples. The intermediate points were collected by pressure cycling under loading rates of 5MPa/18,000s to 5MPa/600s.

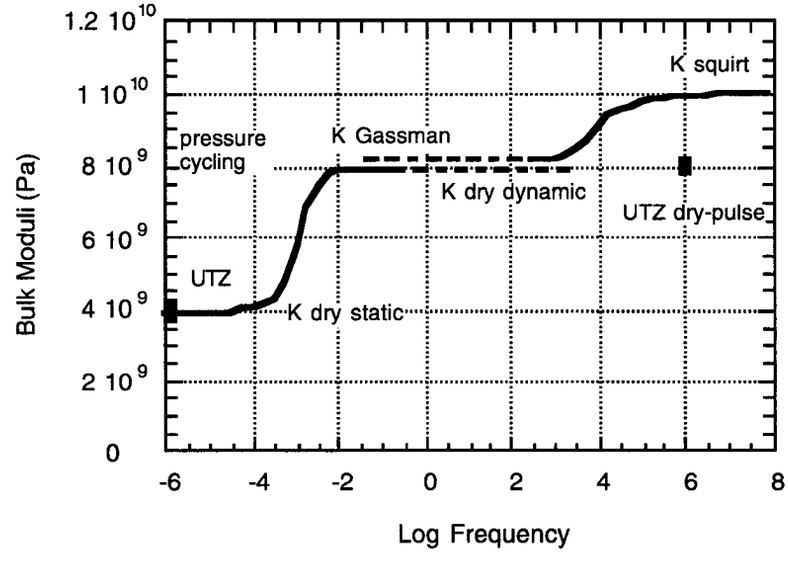

Figure 4.4: Double dispersion in a Wilmington tar sand (w34). Two data points for UTZ static and UTZ dry-ultrasonic pulse transmission are shown along with model.

Although the calculated modulus under-predicts the saturated bulk modulus data from tests o14 and o15 by about 10% (Figure 7), it clearly demonstrates that fluid saturation in the samples results in dispersion. For squirt, the low-frequency limit is the Gassman bulk modulus, which is saturated at low frequency. This nearly equals the dry bulk modulus, which explains the discontinuity between the standard linear solid curves and the squirt curves.

Figure 7 shows the dependence of increasing clay content on double dispersion. Besides increasing the bulk modulus at single frequencies, increasing clay content results in greater amounts of rock viscosity. Small amounts of clay can strongly alter the bulk modulus at frequencies between 10^{-2} and 10^{2} Hz. While an extrapolation of the low-frequency bulk modulus ($\sim 10^{-4}$ Hz) made from measurements taken at about 1 Hz would produce only a small error in clean sand, a significant error will occur when the same measurements are done with a sand containing 10% clay.

In summary, the material shows two types of dispersion as calculated by viscoelastic theory and squirt theory. These theories predict three different regimes of bulk moduli that explain the dispersion measured in the laboratory between high-frequency, low-frequency, and saturated measurements of bulk moduli; they also show the strong effect of clay content on rock modulus dispersion. The models establish a possible connection between the dispersive data and provide a link between various types of measurements using straightforward modeling of dry frame creep and squirt flow.

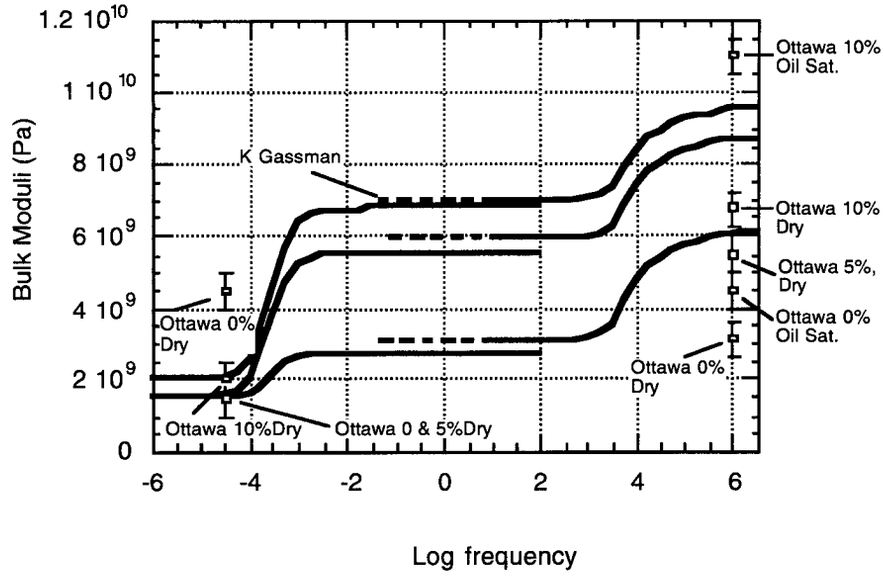

Figure 4.5: Dispersion curves derived from the standard linear solid and the Mavko-Jizba squirt relationships. The models suggest three possible frequency-dependent moduli. A critical frequency at approximately $10^{-3.5}$ Hz arises from dry matrix viscoelasticity. At about 10^{-4} Hz, another jump in moduli associated with fluid saturation occurs.

4.5 Discussion

The data and modeling presents compelling evidence for double dispersion in unconsolidated materials. According to our results, the dry dispersion is apparently related to the time-dependent deformation of the matrix. Moreover, poroelastic effects associated with saturation give rise to a secondary step on the dispersion curve.

Our analysis suggests that small amounts of clay minerals are required for double dispersion to occur. Tutuncu et al (1995) found that frequency dependence in the Young's modulus of cemented sandstone decreased in cleaner samples. This appears to happen in the bulk modulus of the unconsolidated samples studied in this text as well. Creep tests o6, o7, and o9 demonstrate the relationship between viscoelasticity and clay content. Although

the samples consisted of identical grains, the amount of creep they displayed was proportional to the amount of Montmorillonite clay added to each. While the turbidite sample had a relatively low clay content (~10%), its high mica content may have been responsible for its strong viscoelastic character. In the cleanest sample, o9, there is almost no double dispersion, suggesting that a straight transformation based on poroelastic theory could map ultrasonic data to seismic data and stress cycling measurements.

The close fit of the data collected using multiple loading rates with the standard linear solid model in Figure 5 suggests that the model appropriately describes the mechanical properties of the Ottawa sand and clay mixture. In theory, all viscoelastic materials can be fitted with an infinite chain of viscoelastic elements (Gross, 1947). With more elements, transition from stiff to compliant behavior will occur less abruptly with frequency. If a material has a narrow distribution of relaxation times, its mechanical behavior can be approximated using a single viscoelastic element, as we did. For test o7 - Ottawa sand with 10% Montmorillonite, this approach appears to be correct, since the fit to the creep data coincides with the fit to the frequency response of a single viscoelastic element. This result implies that the distribution of relaxation times for the unconsolidated materials is very narrow. Under-prediction of initial strain on the creep fits suggests that more than one element would be necessary to pick-fit the shorter period data, thereby possibly improving the fit in the frequency domain.

Double dispersion provides a frequency-dependent modulus for both saturated and dry rock. Dry rock should only show two frequency regimes: one under the critical relaxation period of the rock and one above. For saturated unconsolidated materials, three different moduli should be seen. For subsonic frequencies, the moduli of the dry and

saturated samples should be the same, as long as the pore fluid is relaxed in the matrix. For saturated rock, the additional ultrasonic transition frequency is7 associated with the inertial effects of the fluid under high-frequency perturbations.

4.6 Conclusions

When extrapolating low- or high-frequency moduli from high-frequency measurements on unconsolidated reservoir rock under saturated conditions, one must consider the effects of both fluid and viscoelastically induced dispersion. This study implies that small amounts of clay can be attributed to appreciable viscoelastic dispersion in unconsolidated reservoir rocks. Combining the two models produces a more realistic relationship between frequency and bulk modulus for unconsolidated reservoir rocks. The resulting estimates of low-frequency moduli can condition models that describe the state of the reservoir and changes associated with drawdown, subsidence, and deformation in the near wellbore field. Thus, when modeling the effects of low-frequency perturbations, a moduli8 determined from sonic logs or seismics may over-predict the in situ mechanical properties if double dispersion is not considered.

4.7 References

Biot, M.A., 1956, Theory of propagation of elastic waves in a fluid saturated porous solid. II. Higher- frequency range, J. Acoust. Soc. Amer., **28**, 168-178.

Bourbie, T., Coussy, O. and Zinser, B., 1987, Acoustics of porous media, Gulf Publishing Company.

Dudley, J., Myers, M., Shew, R., Arasteh, M., 1994, Measuring compaction and compressibilities in unconsolidated reservoir materials via time-scaling creep, Eurock 94, meeting proceedings, Balkema, Rotterdam, 45-54.

Dvorkin, J., Mavko, G., and Nur, A., 1995, Squirt flow in fully saturated rocks, Geophysics, **60**, 97-107.

Dvorkin, J., Nolen-Heksema, R., and Nur, A., 1994, The squrit-flow mechanism:macroscopic description, Geophysics, **59**, 428-438.

Dvorkin, J. and Nur, A., 1993, Dynamic poroelasticity: A unified model with the squirt and the Biot mechanism, Geophysics, **58**, 524-533.

Dvorkin, J., Mavko, G., and Nur, A., 1995, Squirt flow in fully saturated rocks, Geophysics, **60**, 97-107.

Gross, B., 1947, On creep and relaxation, Journal of Applied Physics., **18**, 212- 221.

Marion, D., Nur, A., Yin, H., Han, D., 1992, Compressional velocity and porosity in sand-clay mixtures, Geophysics, **57**, No. 4, 554-563

Mavko, G. and Jizba, D., 1991, Estimating grain-scale fluid effects on velocity disperion in rocks, Geophysics, **56**, 1940-1949.

Mavko, G., and Nur, A., 1979, Wave attenuation in partially saturated rocks, Geophysics, **44**, p.161-178.

Murphy, W. F., III, Winkler, K.W., 1983, Acoustic relaxation in sedimentary rocks; dependence on grain contacts and fluid saturation, Geophysics, **51**: 3, p. 757- 766.

Ostermeier, R.M., 1995, Deepwater Gulf of Mexico turbidites-Compaction Effects on Porosity and Permeability, SPE Formation Evaluation, June, 79-85.

Tchoegl, N.W., 1989, The Phenomenological Theory of Linear Viscoelastic Behavior, Springer - Verlag, 1989, 35-156.

Tutuncu A.N., Podio A.L., Sharma M.M, Nonlinear Viscoelastic Behavior of Sedimentary Rocks: I. Effect of Frequency", submitted to Geophysics, February 1995

Winkler, K.W., 1983, Frequency dependent ultrasonic velocities of high porosity sandstones, Journal of Geophysical Research, **88**, 9493-9499.

CHAPTER 5

TRIAXIAL COMPRESSION EXPERIMENTS ON UNCONSOLIDATED SAND SAMPLES

Abstract

Observations of triaxial creep and stress relaxation in unconsolidated reservoir sands imply that state of stress and strain can vary with time. Triaxial testing performed on 1-inch plugs of reservoir sands under both stress- and strain-controlled conditions shows transient stresses and strains. This effect may explain observations of very low differential stresses found in the Wilmington Field in California, the South Eugene Island Field in the Gulf of Mexico, and elsewhere. All tests were performed under dry (or drained) conditions to eliminate poroelastic effects. Previously we observed creep under hydrostatic stress conditions in these unconsolidated sands. The resulting strain vs. time curves could be fitted with a standard linear solid viscoelastic model that had a relaxation time of about 10 hours. The data demonstrates the capacity of the rock to dissipate stress through relaxation and creep. The reservoir material shows viscoelastic rheological behavior in both creep and relaxation tests, which appears to be related to the presence of intergranular clay. Measurements of the static Poisson's ratio under large strains yield values of ~.29.

5.1 Introduction

Time-dependent deformation of unconsolidated sediments is traditionally understood to arise from pore fluid expulsion in saturated earth materials (Terzaghi, 1941; Bishop, 1966). Although many accounts have been published relating the apparently viscous behavior of soils at shallow depth associated with dewatering, there have been few studies

of time-dependent deformation of poorly consolidated rocks under drained or dry conditions at the high pressures encountered in hydrocarbon reservoirs. We observed earlier that unconsolidated sands can creep during compressional testing at elevated pressures (Chang et al, 1997) and related this behavior to their frequency-dependent elastic moduli; high differential stresses, saturation, and high temperatures were not necessarily required. This study examines time-dependent stress and strain in viscoelastically deforming sediments under dry or drained conditions and demonstrates how creep effects can control the state of differential stress in unconsolidated reservoir rocks. As highly variable (and often very low) differential stress states are commonly seen in poorly consolidated clastic reservoirs (e.g., Finkbeiner and Zoback, 1998), these observations could be explained if poorly consolidated sands were characterized by a viscoelastic rheology.

There are numerous studies of strength, stiffness, and deformation of unconsolidated or weakly consolidated sands in the rock mechanics literature. These tests were performed at pressures more relevant to those encountered during hydrocarbon recovery (Karig, 1992; Ostermeier, 1993; Dudley et al, 1994; Chang et al, 1997). However, very few of these accounts report the existence of time-dependent stress and strain when dealing with the compressive testing of dry sediments. In some investigations (e.g. Karig, 1996), time-dependent deformation can be observed as flat plateaus on stress vs. strain curves, but it is rarely addressed directly. As in the soil mechanics literature, if time-dependent deformation is addressed, it is associated with pore fluid expulsion during consolidation. Such tests are performed under partially drained conditions arising from limited permeability, such as in the study by Lo and Lee (1990) that reported time-dependent

deformation in saturated shales. However, thixotropic or poroelastic phenomena associated with low permeability rocks are probably not relevant in the deformation of highly permeable dry sand.

Time-dependent deformation in poorly consolidated rock at high pressures under drained conditions was examined by Dudley et al (1994) and Ostermeier (1993). These investigations reported time-dependent deformation of unconsolidated reservoir rocks at pressures above 20 MPa in triaxial loading configurations. Both studies observed the creeping behavior of sand at low temperatures. Their samples were saturated yet drained, and had a high permeability that prevented the development of unrelaxed pore fluids during consolidation. These triaxial loading tests exhibited long-term creep strain that could be fitted with a power law creep model. These observations of time-dependent creep in Gulf of Mexico turbidites and river sands suggested that the rocks have a viscoelastic character. However, their boundary conditions were constant axial or hydrostatic load and zero pore pressure, which prevented the observation of stress relaxation or transient pore pressure, thus leaving the question of time-dependent stress unanswered.

Poisson's ratio describes how well the principal strains in a material are coupled. Spencer (1994) provided extensive experimental results showing that clean dry sands tested in the laboratory using ultrasonic techniques have Poisson's ratios between .15 and .20. Karig (1996) performed static experiments on silty clay rich sediments from the Nankai trench that gave values of approximately .20 to .25. These values implied changes in ε_{11} resulted in notable changes in ε_{22} suggesting that the two strains were mechanically coupled. For coupling to be observed between the principal strains, the material must be deformed past its virgin consolidation state. This cannot be measured by ultrasonic

techniques, which use smaller strain perturbations. Large strain perturbations would be a simple way to observe the degree of coupling between the principal strains. The static Poisson's ratio is as important as the ultrasonic information because it governs how unconsolidated reservoir rock behaves under large displacements and over long time periods.

Viscoelastic theory states that if a material creeps, it will relax under appropriate boundary conditions (Cole and Cole, 1941; Tchoegel, 1978). Creep is time-dependent deformation under constant stress while relaxation is stress decay under constant strain. Viscoelastic theory states that if a material creeps viscoelastically, the relaxation stress can be derived mathematically (See Appendix). This means that if a sample is viscoelastic, time-varying stresses should be seen under constant strain boundary conditions. For an illustration of the relationship between creep and relaxation, consider the creep strain in Figure 1. By fitting the data with a standard linear solid model (Figure 1 inset), we can obtain a creep function for the material. Using viscoelastic theory (e.g. Tchoegel, 1978 and Appendix), we can use the creep data to calculate the expected time-dependent stress as seen in Figure 2.

Viscoelastic creep (but not stress relaxation) under hydrostatic pressures in unconsolidated sands has already been documented by Chang et al (1997). This data set was collected under exclusively hydrostatic boundary conditions. It is implied from the mechanical behavior of the sediments that such time-dependent phenomena will occur under triaxial loads as well. The occurrence of triaxial creep and relaxation in unconsolidated sediments may suggest that unconsolidated sands may influence the in situ differential stress state significantly.

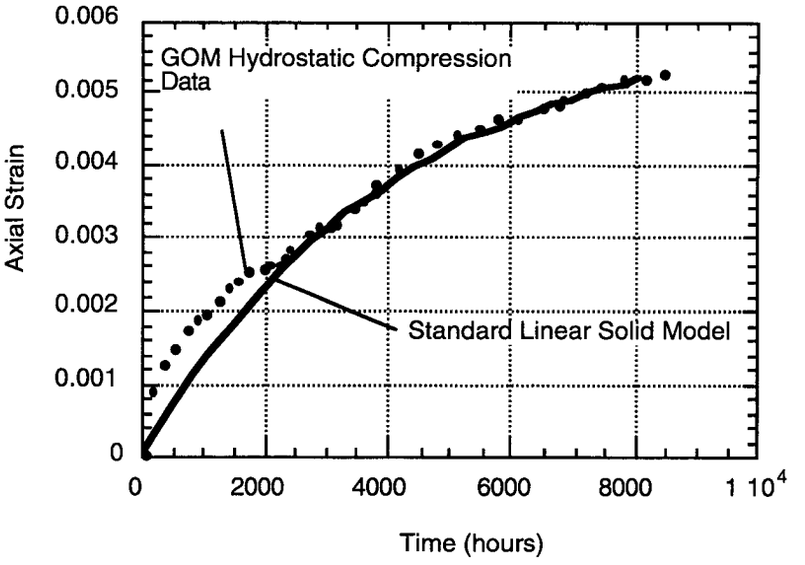

Figure 5.1: A fit to hydrostatic creep data from an unconsolidated sand. This is a Gulf of Mexico sample fitted with a standard linear solid model. The fitting parameters give parameters necessary to predict the theoretical stress relaxation response.

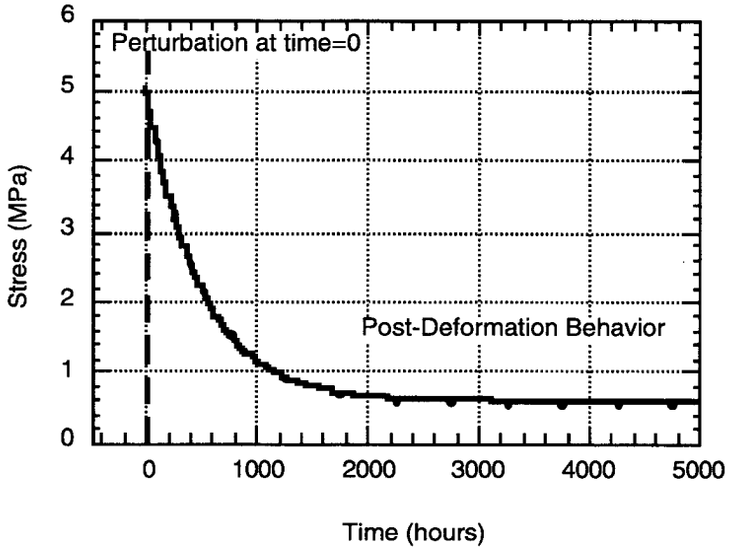

Figure 5.2: Predicted theoretical stress relaxation derived from the experiment shown in Figure 1 assuming viscoelasticity. Following a step increase in strain, the transient stress decays away with time.

5.2 Experimental procedures

The samples used in this study were all unconsolidated sand as described in Table 1. All samples were unconsolidated quartz sands with mean grain of 300 μm or less and porosities between 30 and 40%. The sands were clean, containing less than 10% clay.

Table 1: The samples and their properties

sample	porosity	mean grain size	clay content	grain morphology
Ottawa Sand	34%	500 μm	5-10% as added by volume	Rounded well sorted
Wilmington	35-39%	300 μm	<10%	Angular poorly sorted
Lentic	36%	100 μm	<5%	Angular well sorted

5.2.1 Loading procedures

Core samples of unconsolidated sediments were obtained from two hydrocarbon reservoirs. The Wilmington samples were obtained from the Wilmington field, Long Beach, California from a depth of approximately 3000 feet in wells UP941B and 169W. They were jacketed in PVC at the wellsite and refrigerated until testing to preserve the natural state of the matrix and fluids. The Lentic sample came from a refrigerated split core which was extracted at the South Eugene Island field in the Gulf of Mexico, from a depth of 7883 feet in well SEI-613/A12. Ottawa sand samples were prepared in the laboratory.

The samples were extracted from the whole cores by coring at room temperature with steel tubing and then by extruding the sand into soft polyolefin jacketing. The jacketed specimen was 1 inch in diameter and 2 inches long. For the samples to be tested "dry," residual heavy oil was removed from the samples by flushing, first with mineral spirits and

then with air to dry the pore space. The samples were then wired to a transducer stack and placed in a pressure vessel for testing under room-dry conditions at room temperature.

The Ottawa sand Montmorillonite clay samples were prepared by mixing Ottawa sand with 5% Montmorillonite clay by volume. The laboratory-grade clay was moistened then dried in circulating air for one day before testing. This procedure was motivated by the lack of viscous effects in the absence of premoistened clay. The residual water content was estimated to be below 5% by gravimetric analysis. Polyoelfin jacketing enclosed the mixtures while the samples were sitting between the loading endcaps.

We used a triaxial loading frame instrumented with axial strain and radial strain measurements. A PC-based data acquisition system continuously monitored stress, strain, temperature, and pore pressure over time. An internal load cell measured the differential load. Hydraulic servo-controllers allowed for precise stress ramps and stress holds. Feedback circuitry connected to the LVDT strain measurement system also allowed experiments to be conducted at constant stress boundary conditions. Temperature was maintained at room conditions.

(I) Creep testing

Constant load creep tests were performed by raising the axial load at 10 MPa/minute and then holding the load constant while maintaining a constant confining pressure. Maintaining a constant axial load resulted in axial creep. PC data acquisition monitored the transient creep response for up to 10 hours.

Uniaxial creep strain experiments were performed in a similar manner, except that the confining pressure was no longer constant. Instead, the radial strain gauge adjusted the confining pressure to maintain constant radial strain while holding the differential load

constant.

(II) Relaxation testing

The analog of creep can be achieved by holding the axial strain boundary condition constant following a step displacement of the axial piston. Relaxation tests were performed under triaxial conditions by step-loading the stress and allowing the axial piston to advance to a predetermined position. A closed-loop feedback controller maintained this position by adjusting the axial stress. An internal load cell directly measured the vertical load on the sample. PC data acquisition performed prior to and following loading recorded both the impulse and transient response of the displacement and load. These tests were run dry or drained. The Ottawa sand/5% Montmorillonite clay sample was run "room dry" with pre-wetted laboratory-grade Montmorillonite (see description in Chang et al, or Chapter 3).

(III) Pore pressure transient tests

The pore pressure transient testing was performed in a manner similar to (II). The major difference was that the samples were saturated. The pore pressure control system was shut in to maintain constant pore volume. These tests were essentially performed under undrained triaxial and uniaxial conditions. The differential load was stepped and held at a nominal value, and the axial displacement was allowed to creep at constant confining pressure in the triaxial case (or constant radial strain in the uniaxial case). The PC acquisition system monitored the time history of the pore pressure prior to and following the stress perturbation. These tests were run saturated with denatured alcohol to avoid chemical interactions with the rock fabric.

(IV) Poisson's ratio by stress and strain

To determine Poisson's ratio at large displacements, a direct measurement of principal

strains (axial and radial) is required during triaxial loading. By measuring the stress ratio under uniaxial strain, we can also estimate Poisson's ratio if we assume linear elasticity of the sample. Under uniaxial strain loading, the sample was monitored while we increased the confining pressure to determine the stress ratio up to 27 MPa of vertical stress. These are both large-strain measurements of the degree of coupling between the principal strains under large displacements.

5.3 Results of laboratory testing

5.3.1 Creep testing

As in the hydrostatic loading cases, the rock samples exhibited creep deformation in uniaxial and triaxial loading configurations when loading ramps were paused at a constant pressure. All of the samples crept axially under constant loads in both triaxial stress and uniaxial strain configurations.

The creep response under triaxial loading (Figure 3) resembles that measured under hydrostatic boundary conditions (Chang et al, 1997). Table 2 summarizes the relaxation time constants and loading conditions. For the triaxial cases, it is clear that the Lentic sand time constants are shorter than those of the Wilmington sample.

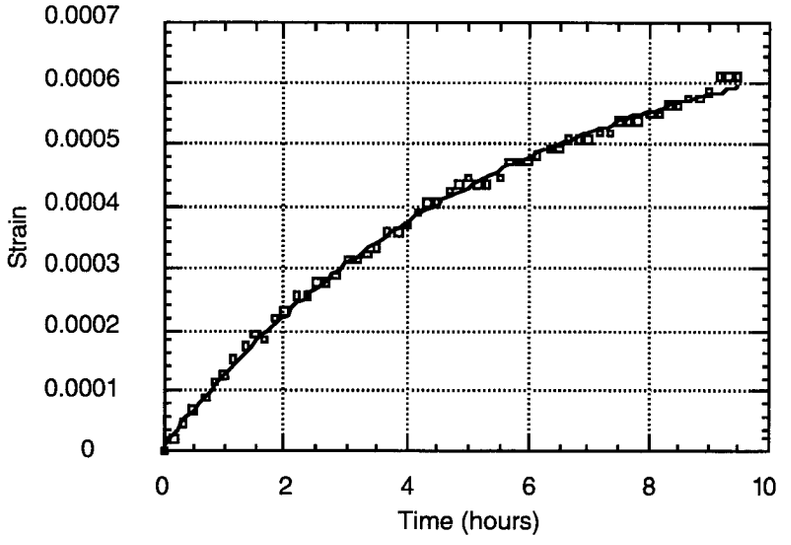

Figure 5.3: Creep response of the Wilmington sand under triaxial loading conditions. The solid line is an exponential fit to the data.

Table 2: Creep parameters

Sample	loading condition	Relaxation time (hours)	Pc (MPa)	Sv (MPa)
Wilmington	uniaxial strain	13.0	30	40
Wilmington	triaxial stress	5.70	22	25
Lentic	uniaxial strain	0.37	15	18
Lentic	triaxial stress	1.88	10	18

During testing of the Wilmington sample under uniaxial strain (Figure 4), the radial strain gauge and pressure feedback controller had a tendency to give a step-like response when the sample crept. Since all strain changes lagged the stress perturbations in the sample, controlling stress with strain measurement (as in the uniaxial strain case) led to the

types of minor instability observed in Figure 4. Although the data contains more irregularity than the other results obtained under triaxial compression, it is evident that the sample crept under these boundary conditions as well.

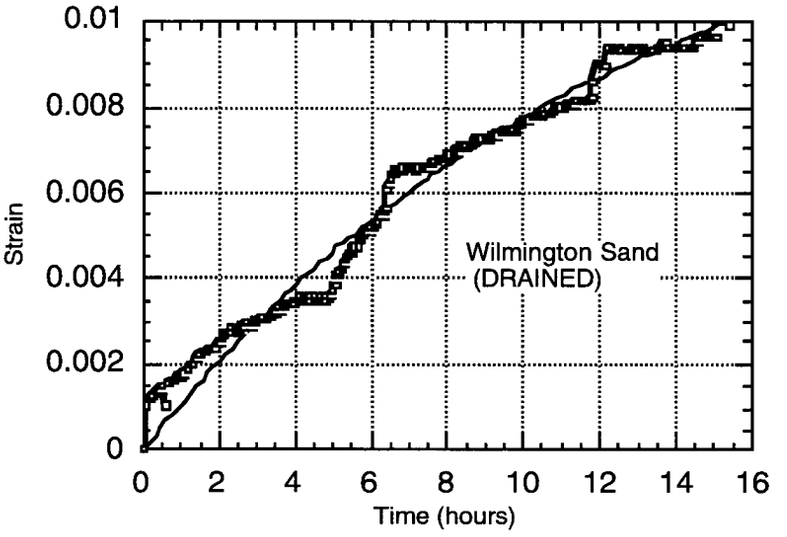

Figure 5.4: Creep in the Wilmington sand under uniaxial strain conditions. The solid line is an exponential fit to the data.

In the Lentic sand tests, the triaxial and uniaxial results are strikingly similar to triaxial stress, uniaxial strain, and hydrostatic stress tests of the Wilmington sands. The triaxial compression results were fitted to an exponential creep function of a standard linear solid (Figure 5), and resembled creep measured triaxially and hydrostatically on Wilmington cores.

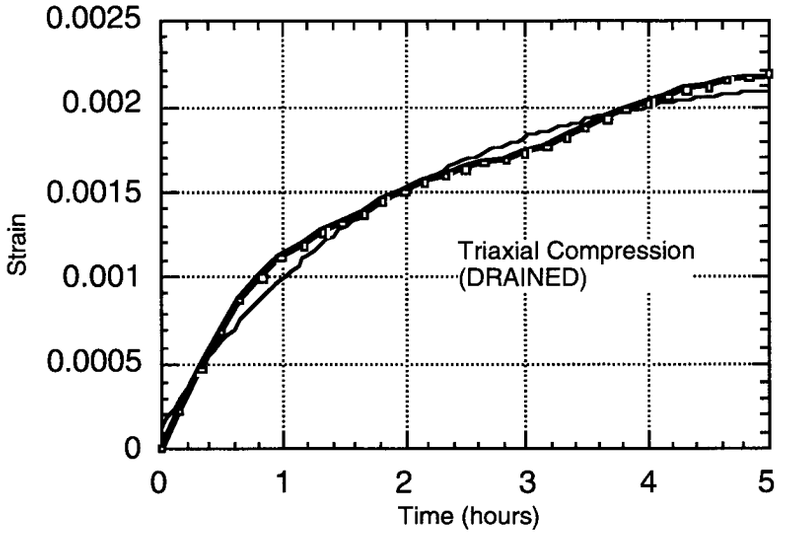

Figure 5.5: Creep in the Lentic sand under triaxial conditions. The solid line is an exponential fit to the data.

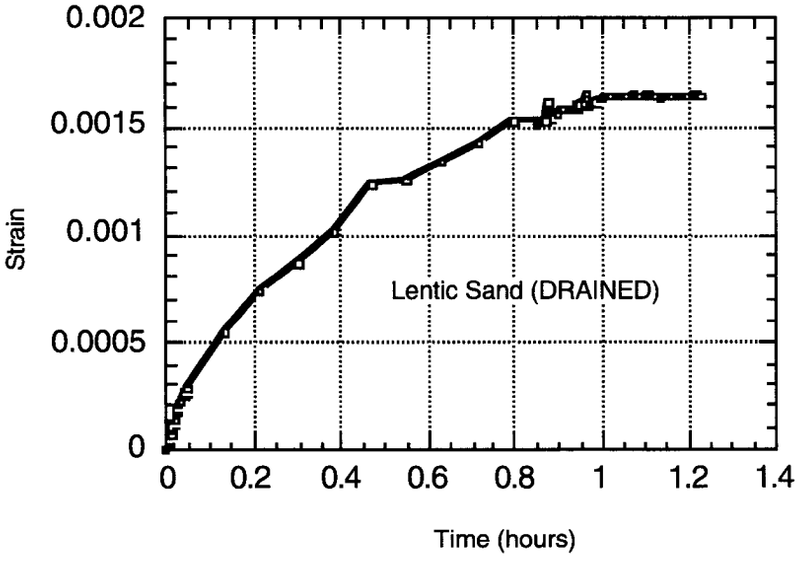

Figure 5.6: Creep in the Lentic sand under uniaxial strain conditions. The solid line is an exponential fit to the data.

The uniaxial compression of the Lentic sand (Figure 6) had a much lower time constant

than the other tests and thus equilibrated much faster. Evidently the time constant is a function of the boundary conditions. As in the Wilmington uniaxial strain test, the difficulties of controlling the confining pressure using strain feedback caused noise in the data. However, the signal was sufficiently clear to demonstrate the effects of creep under uniaxial strain compaction.

Although there is not a clear connection between boundary condition and relaxation time, it appears that the Wilmington sample deforms with a longer time constant than the Lentic sample in the more stable triaxial cases. All tests have relaxation times under 13 hours, as in the hydrostatic cases. The irregularity between the time constants of uniaxial creep and triaxial creep may reflect the instability of the uniaxial creep tests. Still, the Lentic sand appears to be a softer material that equilibrates quickly under triaxial loading.

5.3.2 Triaxial stress relaxation experiments

Under constant strain steps, stress relaxation occurred in both the samples of Wilmington sand and Ottawa sand/Montmorillonite. In the Ottawa sand sample, the transient stress peaked at 36 MPa differential stress and came to equilibrium 5 hours after the step displacement of the axial piston (Fig. 7). The differential stress is monitored by the internal load cell as long as the piston maintains contact on the sample. The fine line denoting the axial strain shows that the feedback control circuitry maintains constant axial strain to an accuracy of less than +/- 0.0001. The piston remained motionless after the step displacement. At zero differential stress the dashed line represents the hydrostatic background stress.

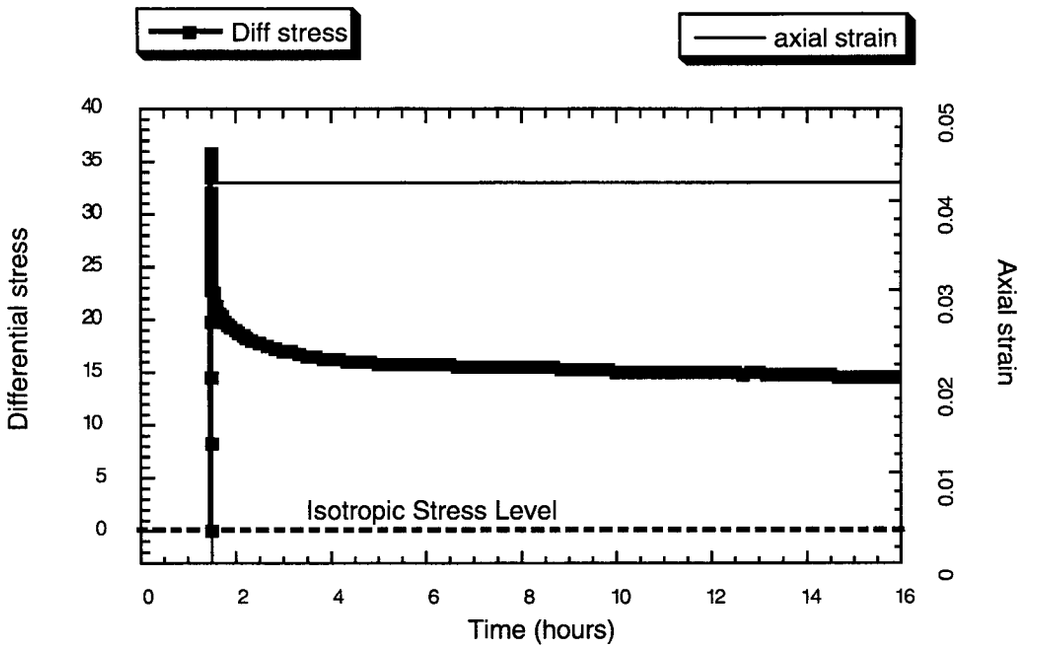

Figure 5.7: Ottawa sand + 10% Montmorillonite clay stress relaxation under triaxial loading conditions and constant axial strain.

The stress, monitored using an internal load cell mounted directly to the sample, decayed exponentially as a function of time and resembled the theoretical predictions made for viscoelastic media (Figure 2). The sample was under dry and drained conditions. Although the sample displayed some degree of fluidity under compression, the shear stress did not decay to 0 MPa, suggesting that the sample did not reach the isotropic stress state. The residual stress after equilibration suggests that a static modulus of this material maintains a finite differential load over time. This indicates that the rock material is not totally fluid-like.

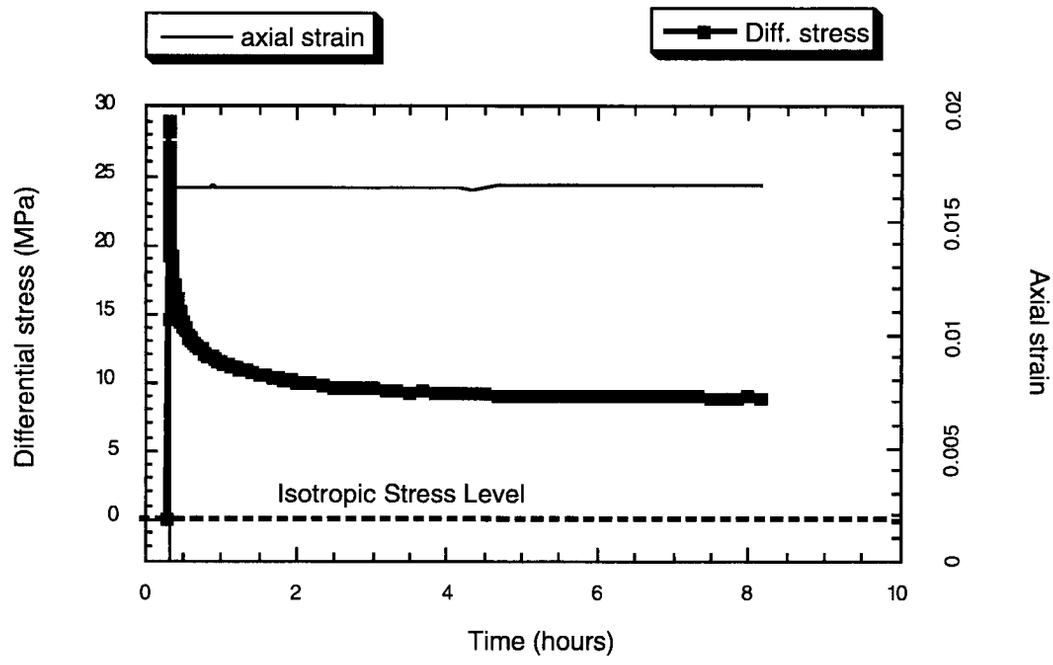

Figure 5.8: Wilmington sand sample stress relaxation under triaxial loading conditions and constant axial strain.

A similar response is seen in the Wilmington turbidite sample (Figure 8). In this case, the sample stress increased to a transient peak following the step strain axial displacement and then decayed over a period of several hours. The hydrostatic stress was held at a constant pressure of 20 MPa. This sample required more strain to obtain the same peak stress as that observed in the Wilmington sample. The Ottawa sand/Montmorillonite sample lost 58% of its initial strain by the time it reached equilibrium. The sample could not maintain the initial 36 MPa of differential stress indefinitely; however, it did maintain a finite load over time.

5.3.3 Pore fluid compression experiments

The objective of the pore fluid compression experiments was to observe the transient increase of pore pressure associated with creep compaction under polyaxial stresses. Under polyaxial compression, sealing the pore fluid system allowed constant pore volume to be maintained without the effects of fluid compressibility. After step axial loads were applied under both triaxial stress and uniaxial strain boundary conditions, the acquisition system collected data of axial creep, volumetric strain, and pore pressure.

The triaxial case showed a time-dependent increase in pore pressure. This increase was accompanied by pore volume compaction (Figure 9) under constant loads as shown in Figure 10. The flat stress data demonstrates the ability of the system to hold the principal stresses constant during the creep process. Pore pressure increased transiently and approached the confining pressure, which was also the least principal stress. The experiment was terminated to prevent the sample jacket from rupturing in a "self-hydrofracing" mechanism. The experiment demonstrated the possibility of transient pore pressure changes occurring after deformation events capable of changing the effective stress state.

The second time-dependent pore pressure experiment involved compacting the Lentic sand under uniaxial strain. As is seen from the strain history in Figure 11, most of the strain occurs during the step increase in differential stress. The axial creep strain follows the instantaneous step in stress for several hours. Because of the uniaxial strain boundary condition, there was no radial strain in this case.

The stress history is shown in Figure 12. Since the sample crept axially after a step load of 22 MPa was exerted in the vertical direction, the confining pressure had to increase to

balance the resulting change in horizontal strain due to Poisson's effect. This led to a transient increase in hydrostatic stress, followed by a transient increase in pore pressure. The latter was corrected for the volume of fluid in the pore pressure plumbing.

In these experiments, the time-dependent pore pressure can be connected to the viscous creep of an unconsolidated sand under constant load. In both cases, after the total stress is perturbed, a transient pore pressure response occurs under undrained conditions. In both experiments, time-varying changes in pore pressure that follow an instantaneous stress perturbation lead to transient changes in the effective stress field.

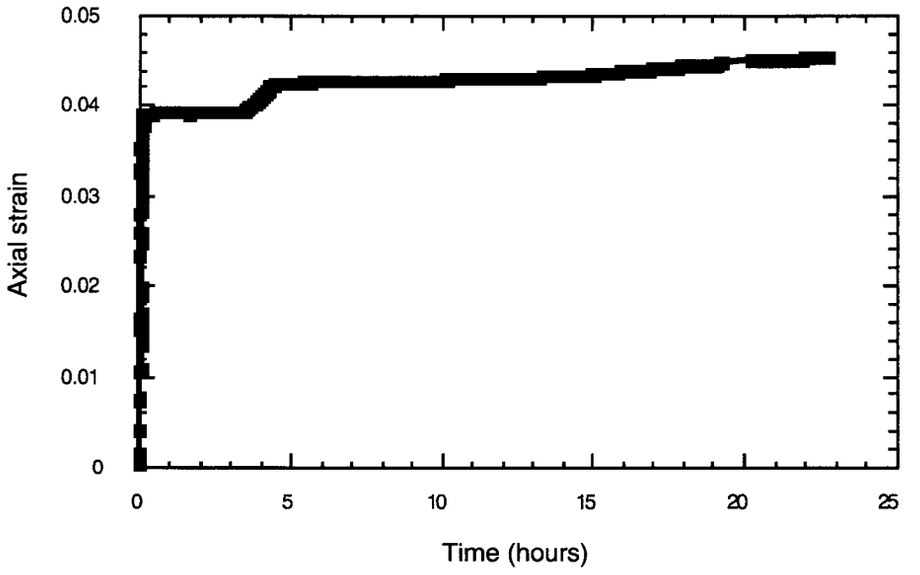

Figure 5.9: The strain history of the Lentic sand under triaxial compression.

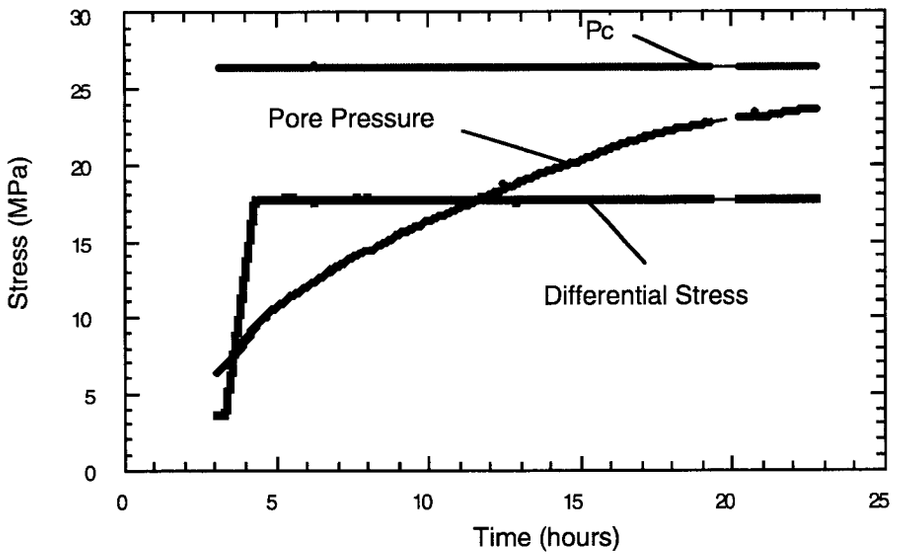

Figure 5.10: The stress history of the same test showing the transient increase of pore pressure under triaxial compression boundary conditions..

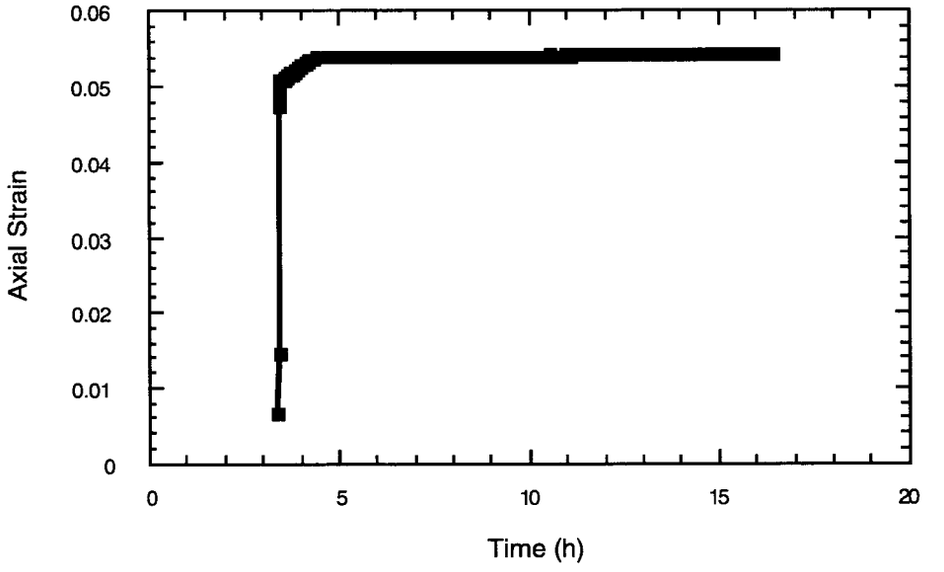

Figure 5.11: The strain history of the uniaxial strain test on the Lentic sand subject to a step strain.

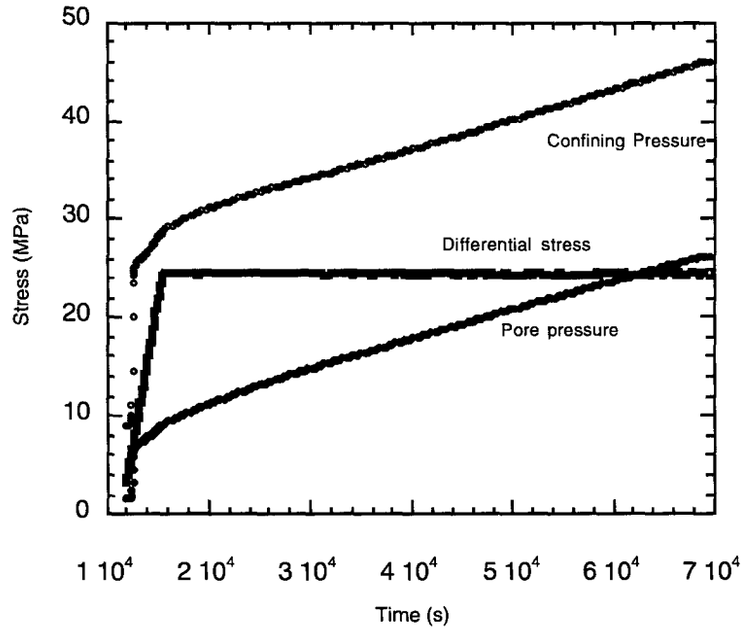

Figure 5.12: Following the step strain, both the pore pressure and confining pressure increase in the Lentic sand under uniaxial strain boundary conditions.

5.3.4 Estimates of Poisson's ratio

Poisson's ratio can be measured using either the stress or strain ratio. By definition, Poisson's ratio is the ratio of the principal strains under uniaxial stress. A second, less robust measurement of Poisson's ratio can be determined using the stress ratio if one assumes that the material deforms as a linear elastic material.

Compressing the Lentic sample under triaxial conditions with constant confining pressure gave a direct measurement of the principal strains. The results of radial and vertical strains on the cylindrical plug sample are shown in Figure 13. The slope of the curve gives Poisson's ratio, which in this case is approximately 0.293. Despite this being a large-strain experiment with plastic deformation, it is close to the definition of Poisson's ratio. The curvature of the data in Figure 13 suggests that the material displayed nonlinear

behavior. Although the curvature suggests a strain dependent Poisson's ratio, a linear fit was used on the strain data to attempt to capture the average value over the range of axial strains. The localized nonlinearity of the curve would have given higher and lower estimates of the Poisson's ratio. Two lines of 0.43 and 0.20 are superimposed on the plot to indicate the degree of variability in the data associated with the low quality of the linear fit.

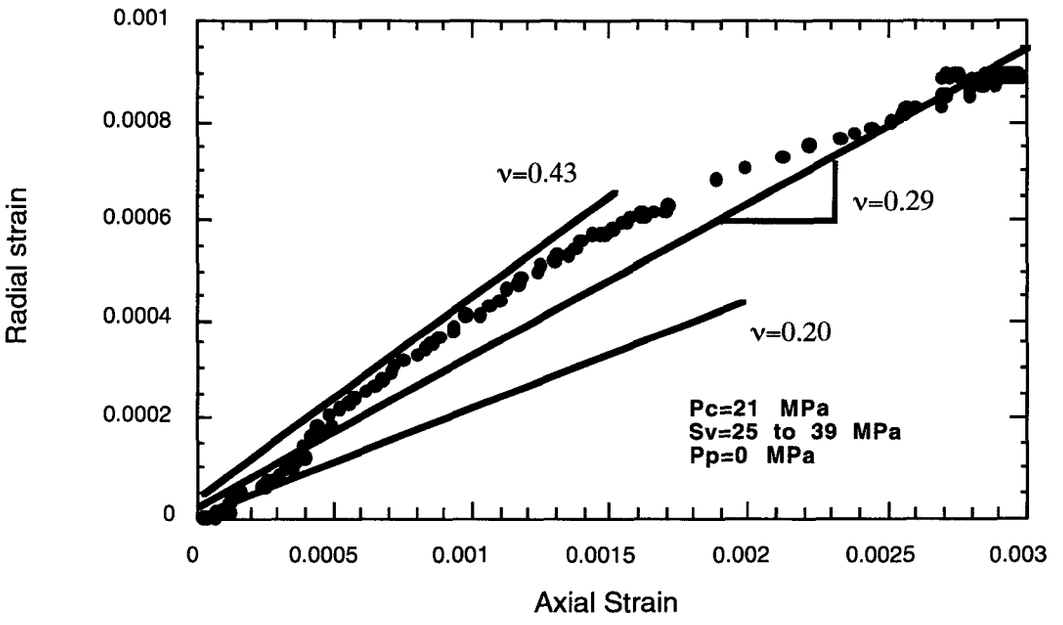

Figure 5.13: Strain history of the uniaxial strain experiment to obtain the stress ratio of the Lentic sand.

Figure 14 is the strain history of the Lentic sand compacted under uniaxial strain conditions. The strain rate corresponded to approximately 1.55e-7/s. This was also the total volumetric strain and was approximately equal to the porosity loss of the sample. The data shows some irregularity at the beginning of the experiment because the hydraulic control system had trouble coming to equilibrium when the sample was weak and poorly

packed. As the material packed more densely, the axial deformation became more regular (time > 2.5 hours).

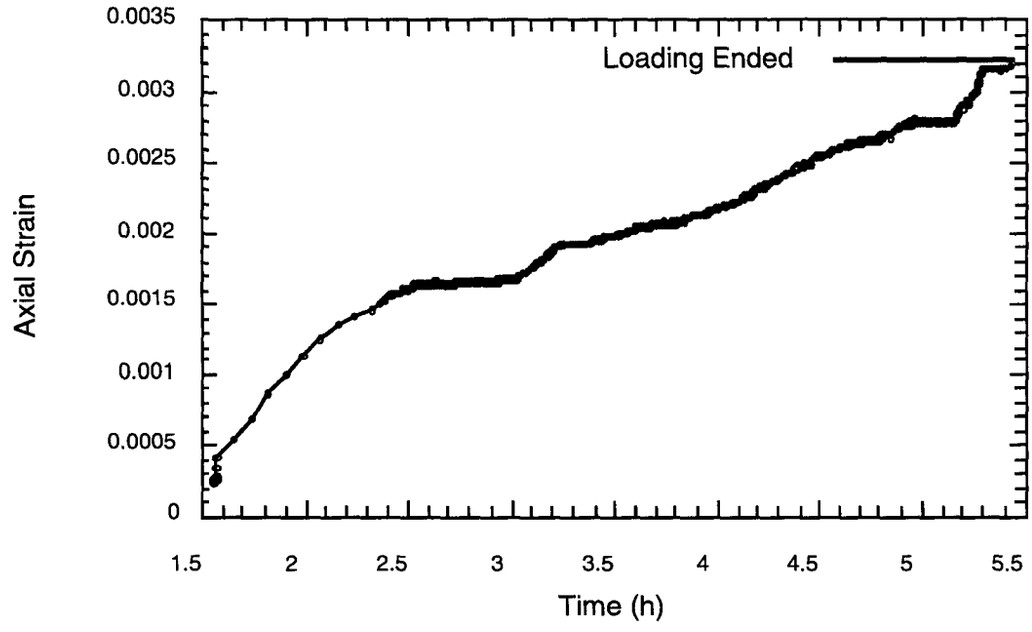

Figure 5.14: Strain history of the uniaxial strain experiment to obtain the stress ratio of the Lentic sand.

The relationship between vertical and horizontal stress is summarized in Figure 13. The change in vertical stress causes the horizontal stress to increase in order to maintain uniaxial strain. Assuming that the material behaves as a linear elastic solid at times between 2.5 and 5 hours, where the constitutive behavior is close to linear, we can relate the stress ratio and Poisson's ratio by

$$\upsilon = \frac{\Delta P_c}{\Delta P_c + \sigma_1} \tag{1}$$

Plotting the principal stresses (Figure 15) and solving for Poisson's ratio gives a value of approximately 0.27. Localized nonlinearity on the curve suggests that Poisson's ratio is not constant over the interval. Although the variation between small intervals is evident, a straight line captures the average behavior of the stress ratio well. In summary, four different types of tests have demonstrated the physical manifestations associated with viscoelastic rheology. Creep tests at constant load exhibited time-dependent

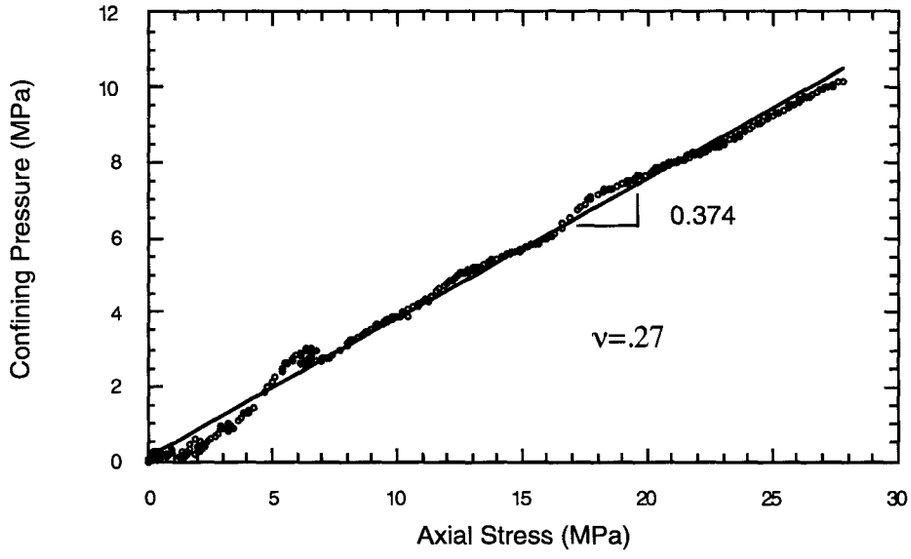

Figure 5.15: The principal strains of the Lentic sand under triaxial compression with a constant confining pressure.

deformation. Stress relaxation tests on dry samples showed exponentially decaying transient stresses and the tendency for unconsolidated materials to approach isotropic (low-shear) stress states over time. Undrained compaction tests under triaxial loads developed transient pore pressure, demonstrating the time dependence of effective stress in unconsolidated sediments. High Poisson's ratios were found when the Lentic sand was compressed, suggesting well-coupled principal strains.

5.3.5 Summary of results

Four different types of tests demonstrated the physical manifestations of viscoelastic rheology. Creep tests at constant load exhibited time-dependent deformation. Stress relaxation tests on dry samples showed exponentially decaying transient stresses and the tendency for unconsolidated materials to approach isotropic (low-shear) stress states over time. Undrained compaction tests under triaxial loads developed transient pore pressure, demonstrating the time dependence of effective stress in unconsolidated sediments. High Poisson's ratios were found when Lentic sand was compressed, suggesting a fluid rheology.

5.4 Discussion

In all of the experiments presented here, unconsolidated reservoir sand and synthetic sand have a viscoelastic character. As predicted from viscoelastic theory and the hydrostatic creep data sets published previously (Chang et al, 1997), creep can diminish differential stresses under constant strain boundary conditions, and pore pressure can increase due to time-dependent pore volume compaction. Given this time-dependent dynamic rheology, it appears that the rock matrix, with or without pore fluid, will deform viscously under the applied static loads. Poisson's ratio measured under large-scale strains indicates that this may occur by granular flow.

The triaxial stress relaxation tests confirm that rock stresses can relax over time in constant strain cases, given the proper boundary conditions and rock materials. In Figures 7 and 8, samples that began with an instantaneous differential stress of around 30 MPa lost their ability to maintain shear stress over time. The steady state stresses in these cases do not approach zero (isotropic stress) because the rock is viscoelastic, not a viscous fluid.

The stress decays to the steady state differential strength of the material, which can be related to the static Young's modulus. Because the load-bearing capacity of the medium decays, it can be thought of as the time-dependent strength. Although the sample is not in failure mode during these experiments, the relaxation of differential stress can be regarded as a weakening. Over 5 hours, the rock sample loses its ability to carry load by approximately 60% in the Ottawa and Wilmington sands.

Poisson's ratio was higher than that expected for an elastic crystalline rock material (~0.25), but lower than that of an ideal incompressible fluid (~0.5), and much larger than that from ultrasonic measurements. Ultrasonic testing usually gives higher values for Poisson's ratio closer to 0.20 for unconsolidated reservoir rock (Spencer, 1994). However, a small amplitude ultrasonic wave does not move the grains in the same way that a static test does. Because the large strain compacts the pore space, it increases the interaction between loosely packed grains. These increases intensify the degree of coupling between the principal strains, thus increasing Poisson's ratio. Since the materials deform viscoelastically at large strains, it may not be appropriate to compare these values to small-strain ultrasonic measurements.

Our tests on Ottawa sand samples suggest that the time-dependent deformation arises from small amounts of clay added to the matrix. Although the sample was not saturated, minute amounts of water may have mixed with the intergranular clay, allowing the grains to repack viscously. This appeared to be a micro-poroelastic effect where clay poroelasticity at the grain boundaries determined the time constant. Since this process is highly dependent on small amounts of residual moisture in the clay, this may also explain the variation in relaxation time constants found in the triaxial creep experiments. To test

this idea, we hydrostatically compressed a thin piece of the same clay corresponding to the amount found in the 5% Ottawa sand/clay synthetic mixture; having done so, we observed creep displacements of the same magnitude as those observed in the Ottawa sand/clay synthetic samples (Figure 16). This observation clearly establishes the relationship between the semi-dry clay and the creep.

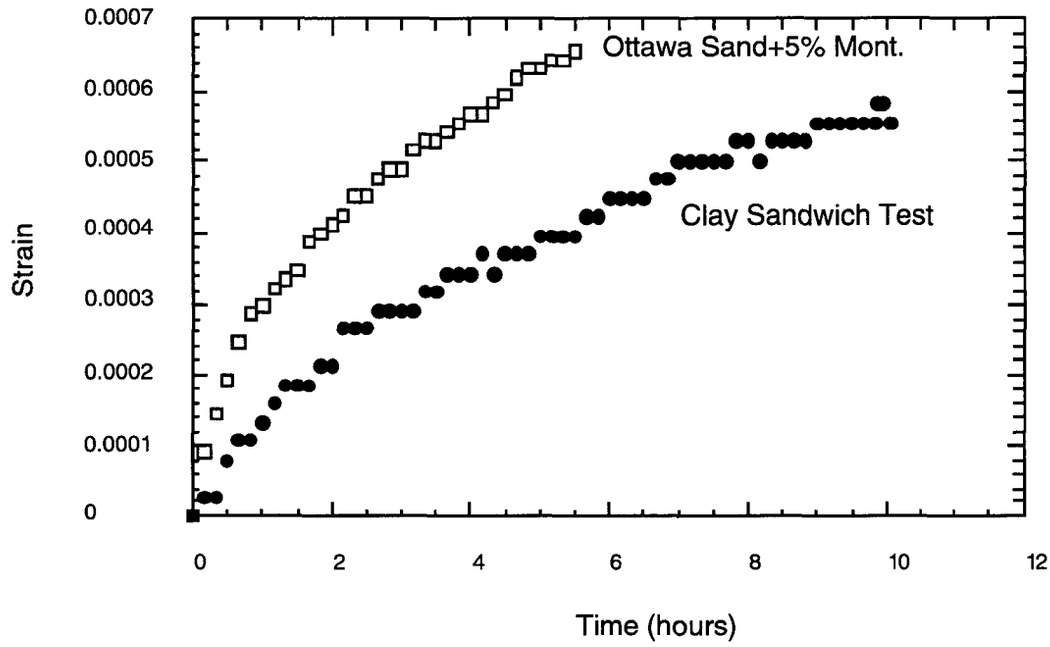

Figure 5.16: The compression of pure clay discs made from the same clays as those used in the Ottawa sand synthetic rocks (closed markers), compared to creep in a sample of Ottawa sand + 5% Montmorillonite clay. Both samples contained equivalent volumes of the same clay.

Even with very low water content, clay displays viscoelastic behavior at high stresses. Our samples required premoistened, dried clay to generate creep effects. During the experiments, the porosity often changed by up to 20%. As the pore volume of the clay got smaller, the minute amounts of residual pore water consumed more of the once-dry pore spaces in the clay clusters. Localized increases in saturation resulted. Since permeability

can drop very low at this scale, it is possible that these minute amounts of pore water were unrelaxed — regardless of the state of drainage in the overall sand sample. This type of mechanism, referred to as "domain compaction" in the clay mechanics literature, provides an explanation for creep in partially saturated clay (Pusch, 1979). If this applies to our samples, the degree of saturation, clay micro-porosity, and thus micro-permeability should determine the relaxation time constant.

The viscoelastic mechanism controlled the stress, stiffness, and strength of our rock samples over time. Depending on the time scale, the rock stress will vary. Because this only occurs after a sudden perturbation of the stress field, it is most relevant to engineering practices where loading rates and observation periods may last from hours to days. Without understanding this phenomenon, it is difficult to make consistent strength estimates from log or seismic measurements alone. A combined analysis, including a variety of data types at different frequencies, better constrains the time-dependent material properties. The stress relaxation experiments suggest that a high-frequency measurement will never see the low-frequency (long-term) modulus or the residual stress. This results in a gross over-prediction of the stiffness and load-bearing capacity of the sand.

5.5 Conclusions

Deformation experiments performed on the Lentic sand, Wilmington sand, and Ottawa sand/Montmorillonite synthetic samples indicate viscoelastic behavior unrelated to pore fluid expulsion or dewatering. This type of mechanism may explain low differential stresses observed in poorly consolidated sand. It may also explain the differences observed between static and dynamic moduli. The experiments successfully demonstrate

viscoelastic behavior in unconsolidated sediments under various types of triaxial loads and allowed us to associate the viscoelastic nature of the sands with the presence of intergranular clays.

5.6 References

Bishop, A.W., 1966, The Strength of Soils as Engineering Materials, Geotechnique, 16, 91-128.

Chang, C., Moos, D., Zoback, M.D., 1997, Anelasticity and dispersion in unconsolidated reservoir rocks, Int. J. Rock Mech. & Min. Sci., 34, No. 3-4, Paper No.048.

Clough, G.W., Sitar, N., Bachus, R.C., Rad, N.S., 1981, Cemented sands under static loading, Proceedings of the American Society of Civil Engineers, 107, No. GT6, 799-817.

Cole, K.S., Cole, R.H., 1941, Dispersion and Absorption in Dielectrics, Journal of Chemical Physics, 9, 341-351.

Dudley, J.W., Myers, M.T., Shew, R.D., Arasteh, M.M., 1994, Measuring compaction and compressibilitites in unconsolidated reservoir materials via time scaling creep, Proc. of Eurock '94 Balkema, Rotterdam, 45-54.

Finkbeiner, T. and Zoback, M.D., 1998, In situ stress, pore pressure, and hydrocarbon migration in the South Eugene Island field, Gulf of Mexico, paper SPE 47212 presented at the 1998 SPE European Rock Mechanics Meeting, Trondheim, Norway, July 8-10.

Gross, B., 1947, On creep and relaxation, Journal of applied physics, 18, 212-220.

Karig, D.E., 1992, Uniaxial reconsolidation tests on porous sediments: mudstones from site 897, Ocean Drilling Program, Scientific Results, 149, 363-373.

Lo, K.Y., Lee, Y.N., 1990, Time-dependent deformation behavior of Queenstown shale, Can. Geotech. J., 27, 461-471.

Ostermeier, R.M., 1993, Deepwater Gulf of Mexico turbidites: compaction effects on porosity and permeability, SPE Formation Evaluation, June

Pusch, R., 1979, Creep mechanisms in clay, Mechanisms of deformation and fracture, ed: Easterling, K. E., 351-359.

Spencer, J., 1994, Frame moduli of unconsolidated sands and sandstones, Geophysics, 59:9, 1352-1361.

Tchoegel, N.W., 1978, The Phenomenological Theory of Linear Viscoelastic Behavior: An Introduction, Springer-Verlag, Berlin, 39.

Terzaghi, K., 1941, Undisturbed clay samples and undisturbed clays, J. Boston Soc. Civil Eng, 29:3, 211-331

Vernik, L., Bruno, M., Bovberg, C.1993. Empirical relations between compressive strength and porosity of siliciclastic rocks, Int. J. Rock Mech. Min. Sci. & Geomech. Abstr, 30:7, 677-680.

Yamamuro, J.A., Bopp, P.A., Lade, P.V., 1996, One-dimensional compression of sands at high pressures, Journal of Geotechnical Engineering, 122:2, 147-154.

5.7 Appendix

The standard linear solid equations for creep strain and stress relaxation are given by

$$\varepsilon = \left[\frac{1}{G_1} + \frac{1}{G_2}\left(1 - e^{-\frac{t}{\tau}}\right)\right](\sigma_0 \cdot u_t) \qquad \{A.1\}$$

and

$$\sigma = \varepsilon_0 \cdot \left(\frac{G_1 G_2}{G_1 + G_2} + \frac{G_1^{\,2}}{G_1 + G_2} \cdot e^{-\left(\frac{G_1 + G_2}{G_2}\right)\frac{t}{\tau}}\right) \qquad \{A.2\}$$

σ = 1-D stress

ε = 1-D strain

E_1 = outer spring (see Figure 1)

E_2 = inner spring

σ_0 = stress perturbation

ε_0 = strain perturbation

t = time

τ = relaxation time constant

CHAPTER 6

MICROMECHANICS OF CREEP AND RELAXATION IN UNCONSOLIDATED SANDS

Abstract

To understand better the micromechanics of creep observed in dry unconsolidated sands, we performed two distinct types of experiments. First, we performed thin section analyses on deformed and undeformed Ottawa sand samples. Microscopic analysis showed that creeping and non-creeping samples contained the same microfractures, and grain-size analysis of deformed samples indicated that very little change in the grain size distribution occurred during testing. These observations suggest that grain-crushing and microcracking mechanisms were not important deformation mechanisms in these samples. Second, to investigate the role of intergranular clay, we tried to isolate most of the creep strain. Pure clay samples were deformed under hydrostatic conditions between two blocks of Berea sandstone under drained conditions. The sample was assembled with room-dried Montmorillonite (5% by volume) and then compressed in the pressure vessel. The resulting creep was comparable to that observed in the Ottawa sand mixtures containing the same amount of clay. It thus appears that compaction of small amounts of clay results in viscous creep at high pressures. Perhaps this arises from a micro-poroelastic phenomenon in the clay under high volumetric strains encountered under high pressures.

6.1 Introduction

In our previous studies (Chang et al, 1997; Chang and Zoback, 1998; and Chapter 3),

we described the time-dependent deformation behavior of unconsolidated sediments. The creep and relaxation behavior was observed under triaxial and hydrostatic loading conditions in fine-grained reservoir sands and synthetic Ottawa sand samples having small (< 10%) amounts of clay. Although the strain rate dependence of the deformation could be described using a viscoelastic rheology, viscoplasticity was also observed and the micromechanical mechanism of time-dependent deformation in these dry sands was not determined.

A number of physical phenomena such as grain-crushing, time-dependent microcracking, grain dissolution, and grain repacking might give rise to creep in these dry unconsolidated reservoir rocks. Of these, grain crushing, time-dependent microcracking, grain dissolution, and grain repacking seem most likely to result in creep. To identify which mechanism governs the deformation of our samples of dry reservoir rock, it was necessary to consider the conditions under which they occurred.

Grain-crushing and microcracking have been thought to produce time-dependent deformation in geologic materials (Brzesowsky, 1995). Acoustic emission tests established that the creep strain rate was related to microcracking and grain-crushing. Zoback and Byerlee (1976) and Brzesowsky (1995) observed creep under uniaxial strain in dry quartz sands and correlated its onset with acoustic emission. In triaxial experiments Zhang et al (1990) observed a similar result but demonstrated that it does not occur under hydrostatic loads of less than 200 MPa. It is therefore difficult to explain the creep observed in our experiment at hydrostatic pressures of 10 - 30 MPa as grain crushing.

Time-dependent microfracture has been studied in the laboratory and used to explain creep in rocks (Costin, 1987). Martin (1972) demonstrated that this process is accelerated

by corrosive fluid flow at high temperatures in quartz. Stress concentrations at the grain contacts can lead to time-dependent grain fracture. This can result in creep such as that observed in the Ottawa sands tested by Chang et al (1997). Although the experimental temperature, shear stress, and fluid conditions of our experiments do not support this mechanism, this phenomenon can be easily checked by comparing thinsections of tested and untested sands.

Solution surface transport is a well-established mechanism for time-dependent compaction of quartz sediments by Borg et al (1960), deBoer et al (1975), and Schutgens (1991). Their laboratory tests demonstrated that chemically reactive fluids corrode grain contacts and cause the quartz grains to lose volume over time, as shown schematically in Figure 1. Although the same phenomenon has been observed in situ using core analysis of naturally consolidated reservoir sands (Bjorkum, 1996), these studies all involved high temperatures and corrosive fluid saturation. It is therefore difficult to explain the large strains and strain rates we observed in the samples of Ottawa, Lentic, and Wilmington sand (Chapter 5) at room temperature using solution surface mechanisms.

Grain repacking is another mechanism that could explain the creep and relaxation observed in our previous study. Figure 2 demonstrates how this process might result in compaction. Repacking is not necessarily time-dependent. For instance, it occurred instantaneously in the pure Ottawa sand samples tested in Chang et al (1997). This may not be the case in sands containing small amounts of clay, as time-dependent compaction was observed in samples containing small amounts of premoistened, room-dried clay. It is possible that the dried Montmorillonite fraction provides a viscous time constant to the repacking process.

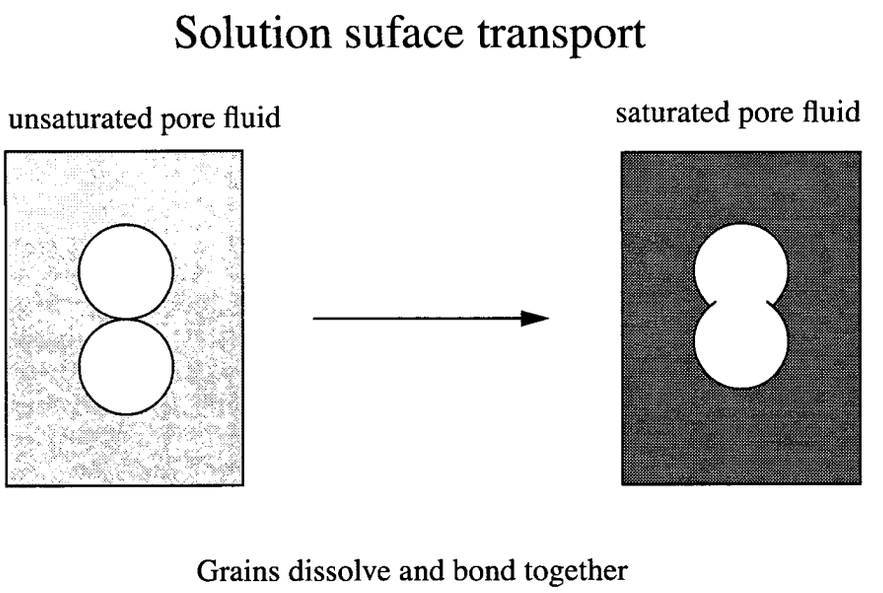

Figure 6.1: Solution surface transport. Grain boundaries dissolve and the material compacts. Since the dissolution process is time-dependent, the compaction of the material is observed as creep.

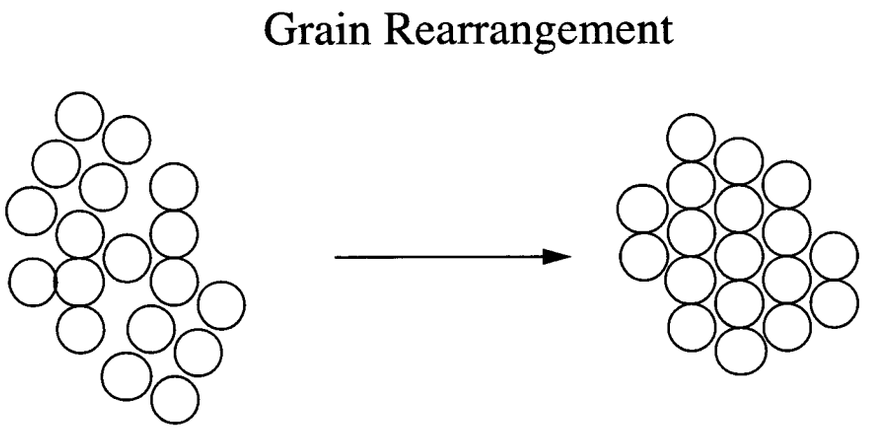

Figure 6.2: Grain rearrangement. Here the particles find a denser way to pack themselves as external stresses increase.

Grain repacking can become time-dependent if the localized stresses in the sand are heterogeneous and not in equilibrium. Although theoretical studies of granular media often postulate that all grains see the same stresses, the distribution of stress in an unsorted sand

sample is not homogenous: neighboring grains do not necessarily carry the same loads. Given a viscous repacking process, the stress will migrate around the sample as localized load-bearing grain structures collapse within the sample. This stress migration process was originally postulated by Barden (1969) to describe secondary consolidation of clays. It is treated theoretically in Pusch (1979) to describe time-dependent collapse of granular materials. The theoretical analysis suggests that the velocity at which stress migrates through a packing of flocculated grains determines a material time constant. Although this analysis has not been applied to sand grains, it may have some relevance to observations of creep in dry sand.

6.2 Experimental procedures and results

6.2.1 Procedure for thin section analysis

To explain the micromechanism of granular creep in dry sands, we performed two types of experiments. The first involved collecting and examining thin sections from the Ottawa sand in cases with clay and no clay, and before and after testing. The second experiment involved the hydrostatic compression of Montmorillonite clay between two large Berea sandstone blocks. These tests were intended first to identify the degree of grain-crushing and microfracturing, and second to isolate the role of clay deformation in the various unconsolidated sands.

The thin sections of Ottawa sands were easiest to interpret and are shown here. Grain statistics were calculated using NIH Image software on 4x scans of the sands. The intent was to identify grain-crushing (if it occurred) and to document a shift in the mean grain size as evidence of grain breakage.

TABLE 1. The sectioned samples

test	condition	sample type	creep
o9	hydrostatically compressed	clean Ottawa sand, 300 um mean grain sz	none
vo	virgin - untested	clean Ottawa sand, 300 um mean grain sz	not applicable
o6	hydrostatically compressed	5% Montmorillonite clay and clean Ottawa sand, 300 um mean grain sz	yes

A collection of thin section images from the Wilmington, Lentic, and Ottawa sand samples provided microstructural information on the grain scale. Unfortunately, the thin sectioning process made the natural samples difficult to interpret, as it was difficult to determine whether cemented grains were formed during diagenesis, or during testing in the natural samples. Of the three rock types (Wilmington, Lentic, and Ottawa sands) only Ottawa sand images and a reference case of untested Ottawa sand will be included here. Table 1 describes the samples and the conditions under which they were tested. Samples of the Wilmington and Lentic cores were sectioned. However, their poor quality (caused by the difficulty of sectioning) made it impossible to analyze these sections.

6.2.2 Results of thin section analysis

Thin section analysis provided information about the micromechanics of the Ottawa sands. In the tested samples, grain fracturing occurred. Though the untested sample showed grain microcracking, it was not as extensive as in the tested samples. Grain counting by NIH Image software provided statistical distributions of the grain sizes in three samples in nine different areas of the section. The sectioning suggested that the grain size distribution was not changed during the hydrostatic loading process. Inspection of the

sections for clay particles showed that the sample preparation had disturbed the intergranular clay, thus making it difficult to form conclusions about clay/quartz interactions.

Figure 3 is a photomicrograph of the virgin Ottawa sample. Although this sample was never compressed, there were visible microcracks in the grains. The cracks did not appear to penetrate the entirely through individual grains. In this sample there was no clay added before sectioning. Some grain microcracking was observed in all samples of the Ottawa sands, whether they were tested or not. Whether the microcracks were pre-existing or induced during thin sectioning is unknown. This image served as a reference for the hydrostatically compressed images.

Figure 4 is the statistical distribution of grain sizes in the reference sample. Although the number of grains is not large, the grain counting software provides a normal distribution of grain sizes. Two other images of this sand were taken from different areas of the sample but are not shown here. They appeared to have similar grain morphology as suggested by the micrograph, as well as nearly identical grain-size distributions (corresponding to samples o9, vo and o6.

The following microsections in Figures 5 and 7 were almost indistinguishable from the virgin samples, although they had been subjected to 30 MPa of hydrostatic stress. The corresponding grain-size distributions (Figures 6 and 8) indicate that these samples did not undergo significant grain-crushing or cataclasis during loading. The size distribution remained the same before and after loading.

Observations of the grains implied that the rounded quartz particles were mostly unchanged by testing. Microfracturing appeared to occur in all samples with slightly larger

counts of fractured grains in the tested samples. This did not change the grain-size distribution because few of the fractures completely penetrated the grains. None of the samples appeared to have solution surface interfaces between connected grains, but these were not necessarily expected because of the low temperature, saturation, and duration of the experiments.

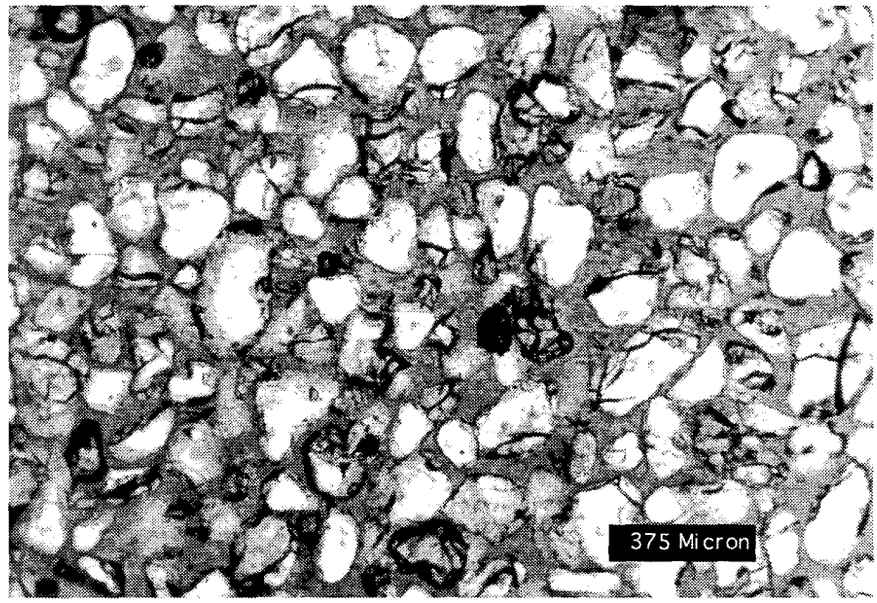

Figure 6.3: Photomicrograph of an untested (virgin) Ottawa sample at 4x magnification. The darker grains are microfractured.

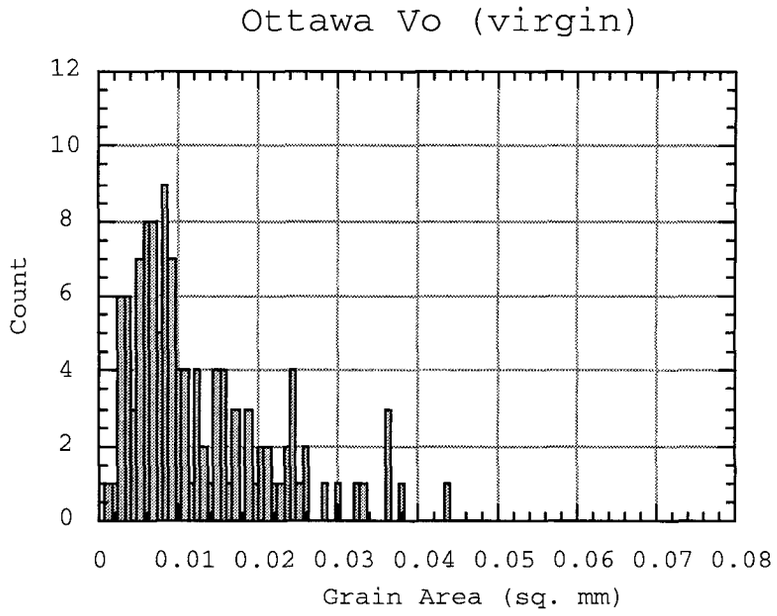

Figure 6.4: The grain-size counting statistics of the virgin Ottawa sand shown in Figure 3.

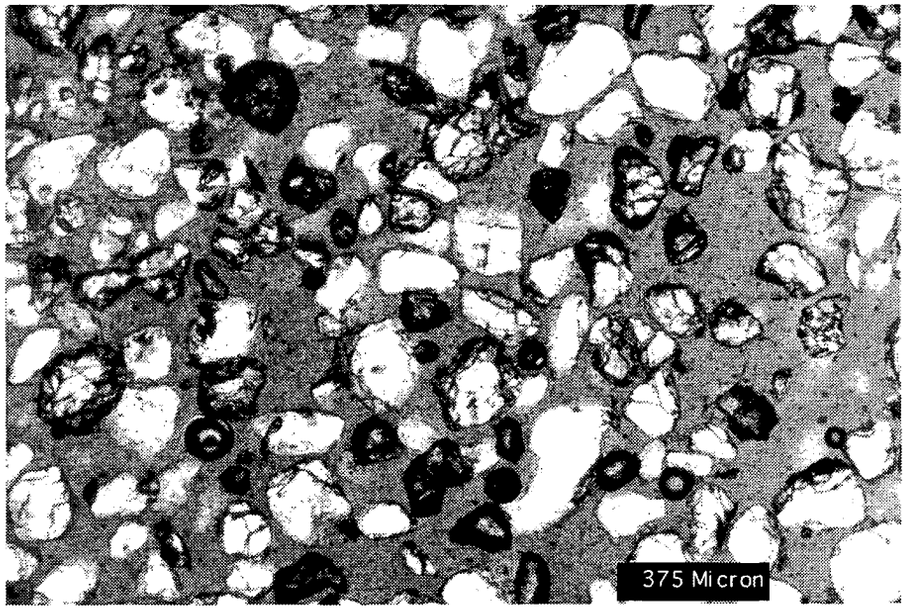

Figure 6.5: Montmorillonite/Ottawa sand sample (o6) following testing. Note the microfractured (darker) grains.

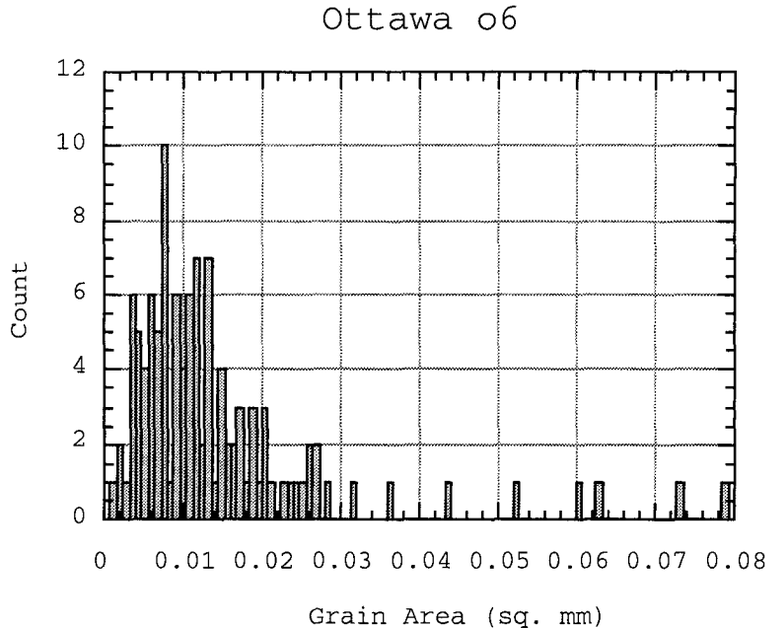

Figure 6.6: Grain-size statistics for the Ottawa sand + 5% Montmorillonite sample following loading.

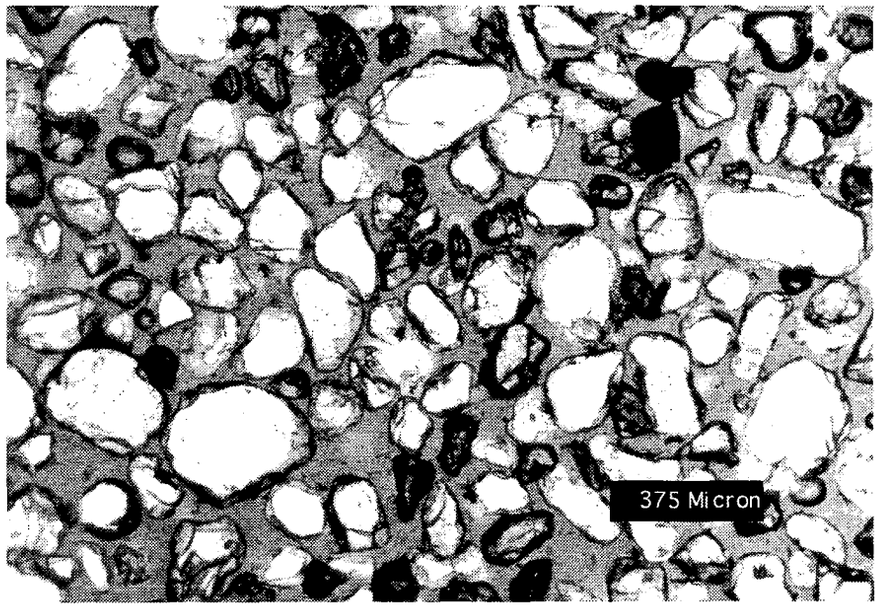

Figure 6.7: Thin section of clean Ottawa sand sample (o9) following testing.

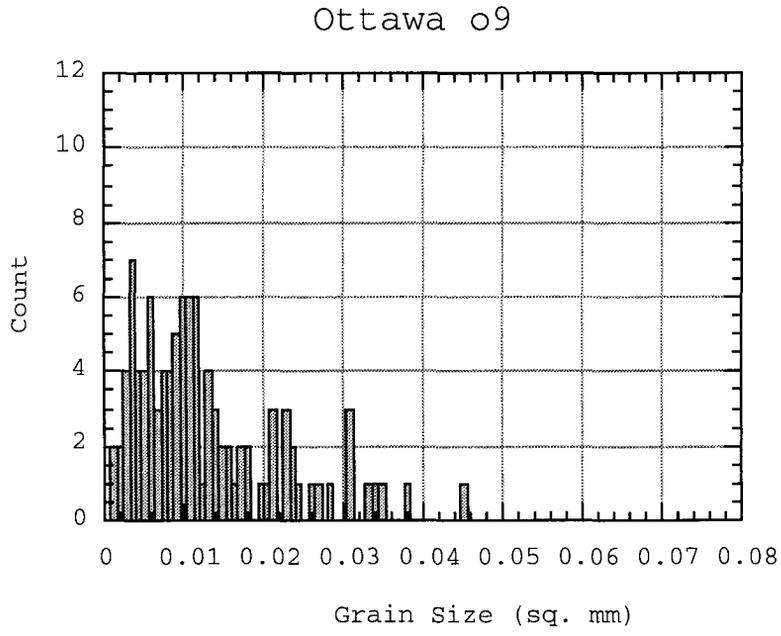

Figure 6.8: Clean Ottawa sand following testing. Note the similarity with the previous histograms.

6.2.3 Experimental procedures for clay compression testing

Montmorillonite clay appeared to be the time-dependent agent in the tests as reported in Chapter 3 and by Chang et al (1997). Block tests using hydrostatic pressurizing thus provided information on the time-dependent rheology of the clay bounded by two Berea sand cores. Berea was chosen to provide a stiff yet permeable barrier to the clay. To prevent unwanted pressure discontinuities from developing at the interface, we used a highly permeable sandstone to drain the surface of the clay adequately.

As in the previous mixing experiments, the clay was wetted and then room-dried for a day. On completion it appeared dry and dusty. The clay was placed between two cores of 100 mD Berea sandstone 1 inch (2.5 cm) in diameter and 1 inch (2.5 cm) long (Figure 9).

The thickness of the clay layer was 1.27 mm, which corresponded to a total clay content of 5% by volume over the 2-inch-long sample. This was intended to replicate the behavior of a granular mixture of 5% clay and 95% quartz sand. The saw-cut sample was compressed at hydrostatic pressures of 10, 20, 30, 40, and 50 MPa, with pauses at each load to allow for creep equilibration. Axial displacement, stress and time were continuously monitored.

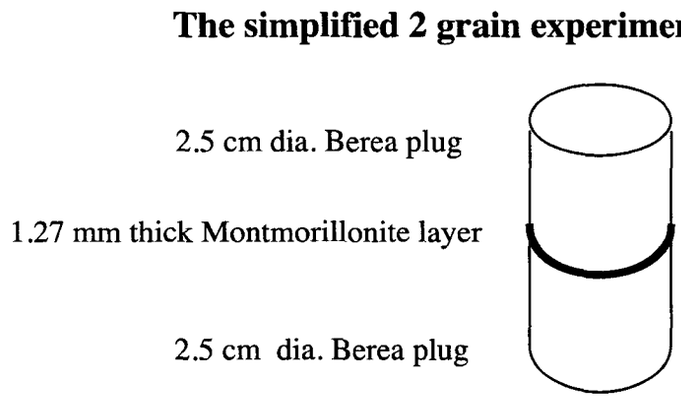

Figure 6.9: The schematic of the simplified clay compression experiment

The samples used in this study are described in Table 2. As in the hydrostatic loading cases discussed in Chapter 3, these tests used hydrostatic pressure steps and unloadings to obtain creep strain data.

TABLE 2.

sample	berea blocks	amount of clay	loading
#1	2x1"	5%	0-34 MPa, 3 steps
#2	2x1"	5%	0-55 MPa, 5 steps

6.2.4 Results for clay compression tests

Figure 10 shows the stress vs. time histories of the samples. The loading procedures and external boundary conditions of this saw-cut sample and those of the creeping Ottawa sand (o6) sample are similar. Rather than having tens of thousands of grains and contacts, the block sample has only two, isolating the compaction strain to the soft Montmorillonite clay. The rounded plateaus in Figure 10 shows that the block sample exhibits creep strain while stress is held constant. Figure 11 shows the creep strains of the saw-cut block test sample #1 overlaid at different pressures. The amount of creep appears to decrease with increasing pressure. It is not clear from these simple tests whether this results from the effects of strain history or stress magnitude. The form of the creep curve and the total amount of strain are remarkably similar to those observed in the 5% Montmorillonite/Ottawa sand mixture under 30 MPa of pressure. The total amount of creep strain does not fall into a predictable order in Figure 11. Intuitively, the creep strain for 30 MPa seems as if it should fall below the creep strain for 20 MPa rather than in between 10 and 20 MPa. The heirarchy suggests that a combination of processes is occurring. First, the total amount of creep for each stress step must decrease since it originates from the loss of clay porosity in the clay layer which would imply that the 30 MPa curve had seen a longer compaction history and lost its ability to creep unlike the 10 MPa curve which occurred earlier in the test. However, the stress magnitude also increases in the 30 MPa test making the driving force higher. In the case of a viscoelastic solid model as seen in Chapter 3, the total amount of creep strain is proportional to the driving stress suggesting a possible explanation for the apparent disorder seen in Figure 11.

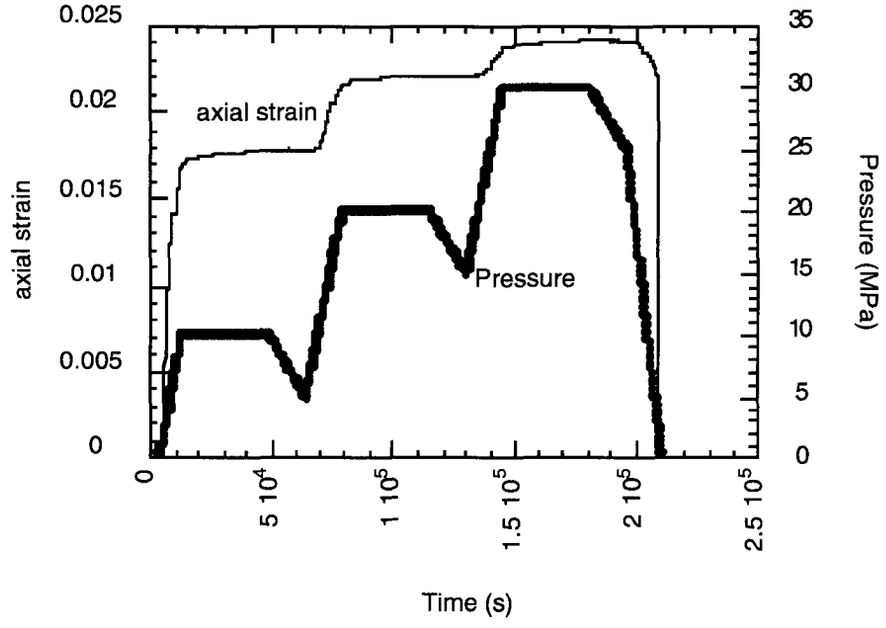

Figure 6.10: The stress and strain history of the block test sample #1. The creep deformation can bee seen as curvature in the strain response at constant pressure.

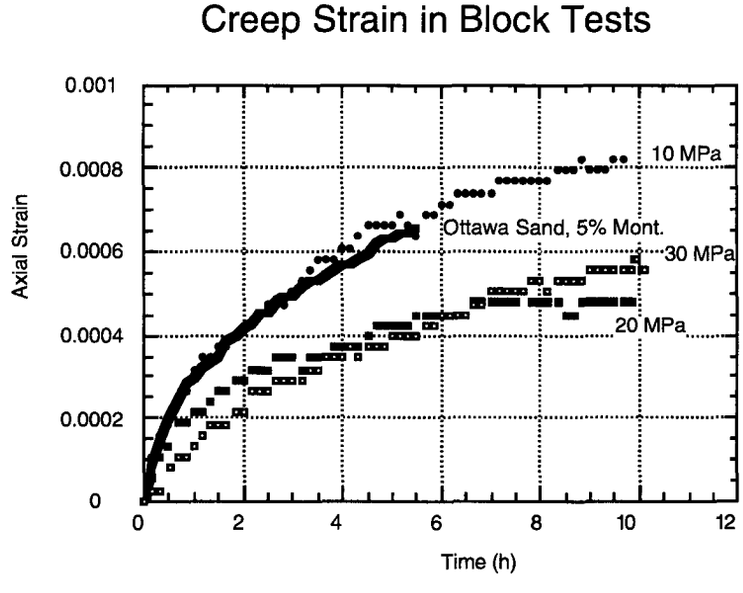

Figure 6.11: Creep curves from test #1. In this test the amount of creep strain decreases with pressure.

A similar test, test #2, was performed to examine the creep behavior in the clay at higher

pressures as those encountered in test #1. Figure 12 shows the strain history of this tests during 5 steps of pressure from 0 to 55 MPa. It is evident that the total amount of creep strain decreases with increasing pressure. This is also observed in enlarged and overlaid strain versus time curves shown in Figure 13. The flattening of the creep response implies that the creep does not continue indefinitely and is dependent on the initial state of deformation.

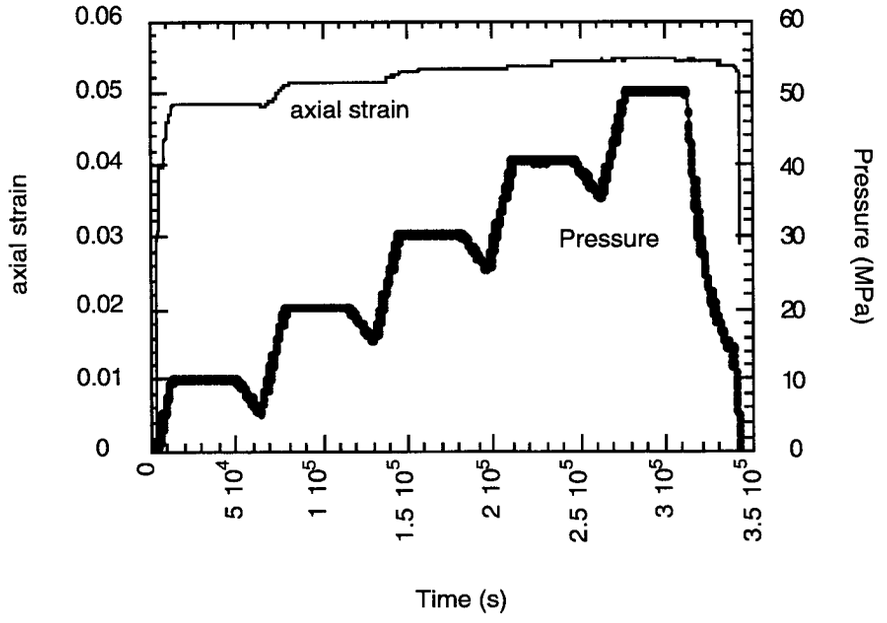

Figure 6.12: The stress and strain history of the block test sample (#2) showing creep in the pure clay contact boundary. This test went to higher pressures. There was little creep at 40 MPa and above.

In test #2, compaction appeared to control the total amount of creep strain in each step. As the experiment progressed, and stresses became higher, the total amount of creep strain decreased. The upward tail of the creep curve in Figure 13 might have been caused by sample buckling towards the end of the experiment after the sample has undergone very large axial displacements.

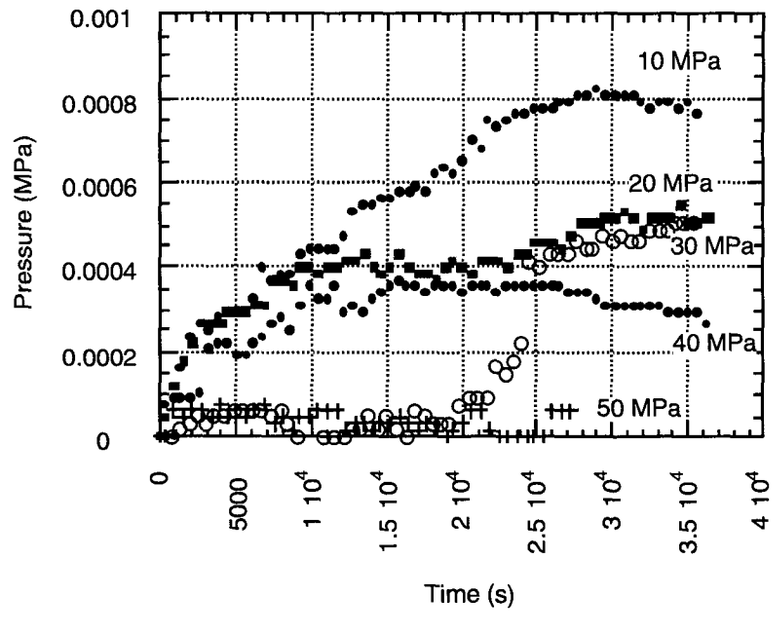

Figure 6.13: Creep curves from test #2. In general, creep strain decreases with increasing pressure

6.3 Discussion

The results of the thin section analysis, grain-size analysis and the clay layer experiment provide evidence that intergranular clay compaction was the predominant mechanism controlling the viscous creep of the unconsolidated sands.

The thin section data shows that the Ottawa sands do not creep because of grain-crushing or solution surface processes. All thin sections show a small degree of grain microfracturing but only o6, the Montmorillonite/Ottawa mixture, exhibited creep. Although some grains have microfractures, they do not appear to fully penetrate and dissociate the grain, as evidenced by the thin sections and the unchanging grain-size distributions.

Solution surface transport does not appear to be an influential factor in the time-dependent deformation of the sand. Although it has been documented to give rise to creep in numerous laboratory studies, it requires high temperature, corrosive fluid saturation, and long time intervals, none of which are present in the experiments we have carried out. The viscous behavior of the dirty sands occurred at room temperature and without pore fluid. Under microscopic investigation, solution surface contacts were not observed in the micrographs of the synthetic sand samples.

The deformation of clay appeared to play an important role in the time-dependent stress and strain characteristics of the tested samples. First, it was observed that creep in Ottawa sand/Montmorillonite mixtures could be controlled by adding small amounts of clay (Chang et al, 1997). Second, the block tests clearly demonstrated that the same clay could give rise to time-dependent deformation, even when distributed between only two grains.

Clay creep is usually classified into two successive stages: primary consolidation associated with fluid expulsion, and secondary consolidation, which is creep after the elevated pore pressures have equilibrated (Mitchell, 1976). The creeping clay observed in Figures 13 and 14 probably originates from high-pressure secondary consolidation. Secondary mechanisms occur after the transient pore pressure equilibrates. A secondary mechanism classified by Barden (1969) was micropore-macropore communication under poorly saturated conditions. These localized flows in the clay do not give rise to external pressure transients and establish a deformation time constant. The time constant is determined by the pore size distribution. Even though the samples were room-dried, evidence from Spoor and Goodwin (1979) of shear tests on different moisture contents in clay suggests that full saturation is not necessary to promote secondary consolidation of

clay. This appears to be what we have observed (Figures 12 and 13). As with all compaction mechanisms, compaction cannot occur indefinitely (except under solution surface failure). Figure 13 suggests that the clay compaction in the block experiments is finite, and is highly dependent on the samples loading history as suggested in the triaxial creep tests in Chapter 5.

In the sample of Montmorillonite clay tested here, it was evident that a small amount of water was necessary to facilitate creep. Premoistening and drying were required to obtain creep strain in the sands. The results of Spoor and Goodwin (1979) and Holzer et al (1973) suggest that the strength of clay can be influenced by small amounts of moisture. This is probably why premoistening and drying was required in the block tests (Figure 14) to produce creep. This property strongly suggests a micro-poroelastic mechanism that is undetectable using conventional pressure measurements.

Combining the concept of stress migration (Barden, 1969; Pusch, 1979) and ductile behavior in clay may give rise to a possible explanation for viscous deformation of sands. If there were no clay, all responses to stress perturbations would happen instantaneously, with no phase lag between stress and strain. With the presence of clay, localized viscous deformation can lead to time-dependent compaction of localized load-bearing structures in the sample. This explains why we observed more viscous behavior in loading than in unloading. Rearrangement can occur relatively easily as the clay slowly loses its volume under load.

6.4 Conclusions

1) Creep observed under hydrostatic stress and room temperature in the Ottawa sand/

Montmorillonite clay samples is not related to grain-crushing, time-dependent microfracturing, stress corrosion, or solution surface effects.

2) Secondary consolidation of room-dried clay on the grain contacts gives rise to time-dependent grain rearrangement. This motion manifests itself as volumetric creep during hydrostatic loading tests on unconsolidated sands.

3) This mechanism most likely explains the creep observations made in the unconsolidated Lentic sands from the Gulf of Mexico and the Wilmington sands from the Wilmington Field in Long Beach, California.

6.5 References

Barden, L., 1969, Time dependent deformation of normally consolidated clays and peats, Journal of the Soil Mechanics and Foundations Division, ASCE, 95:SM1, 1-31.

Bjorkum, P.A., 1996, How important is pressure in causing dissolution of quartz in sandstone?, J. Sed. Res., 66, 147-154.

Borg, I., Friedman, M., Handin, J., and Higgs, D.V., 1960, Experimental deformation of St. Peter Sand: a study of cataclastic flow, in: Rock Deformation, eds. D.Griggs and

Brzesowsky, R., 1995, Micromechanics of sand grain failure, Ph.D thesis, Universiteit Utrecht.

Costin, L.S., 1987, Time-dependent deformation and failure, in: Fracture Mechanics of Rock, edited by B.K. Atkinson, Academic Press.

deBoer, R.B., Nagtegaal, P.J.C., and Duyvis, E.M., 1977, Pressure solution experiments on quartz sand, Beochim. Cosmochim. Acta, 41, 257-264.

Holzer, T.L., Hoeg, K., Arulanandan, K., 1973, Excess Pore Pressures During Undrained Clay Creep, Can. Geotech. J., 10: 12, 13-24.

Lundegard, P.D., 1992, Sandstone porosity loss - a "big picture" view of the importance of compaction, J. Sed. Petrol., 62, 250-260

Martin, R.J., 1972, Time-dependent crack growth in quartz and its application to creep of rocks, Journal of Geophysical Research, 77: 8, 1406-1419, 1972.

Mitchell, J.K., 1976, Fundamentals of Soil Behavior, John Wiley and Sons, New York.

Pusch, R., 1979, Creep mechanisms in clay, Mechanisms of deformation and fracture, ed: Easterling, K. E.

Spoor, G., Goodwin, R.J., 1979, Soil deformation and shear strength characteristics of some clay soils at different moisture contents: Journal of Soil Science, 30, 483-498.

Schutjens, P.M.,1991, Experimental compaction of quartz sand at low effective stress and temperature conditions: J. of the Geo. Soc. London, 148, 527-539.

Zhang, J., Wong, T.F., Davis, D.M.,1990, High pressure embrittlement and shear- enhanced compaction of Berea Sandstone; acoustic emission measurement and microstructural observation: Rock mechanics; contributions and challenges; proceedings of the 31st U.S. symposium; 31, 653-660.

Zoback, M. D., Byerlee, J., 1976, Effect of high-pressure deformation on permeability of Ottawa Sand, AM. ASSOC. PET. GEOL. BULL, 60: 9, p. 1531-1542.

CHAPTER 7

7.1 Conclusions

The results of experimental deformation testing of poorly consolidated sands show that time-dependent deformation can occur in fine-grained reservoir sands and synthetic samples of Ottawa sand mixed with small amounts of Montmorillonite clay. This creep deformation at hydrostatic and triaxial loads of 10 MPa to 40 MPa suggests that the sands compact visoelastically with time constants between 1 and 10 hours. Since all of the samples that displayed creep behavior also contained small (< 10%) amounts of clay, the presence of clay appears to determine the occurrence of creep. The resulting data suggests that time-dependent deformation mechanisms with time constants between 1 and 10 hours may control the geomechanical behavior of reservoir rock in situ during hydrocarbon production activities, and may possibly explain fault-gouge compaction in active earthquake zones.

The differences between static and dynamic moduli can be attributed to a viscoelastic mechanism. Creep, relaxation, dispersion, and strain rate variation data support the connection between time-dependent deformation and viscoelasticity in the rock samples tested here. The data indicates that a standard linear solid viscoelastic model can describe the transient stress and strain behavior of the rock. The mechanism describes the phase lag observed between the stress and strain during deformation and variation in stiffness at different strain rates. The time-dependent deformation arising from a phase lag between the stress and strain implies that measurements of static and dynamic moduli will differ because of viscoelastic relaxation of the rock matrix.

Although the creep, relaxation, and dispersion data support the viscoelastic phenomena

in the unconsolidated samples of the Wilmington, Lentic, and Ottawa sands, it is apparent that nonlinear elasticity and plasticity strongly contribute to dispersion as well. Curvature in the stress-strain curves under loading and the lack of creep in unloading tests demonstrate the influence of irreversible compaction of the pore volume. This curvature can be interpreted as a strain-dependent anelastic modulus. The resulting modulus could be lower for large-strain perturbations, such as the stress cycling tests, and higher for ultrasonic pulse transmission, thus giving rise to dispersion. Most likely, a combination of strain rate (viscoelastic) and strain amplitude effects is occurring simultaneously during deformation generating differences in the static and dynamic moduli.

The relaxation of stress under constant strain boundary conditions indicates that the shear strength of unconsolidated reservoir rock depends on time. The relaxation observed in the unconsolidated sand tests, which is related to creep, can be regarded as a time-dependent load-bearing capacity. Although the sample is not in failure, as defined by a Mohr-Coulomb relationship with a coefficient of 0.6, it loses its ability to carry load as a function of time. This is probably because the stress relaxation mechanism is not a frictional mechanism that can be modeled using a frictional constant. The loss of 60% of the load-bearing capacity does, however, represent failure if considered in engineering applications associated with drilling and production. This mechanism may explain the often low differential stresses observed in unconsolidated reservoir rocks in situ.

The micromechanical mechanism for creep appears to be the compaction of clays containing very small amounts of water. The compaction experiments on dry Montmorillonite clay suggest that flocculated clay structure formed during clay saturation and drying becomes compacted to planar structure during compression. The flocculated

structure contains less than 10% water; however, it becomes saturated as the pore volume is compacted. This micro-poroelastic mechanism probably gives rise to the time-dependent compaction of clayey sands under dry conditions. For the sand sample, clay particles between the grains govern the overall compaction behavior and contribute a time constant to the overall deformation. This deformation behavior is probably controlled by the amount of clay, its moisture content, and the initial packing of the quartz grains.

The viscoelastic effects described in this dissertation may provide vital keys to unlocking some very perplexing problems of tectonophysics. The near-hydrostatic stress states in the unconsolidated reservoir rocks of the Gulf of Mexico may be controlled by viscoelastically relaxing rock. Time-dependent hole collapse and long-term subsidence in some oil producing reservoirs may be influenced by viscoelastic deformation mechanisms. The state of stress and intensification of pore pressure in fault-gouge materials, such as those observed in the San Andreas Fault, may be characterized by a viscoelastic rheology, which would explain the low shear stresses observed there. At this time, it is speculative that there is a relationship between these problems and the rheology of the rocks dealt with here. Connecting these natural phenomena to the laboratory results will require more investigation in both areas.

7.2 Suggestions for further investigation

Although the micromechanical description of natural unconsolidated reservoir rock creep was connected to the presence of clay, it is not clear what controls the time constant of deformation. The microporoelastic mechanism discussed in this dissertation would suggest that the time constant depends on the hydraulic conductivity of the small amounts

of intergranular clays. Thus, clay permeability and pore fluid viscosity probably play important roles in determining this value. To investigate this phenomena in more depth, the focus of the testing should be directed to the deformation of pure clays. The experimental details of saturation need to be carefully controlled to observe the dependence of creep on fluid saturation.

Because triaxial deformation systems are not designed to follow the motion of individual grains, this study did not examine the phenomena of grain repacking in depth. It was assumed that the viscoelastic clay deformation provided a time-dependent mechanism for grain motion and repacking. It is very difficult to monitor the positions of grains relative to clay before, during, and after deformation. A new technique, possibly utilizing acoustic microscopy during deformation, may provide more detailed information regarding the repacking mechanism that conventional microscopic and SEM analysis cannot provide.

The mechanics of time-dependent deformation in granular materials is not exclusive to rock and soil mechanics literature. Mechanical engineering literature examines similar topics under tribology of granular media to understand the interaction between fluid-coated roller bearings. In chemical engineering literature, one finds studies of the behavior of suspensions and slurries of fluid and grain mixtures to optimize slurry transportation techniques. In ceramics engineering literature there are empirically examinations of the physics of grain lubricants and binders used to facilitate the injection of dry clays into ceramic casting molds at high pressures. Although these fields are related, their approaches and scientific motivation are vastly different from those of geophysics and were not discussed in this dissertation. However, the extensive research in these disciplines may provide insight into the behavior of granular deformation not yet considered by

geophysicists. It would benefit the science of granular material deformation to integrate some of the information from these disciplines.